TECHNICAL REPORT

FINAL REPORT ON A STUDY OF LOW-DENSITY NOZZLE FLOWS, WITH APPLICATION TO MICROTHRUST ROCKETS

CAL No. AI-2590-A-1

Prepared for:

HEADQUARTERS
NATIONAL AERONAUTICS AND SPACE ADMINISTRATION
WASHINGTON, D.C.

PROGRAM MANAGER: Frank E. Compitello
NASA HEADQUARTERS

TECHNICAL MANAGER: Manuel Curtis
GODDARD SPACE FLIGHT CENTER

FINAL REPORT
Contract No. NASW-1668
December 1969

CORNELL AERONAUTICAL LABORATORY, INC.
OF CORNELL UNIVERSITY, BUFFALO, N. Y. 14221

CORNELL AERONAUTICAL LABORATORY, INC.
BUFFALO, NEW YORK 14221

FINAL REPORT ON A STUDY OF LOW-DENSITY NOZZLE FLOWS, WITH APPLICATION TO MICROTHRUST ROCKETS

FINAL REPORT
CAL REPORT NO. AI-2590-A-1
CONTRACT NO. NASW-1668
DECEMBER 1969

Prepared for:

HEADQUARTERS
NATIONAL AERONAUTICS AND SPACE ADMINISTRATION
WASHINGTON, D.C.

PROGRAM MANAGER: Frank E. Compitello
NASA HEADQUARTERS

TECHNICAL MANAGER: Manuel Curtis
GODDARD SPACE FLIGHT CENTER

PREPARED BY: William J. Rae
William J. Rae

APPROVED BY: Charles E. Treanor
Charles E. Treanor, Head
Aerodynamic Research Department

PRECEDING PAGE BLANK NOT FILMED.

ABSTRACT

A method for calculating the effect of viscosity on low-density flow through a nozzle is described, and details of a computer program for applying the method are presented. The analysis is based on the slender-channel equations, with slip boundary conditions at the walls. The solution is started upstream of the throat, using asymptotic results for slow viscous flow in a converging cone. An implicit finite-difference scheme is then used to calculate the pressure, and profiles of velocity and enthalpy at successive stations along the channel.

The cases presented show the effects of the nozzle geometry, the Reynolds number, and the thermal condition of the nozzle wall. The results show that specific impulse is improved by a throat whose longitudinal radius of curvature is small, and that exit-area ratios as low as ten can be used without serious loss of performance.

It is shown that, at sufficiently low Reynolds numbers and low exit-cone angles, there is no solution of the slender-channel equations in which the flow can expand to supersonic conditions. Instead, the boundary layer closes, and the solution resembles a viscous subsonic pipe flow. The implications of this finding on the upstream influence of the exit-plane conditions and on the limits of validity of the slender-channel equations are discussed.

Readers desiring to make calculations can proceed directly to Appendix A, which is a user's manual for the computer program. This program has been deposited at the COSMIC Computer Center, University of Georgia, Athens, Georgia, 30601.

TABLE OF CONTENTS

LIST OF SYMBOLS

a	speed of sound
A	$\dot{m}/2\pi\rho_0\sqrt{2H_0}\ r_*^2$
A/A_*	geometric area ratio
B	$\rho_0\sqrt{2H_0}\ r_*/\mu_0$
D	ρ/ρ_0
F	thrust
$\bar{F}$	$F/p_0\pi r_*^2$
h	static enthalpy
H	total enthalpy
k	thermal conductivity
L	nozzle length
$\dot{m}$	mass flow rate
M	Mach number
$\mathcal{M}$	molecular weight
p	pressure
P	p/p_0
Pr	Prandtl number
r, z	cylindrical coordinates
r_1	longitudinal radius of curvature of the nozzle wall, at the throat
$\mathcal{R}$	universal gas constant
$R(z)$	transverse radius of nozzle wall
R_1	r_1/r_*
T	temperature
u, v	axial and radial velocity components

LIST OF SYMBOLS (Cont)

$\mathcal{U}, V$	$u/\sqrt{2H_0}$, $v/\sqrt{2H_0}$
W	$V - \mathcal{U}\eta \, d\sigma_w/dx$
x, σ	z/r_* , r/r_*
α_u, α_T	accommodation coefficients for velocity and temperature
γ	specific-heat ratio
δ	r/L
δ_1	displacement thickness
η	σ/σ_w
θ	wall angle
θ_1, θ_2	entrance and exit-cone angles
Θ	h/H_0
μ	viscosity
ρ	density
σ	r/r_*
ω	exponent in viscosity, enthalpy relation
$(\ )_e$	denotes conditions at nozzle-exit plane
$(\ )_o$	denotes conditions in reservoir
$(\ )_w$	denotes conditions at the wall
$(\ )_{¢}$	denotes conditions on the axis
$(\ )_*$	denotes conditions at the geometric throat

1. INTRODUCTION

The rocket engines that are used for satellite attitude control are often required to produce a thrust less than one pound force, extending in some instances to values as low as 10^{-6} lbf.[1] Such low values of the thrust dictate the use of low reservoir pressures and small nozzle scale; the result is that the flow takes place at very low Reynolds numbers, where viscous effects are felt all across the nozzle cross-section. Thus, it is not possible to calculate the performance of these devices by the usual inviscid, one-dimensional flow approximation, with a small correction due to a thin boundary layer.

The studies described in this report have led to a method of predicting nozzle performance in most of the Reynolds number range appropriate to microthrust rockets. These predictions show good agreement with experiment. The method is a numerical one, and a relatively simple computer program has been developed for applying the method. The only inputs required for a calculation are the reservoir conditions, the nozzle geometry, the gas properties (such as the specific-heat ratio), and (if heat transfer is allowed) the distribution of wall temperature. The program determines the mass flow, and then prints the pressure, thrust coefficient, and profiles of velocity, density, and static enthalpy at selected stations along the nozzle.

A search of the literature was made at the beginning of this program. The major results of that search are presented in Section 2. It was decided, on the basis of this search, that the theoretical approach which offered the greatest potential was a numerical solution of the slender-channel equations with slip boundary conditions. These equations are derived in Section 3, and a few details of the finite-difference method are given in Section 4. Prior to the present study, no one had demonstrated a routine numerical method of solving these equations for arbitrary nozzle geometry and reservoir conditions. The key to the successful development done in this study was to apply, to internal flows, certain advances that have been made in recent years in the calculation of viscous axisymmetric wakes. In particular, use has been made of implicit finite differences, and inversion of the large matrices which these differences lead to has been done by taking advantage of the tridiagonal nature of these matrices. Perhaps most important of all, the existence of a singular point in the slender-channel equations has been recognized by analogy with the wake problem, and analogous means of passing smoothly through the singularity have been developed.

The approximation inherent in the slender-channel equations is essentially the same as that made when one assumes that the flow has a thick boundary layer, with an inviscid core. The mathematical approach commonly used in this approximation is to solve by an iteration process, in which the first iteration assumes a purely inviscid flow. The pressure distribution of this inviscid flow is then used to calculate a boundary layer, whose displacement thickness is subtracted from the geometric cross-sectional area, to provide the basis for the next iteration on the inviscid core. This iteration method often fails to converge under low-density conditions, where an inviscid flow is a very poor first approximation.

In the present approach, this iteration method is not used; instead, the pressure distribution is found by satisfying, at each step along the channel, an equation which contains information about the singular point. By proceeding in this manner, it has been possible to find solutions at lower densities than those of previous solutions, and in fact it has been possible to identify the density level at which the boundary layer closes and the inviscid core disappears.

The initial profiles that are used to start the solution at near-reservoir conditions are described in Section 5. Results from a variety of cases are discussed in Section 6. Comparisons with experimental data are given first, as a means of validating the theory. These are followed by a set of parametric studies, which show that the maximum thrust is achieved at lower and lower exit-area ratios as the Reynolds number is decreased, and that for sufficiently low Reynolds number the core of the flow cannot expand to supersonic conditions in the diverging part of the nozzle. The influence of heat transfer is found to be significant, and thrust improvements found with a heated wall suggest that engines from which heat is rejected (as for example when a catalyst bed is used) would have better performance if the rejected heat were introduced into the divergent walls of the nozzle.

The present method has application to the design of low-density wind tunnels. The computer program described here has in fact been used for this purpose at several laboratories in the United States.

Under continuing support from NASA, an experimental follow-on program is being pursued, in which profiles of density in a low-density nozzle will be measured by an electron-beam fluorescence probe. This work, which is being done by Dr. Dietmar E. Rothe, will provide a very significant check on predictions of the theory described here. In addition, it can be expected to yield important data on the structure of the flow field at the very low-density levels where no supersonic core is predicted by the present model.

2. LITERATURE SEARCH

At the beginning of this program, a thorough literature search was made. Approximately two hundred references were studied, some of which were provided by automated information - retrieval systems.[2, 3] The most valuable groups of papers were those which presented analytical methods of predicting viscous flow,[4-47] experimental measurements of nozzle performance,[48-68] and general reviews of the problem.[1, 69-72] Two other groups worthy of mention were those describing thrust transients[73-79, 24] and experimental techniques for measuring low thrust levels.[80-86]

The thrust range of interest in the present investigation was that between approximately 10^{-6} and 1.0 lbf. Except perhaps for the lowest decade, most of this range lies in the transitional region between continuum and free-molecular flow (see, for example, Ref. 1, p. 1160). Consequently, in carrying out the literature search, primary attention was directed toward analytical methods based on a continuum model. The analytical methods were essentially of two types: those based on conventional thin-boundary-layer theory, and those based on the slender-channel equations.

In the first type of approach, it is assumed that the flow has an inviscid core that can be treated as an isentropic, one-dimensional channel flow. The boundary layer that forms on the walls is treated in a variety of ways (e.g., by integral methods or by local application of similarity solutions), and its growth rate is usually coupled to the rate of expansion of the inviscid core. In developing this approach, various authors have used a number of further approximations; important among these are the degree to which transverse curvature is accounted for, and the manner of specifying the initial state of the boundary layer. Many of these treatments have been developed to the point of presenting a working computer program, some of which (see, for example, Ref. 33) are very well documented. The major shortcomings of these methods, when applied to the microthrust rocket problem, is that the boundary layer is usually assumed to have zero thickness at the throat, that slip boundary conditions are generally not used, and that the rate of convergence of the iterations between the boundary-layer and core flows becomes slower as the boundary layer thickens.

The slender-channel equations, on which the second type of approach is based, were first proposed by Williams,[43, 44] who simplified the Navier-Stokes equations on the basis that the nozzle walls diverge very slowly. These equations are formally identical with the boundary-layer equations, including the full effect of transverse curvature. They differ only in being written in cylindrical coordinates aligned with the nozzle axis, rather than in surface coordinates. In this approximation the pressure is constant across the channel, varying only with distance along the channel. Thus, except for the boundary conditions, the slender-channel equations are the same as those often used in studies of the laminar axisymmetric wake.

Most of the existing solutions of the slender-channel equations are those of the self-similar variety, done by Williams[43-46] and by Adams.[42] These solutions have given important qualitative information about low-density nozzle flow fields. However, they are of limited value when applied to the direct problem, since the conditions for self-similarity require nozzles whose shape changes when the Reynolds number is changed.

In recent years, many nonsimilar boundary-layer problems have been treated successfully by numerical methods (see, for example, Refs. 87 and 88). Numerical solutions of the slender-channel equations have in fact been presented by Milligan[38] and by Myers;[39] only a few such results are available, however, due primarily to limitations in computational facilities. In addition, finite-difference solutions of the laminar axisymmetric wake problem have been presented by several groups.[89-92]

In the light of these observations, it appeared that the approach most likely to produce useful engineering results was to develop a finite-difference solution of the slender-channel equations, starting with a given nozzle geometry, and given reservoir conditions. It was decided to follow this approach, using slip boundary conditions at the wall, since many studies have shown (see, for example, Ref. 93) that these conditions, with the Navier-Stokes equations, lead to valid results well down into the transition-flow regime.

3. BASIC EQUATIONS

The starting point for the derivation of the slender-channel equations is the Navier-Stokes equations. In cylindrical coordinates, for steady, axisymmetric flow, with zero bulk viscosity, these are:

Continuity:

$$\frac{\partial}{\partial z}(\rho u) + \frac{\partial}{\partial r}(\rho v) + \frac{\rho v}{r} = 0 \tag{3-1}$$

Axial momentum:

$$\begin{aligned} \rho u \frac{\partial u}{\partial z} + \rho v \frac{\partial u}{\partial r} &= -\frac{\partial p}{\partial z} \\ &+ \frac{\partial}{\partial z}\left[\mu\left(2\frac{\partial u}{\partial z} - \frac{2}{3}\left\{\frac{1}{r}\frac{\partial}{\partial r}(rv) + \frac{\partial u}{\partial z}\right\}\right)\right] \\ &+ \frac{1}{r}\frac{\partial}{\partial r}\left[\mu r\left(\frac{\partial v}{\partial z} + \frac{\partial u}{\partial r}\right)\right] \end{aligned} \tag{3-2}$$

Radial momentum:

$$\begin{aligned} \rho u \frac{\partial v}{\partial z} + \rho v \frac{\partial v}{\partial r} &= -\frac{\partial p}{\partial r} \\ &+ \frac{\partial}{\partial r}\left[\mu\left(2\frac{\partial v}{\partial r} - \frac{2}{3}\left\{\frac{1}{r}\frac{\partial}{\partial r}(rv) + \frac{\partial u}{\partial z}\right\}\right)\right] \\ &+ \frac{\partial}{\partial z}\left[\mu\left(\frac{\partial v}{\partial z} + \frac{\partial u}{\partial r}\right)\right] + \frac{2\mu}{r}\left(\frac{\partial v}{\partial r} - \frac{v}{r}\right) \end{aligned} \tag{3-3}$$

Energy:

$$\rho u \frac{\partial h}{\partial z} + \rho v \frac{\partial h}{\partial r} - u \frac{\partial p}{\partial z} - v \frac{\partial p}{\partial r} =$$

$$\frac{1}{r} \frac{\partial}{\partial r}\left(r k \frac{\partial T}{\partial r}\right) + \frac{\partial}{\partial z}\left(k \frac{\partial T}{\partial z}\right)$$

$$+ \mu \left[2 \left\{ \left(\frac{\partial u}{\partial z}\right)^2 + \left(\frac{\partial v}{\partial r}\right)^2 + \left(\frac{v}{r}\right)^2 \right\} + \left(\frac{\partial v}{\partial z} + \frac{\partial u}{\partial r}\right)^2 \right] \qquad (3\text{-}4)$$

$$- \frac{2}{3} \mu \left(\frac{\partial v}{\partial r} + \frac{v}{r} + \frac{\partial u}{\partial z} \right)^2$$

Williams simplified these equations by assuming that the ratio of radial to axial velocity components, and the ratio of axial to radial gradients were each of the order of the slenderness ratio of the nozzle, i. e.

$$O\left(v/u\right) = O\left(\frac{\partial/\partial z}{\partial/\partial r}\right) = O(\delta)$$

$$\delta \equiv r/L$$

This assumption appears to be suitable for flows in which shear stresses produced by transverse gradients are much larger than those produced by axial gradients. The only region that might appear to be excluded from this rule is that near the throat, where the axial acceleration is greatest, and where boundary layers are generally thinnest. Even in this region, however, the ordering used by Williams is acceptable, as can be seen from the following argument: the axial velocity increases from the value a_* at the throat to about $2a_*$ at the point where $A/A_* \approx 5$, according to inviscid, one-dimensional theory.[94] Thus an upper limit for the order of $\partial u/\partial z$ can be taken as

$$\frac{\Delta u}{\Delta z} \sim \frac{\Delta u}{\Delta (A/A_*)} \cdot \frac{d(A/A_*)}{dz} \sim \frac{a_*}{5} \frac{d(A/A_*)}{dz}$$

-But for a slender nozzle, the area ratio is a function of $z \tan\theta / r_*$; thus $d(A/A_*)/dz \sim O(\theta/r_*)$ and

$$\frac{\partial u}{\partial z} \sim O\left(a_* \frac{d(A/A_*)}{dz}\right) \sim O\left(\frac{a_* \theta}{r_*}\right)$$

If in addition it is assumed that $\partial u/\partial r \sim O(a_*/r_*)$ one is led to Williams' ordering, namely that

$$\frac{\partial/\partial z}{\partial/\partial r} = O(\theta)$$

If these approximations, including the assumption that $v/u \sim O(\theta)$, are now used in Eqs. (3-1) - (3-4), the leading terms are

$$\frac{\partial}{\partial z}(\rho u) + \frac{\partial}{\partial r}(\rho v) + \frac{\rho v}{r} = 0 \qquad (3\text{-}5)$$

$$\rho u \frac{\partial u}{\partial z} + \rho v \frac{\partial u}{\partial r} = -\frac{dp}{dz} + \frac{1}{r}\frac{\partial}{\partial r}\left(\mu r \frac{\partial u}{\partial r}\right) \qquad (3\text{-}6)$$

$$\frac{\partial p}{\partial r} = 0 \qquad (3\text{-}7)$$

$$\rho u \frac{\partial h}{\partial z} + \rho v \frac{\partial h}{\partial r} - u \frac{dp}{dz} =$$

$$\frac{1}{r}\frac{\partial}{\partial r}\left(\frac{r\mu}{Pr}\frac{\partial h}{\partial r}\right) + \mu\left(\frac{\partial u}{\partial r}\right)^2 \tag{3-8}$$

These equations are formally identical with the boundary-layer equations, including the radial dependences that account for transverse curvature.

The boundary conditions applied at the walls are those corresponding to first-order velocity slip and temperature jump. The first of these relates the velocity component along the wall to its gradient normal to the wall. When this component is expressed as a linear combination of u and v and is then simplified according to the slender-channel ordering, the result is

$$-u_w = \frac{2-\alpha_u}{\alpha_u}\sqrt{\frac{\pi}{2}}\,\frac{\mu}{p}\sqrt{\frac{RT}{m}}\,\cos\theta\left(\frac{\partial u}{\partial r}\right)_w \tag{3-9}$$

The corresponding condition for the temperature becomes

$$T - T_w =$$

$$= -\frac{2-\alpha_T}{\alpha_T}\sqrt{\frac{\pi}{2}}\,\frac{2\gamma}{Pr(\gamma+1)}\,\frac{\mu}{p}\sqrt{\frac{RT}{m}}\,\cos\theta\left(\frac{\partial T}{\partial r}\right)_w \tag{3-10}$$

In all of the results presented here, the gas has been assumed to follow the perfect-gas law, with constant Prandtl number, constant specific-heat ratio, and with viscosity proportional to a power of the temperature:

$$p = \frac{\gamma - 1}{\gamma} \rho h \quad ; \quad \mathcal{R} = const.$$

$$\mu / \mu_o = \left(\frac{h}{H_o} \right)^{\omega} \qquad (3\text{-}11)$$

Dimensionless Forms

The coordinates are made dimensionless by the nozzle throat radius:

$$x = z/r_* \quad , \quad \sigma = r/r_* \qquad (3\text{-}12)$$

and the dependent variables are made dimensionless with respect to reservoir conditions:

$$U = u/\sqrt{2H_o} \quad , \quad V = v/\sqrt{2H_o}$$

$$P = p/p_o \quad , \quad D = \rho/\rho_o \quad , \quad \Theta = h/H_o \qquad (3\text{-}13)$$

In addition, it is useful to normalize the radial coordinate by its wall value at each station

$$\eta = \sigma/\sigma_w(x) \qquad (3\text{-}14)$$

In terms of these variables, the equations of motion become

Continuity:

$$P \frac{\partial}{\partial \eta} \left(\frac{\eta W}{\Theta} \right) + \sigma_w \eta \frac{\partial}{\partial x} \left(\frac{PU}{\Theta} \right) + 2 \sigma_w' \frac{P \eta U}{\Theta} = 0 \qquad (3\text{-}15)$$

Momentum:

$$\frac{P}{\Theta}\left(\mathcal{U}\frac{\partial \mathcal{U}}{\partial x} + \frac{W}{\sigma_w}\frac{\partial \mathcal{U}}{\partial \eta}\right) = -\frac{\gamma - 1}{2\gamma}\frac{dP}{dx}$$

$$+ \frac{1}{B\eta\sigma_w^2}\frac{\partial}{\partial \eta}\left(\eta\,\Theta^{\omega}\frac{\partial \mathcal{U}}{\partial \eta}\right) \qquad (3\text{-}16)$$

Energy:

$$\frac{P}{\Theta}\left(\mathcal{U}\frac{\partial \Theta}{\partial x} + \frac{W}{\sigma_w}\frac{\partial \Theta}{\partial \eta}\right) = \frac{\gamma - 1}{\gamma}\,\mathcal{U}\frac{dP}{dx}$$

$$+ \frac{1}{B\eta\sigma_w^2}\frac{\partial}{\partial \eta}\left(\frac{\eta}{Pr}\Theta^{\omega}\frac{\partial \Theta}{\partial \eta}\right) \qquad (3\text{-}17)$$

$$+ \frac{2\Theta^{\omega}}{B\sigma_w^2}\left(\frac{\partial \mathcal{U}}{\partial \eta}\right)^2$$

In these equations, the density has been eliminated by use of the equation of state:

$$P = D\,\Theta \qquad (3\text{-}18)$$

The transformed radial velocity W that appears in these equations is

$$W = V - \mathcal{U}\eta\frac{d\sigma_w}{dx} \qquad (3\text{-}19)$$

Note that W is zero both at the wall and on the axis, and that if W is zero elsewhere, it implies that the local streamline deflection is equal to the wall slope, multiplied by the fractional distance to the wall.

The only parameter that appears in these equations (in addition to γ, Pr, ω, and $\sigma_w(x)$) is a Reynolds number based on reservoir conditions and the throat radius:

$$\mathcal{B} = \frac{\rho_o \sqrt{2H_o}\; r_*}{\mu_o} \tag{3-20}$$

This parameter is convenient to use, since it involves only conditions that are known in advance and are accessible to the designer.

The boundary conditions in the (x, η) coordinate system are:

$$\mathcal{U}\Big)_{\eta\to 1} = \tag{3-21}$$

$$- \frac{2-\alpha_u}{\alpha_u} \sqrt{\frac{2\gamma}{\gamma-1}\,\frac{\pi}{2}}\; \frac{\cos\theta_w}{\mathcal{B} P \sigma_w} \left(\Theta_{\eta\to 1}\right)^{\omega+\frac{1}{2}} \left(\frac{\partial \mathcal{U}}{\partial \eta}\right)_{\eta\to 1}$$

If the wall temperature is prescribed, the thermal boundary condition is

$$\Theta\Big)_{\eta\to 1} - \Theta_w(x) = \tag{3-22}$$

$$- \frac{2-\alpha_T}{\alpha_T}\, \frac{2\gamma}{\mathcal{E}(\gamma+1)} \sqrt{\frac{2\gamma \cdot \pi}{(\gamma-1)\cdot 2}}\; \frac{\cos\theta_w}{\mathcal{B} P \sigma_w} \left(\Theta_{\eta\to 1}\right)^{\omega+\frac{1}{2}} \left(\frac{\partial \Theta}{\partial \eta}\right)_{\eta\to 1}$$

If the wall is taken to be adiabatic, this second boundary condition is replaced by (see Eq. (3-31)):

$$\frac{\partial}{\partial \eta}\left(\frac{\Theta}{\mathcal{E}} + \mathcal{U}^2\right)_{\eta\to 1} = 0 \tag{3-23}$$

On the axis, symmetry requires that

$$\frac{\partial \mathcal{U}}{\partial \eta}\Big)_{\eta=0} = \frac{\partial \Theta}{\partial \eta}\Big)_{\eta=0} = 0 \tag{3-24}$$

Conservation Relations

The relations that express the global conservation of mass, momentum, and energy can be written down either from a direct transformation of the integral forms of the conservation laws, or by manipulation of Eqs. (3-15) - (3-17).* The continuity equation, when integrated from zero to η, becomes an expression for W:

$$\frac{\eta W}{\sigma_W \Theta \int_0^{\eta} \frac{\eta U \, d\eta}{\Theta}} + \frac{d}{dx} \ln \left[P \sigma_W^2 \int_0^{\eta} \frac{U \eta \, d\eta}{\Theta} \right] \tag{3-25}$$

In particular, if the upper limit is set equal to one (where $W = 0$), this becomes an expression for the total mass flow:

$$P \sigma_W^2 \int_0^1 \frac{U \eta \, d\eta}{\Theta} = A \equiv \frac{\dot{m}}{2\pi \rho_0 r_*^2 \sqrt{2H_0}} \tag{3-26}$$

The parameter A is proportional to the discharge coefficient of the nozzle:

$$C_D = \frac{\dot{m}_{\text{ACTUAL}}}{\dot{m}_{\text{ISENTROPIC, ONE-DIMENSIONAL}}} = 2A \left(\frac{\gamma+1}{2} \right)^{1/(\gamma-1)} \sqrt{\frac{\gamma+1}{\gamma-1}} \tag{3-27}$$

The constant of proportionality between A and C_D is:

$\gamma =$	1.1	1.2	1.3	1.4	1.667
$A/C_D =$	0.06698	0.09361	0.1133	0.1294	0.1624

*Detailed derivations are given in Appendix B.

A convenient definition of the stream function is

$$\psi = \frac{\displaystyle\int_0^\eta \frac{\mathcal{U}\eta \, d\eta}{\Theta}}{\displaystyle\int_0^1 \frac{\mathcal{U}\eta \, d\eta}{\Theta}} \tag{3-28}$$

Integration of the momentum equation leads to an expression for the variation of the thrust coefficient:

$$\frac{d\bar{F}}{dx} = P \frac{d}{dx}(\sigma_w^2) + \frac{4\gamma}{B(\gamma-1)} \left[\Theta(1)\right]^\omega \left.\frac{\partial \mathcal{U}}{\partial \eta}\right)_{\eta=1} \tag{3-29}$$

where

$$\bar{F} \equiv \frac{F}{p_0 \pi r_*^2} = P\sigma_w^2 \left\{ 1 + \frac{4\gamma}{\gamma-1} \int_0^1 \frac{\mathcal{U}^2 \eta \, d\eta}{\Theta} \right\} \tag{3-30}$$

Equation (3-29) states that the maximum thrust occurs at the point where the contribution from the pressure forces acting on the wall is balanced by the viscous shear stress at the wall, an observation that has been made by many authors (see, for example, Ref. 56).

If the momentum equation is multiplied by $2\mathcal{U}$, integrated, and added to the integrated energy equation, the result is a statement that the flux of total enthalpy is changed only by heat transfer at the wall:

$$\frac{d}{dx}\left\{ \sigma_w^2 \int_0^1 \eta D \mathcal{U} (\Theta + \mathcal{U}^2) \, d\eta \right\} = \frac{1}{B}\left[\Theta^\omega \frac{\partial}{\partial \eta}\left(\frac{\Theta}{Pr} + \mathcal{U}^2 \right) \right]_{\eta=1} \tag{3-31}$$

The adiabatic wall boundary condition, cited above as Eq. (3-23), is found by setting the right-hand side of this expression equal to zero.

Streamtube Relation

In the study of isentropic, one-dimensional channel flows, a very important equation is the one that relates the pressure gradient to the rate of change of cross-sectional area.[94]

$$\gamma \, d \ln \left(A/A_* \right) = \frac{1-M^2}{M^2} \; d \ln \left(p/p_0 \right)$$

For the present problem, this expression can be generalized to include the effects of viscosity. The generalization to viscous, two-dimensional flows was given by Weinbaum and Garvine;[95] the further generalization to the case of axisymmetric flows is given below.*

The equation of state is first used to eliminate the density from the continuity equation; in the resulting expression, the momentum and energy equations are used to replace $\partial u/\partial z$ and $\partial h/\partial z$ in favor of dp/dz . The result is:

$$\frac{\partial}{\partial r}\left(r \frac{v}{u} \right) = - \frac{r}{\gamma p} \; \frac{M^2 - 1}{M^2} \; \frac{dp}{dz}$$

$$- \frac{1}{\gamma p M^2} \; \frac{\partial}{\partial r}\left(\mu r \frac{\partial u}{\partial r} \right) + \frac{\gamma - 1}{\gamma u p} \; \frac{\partial}{\partial r}\left(\frac{\mu r}{Pr} \; \frac{\partial h}{\partial r} \right) \qquad (3\text{-}32)$$

$$+ \; \frac{\gamma - 1}{\gamma} \; \frac{\mu r}{u p} \left(\frac{\partial u}{\partial r} \right)^2$$

---

*The axisymmetric formulas have also been presented in a recent paper by Garvine and Weinbaum.[96]

The left-hand side of this expression is proportional to the radial gradient of the streamline direction, and hence to the axial rate of change of cross-sectional area of the streamtube. If the streamtube area is taken as $2\pi r \, \Delta r$, it can be shown that

$$\frac{1}{r} \frac{\partial}{\partial r}\left(r \frac{v}{u}\right) = \frac{1}{2\pi r \, \Delta r} \frac{d}{dx}\left(2\pi r \, \Delta r\right)$$

Thus, the first two terms in Eq. (3-32) are exactly the same as those familiar from the case of isentropic, one-dimensional channel flows. The additional terms represent the contributions to the area change that come from shear, net heat conduction to the streamtube, and heat generation within the streamtube due to the conversion of kinetic to thermal energy. These terms can be checked against the equivalent expressions derived from first principles by Shapiro.[97]

In terms of the dimensionless variables, the streamtube relation is

$$\begin{aligned} \frac{\partial}{\partial \eta}\left(\eta \frac{V}{U}\right) = {} & \frac{1-M^2}{\gamma P M^2} \, \eta \, \tau_w \, \frac{dP}{dx} \\ & - \frac{2}{(\gamma-1) B \tau_w P M^2} \left\{ \frac{\partial}{\partial \eta}\left(\eta \, \Theta^{\omega} \frac{\partial U}{\partial \eta}\right) \right. \\ & \left. - \frac{U}{\Theta}\left[\frac{\partial}{\partial \eta}\left(\frac{\eta \, \Theta^{\omega}}{Pr} \frac{\partial \Theta}{\partial \eta}\right) + 2\eta \, \Theta^{\omega}\left(\frac{\partial U}{\partial \eta}\right)^2\right] \right\} \end{aligned} \qquad (3\text{-}33)$$

If this expression is now integrated across the channel, it becomes a relation between the rate of change of the total channel cross-sectional area, and the integrated effects of pressure gradient, shear, heat conduction, and heat generation. It is useful to solve the resulting expression for the pressure gradient:

$$\frac{dP}{dx} = \Bigg\{ \gamma P \sigma_w' + \frac{2\gamma}{(\gamma-1) B \sigma_w} \cdot$$

$$\cdot \int_0^1 \frac{\frac{\partial}{\partial \eta}\left(\eta \Theta^{\omega} \frac{\partial U}{\partial \eta}\right) - \frac{U}{\Theta}\left[\frac{\partial}{\partial \eta}\left(\frac{\eta \Theta^{\omega}}{Pr} \frac{\partial \Theta}{\partial \eta}\right) + 2\eta\, \Theta^{\omega}\left(\frac{\partial U}{\partial \eta}\right)^2\right]}{M^2}\, d\eta \Bigg\}$$

$$\div \left\{ \sigma_w \int_0^1 \frac{1-M^2}{M^2}\, \eta\, d\eta \right\} \qquad (3\text{-}34)$$

In the limit of infinite Reynolds numbers, this expression reduces to the familiar inviscid, one-dimensional channel-flow result. At large finite Reynolds numbers, the general character of the solutions for various mass flows is qualitatively the same as that of the inviscid limit, namely: at sufficiently low mass flows, the pressure decreases along the converging part of the channel, reaches a minimum at or slightly beyond the throat, and then rises. For somewhat higher mass flows, the denominator of Eq. (3-34) changes sign upstream of the throat. Thus the pressure gradient becomes infinite, indicating that the flow has choked. At some intermediate mass flow, it is possible to find a saddle point, where the numerator and denominator of Eq. (3-34) vanish simultaneously. This intermediate mass flow is the only one that allows an expansion to conditions that are "supersonic", in the sense that

$$\int_0^1 \frac{1-M^2}{M^2}\, \eta\, d\eta < 0$$

Thus for high Reynolds numbers there is a critical mass flow, which allows a supersonic flow. Greater mass flows lead to choking, while lower ones yield a subsonic flow in which the pressure reaches a minimum near the throat and then rises.* The results given in Section 6 illustrate these types of behavior.

However, the results also show that the saddle point moves farther downstream as the Reynolds number is lowered, and that at low enough Reynolds numbers it does not occur at all within the range of exit-area ratios normally of interest in rocket design. For these cases, there is no mass flow that leads to supersonic conditions in the average sense indicated above. There is a certain mass flow for which choking occurs at the exit plane. For higher mass flows, choking occurs within the nozzle; for lower mass flows, the pressure may either reach a minimum and then rise, or it may decrease monotonically to the exit plane if the pressure drop due to friction is great enough to overcome the effect of nozzle expansion.

It should be noted that in cases where the no-slip condition is applied to the velocity at the wall, the integrals in Eq. (3-34) diverge. In order to obtain a determinate result, some account must be taken of the fact that in Eq. (3-33) the pressure gradient and shear-stress terms, as well as the heat-conduction and heat-generation terms, cancel in pairs in a region near the wall. Thus the simplification employed by Lighthill[98] might be used, in which the integration is stopped short of the wall. In the present paper, all of the cases studied allow slip at the walls, and the integrals can be carried out to $\eta = 1$ without complications.

*In some cases the rate of rise is sufficient to cause reverse flow near the wall. When this happens, the solution must be terminated, since the slender-channel equations are parabolic, and cannot allow an upstream influence.

4. NUMERICAL METHOD

Difference Equations

There are many ways of representing the present set of nonlinear partial differential equations by an equivalent set of difference equations. The choices made here were patterned after those that have been successful in earlier boundary-layer work.

The coordinates are expressed as

$$x = x_0 + (K-1)\Delta x \; ; \quad \eta = (L-1)\Delta\eta \quad , L = 1, 2, \cdots, L_{max}$$

For all the calculations reported here, L_{max} was taken as 101, and that constant is built into the computer program described in Appendix A. Values of the dependent variables at a grid point are represented by the notation:

$$\mathcal{U}(x, \eta) = \mathcal{U}_K^L$$

Crank-Nicholson implicit differences were used, to rewrite the momentum and energy equations in the following form

$$\frac{\eta \bar{P}}{\Theta_K^L}\left[\mathcal{U}_K^L \frac{\mathcal{U}_{K+1}^L - \mathcal{U}_K^L}{\Delta x} + \frac{W_K^L}{\bar{\sigma}_w} \frac{\mathcal{U}_K^{L+1} - \mathcal{U}_K^{L-1} + \mathcal{U}_{K+1}^{L+1} - \mathcal{U}_{K+1}^{L-1}}{4\Delta\eta}\right] =$$

$$= -\frac{\gamma-1}{2\gamma}\eta\frac{dP}{dx} + \frac{(\Theta_K^L)^\omega}{B\bar{\sigma}_w^2}\left[\frac{\mathcal{U}_K^{L+1} - \mathcal{U}_K^{L-1} + \mathcal{U}_{K+1}^{L+1} - \mathcal{U}_{K+1}^{L-1}}{4\Delta\eta}\right.$$

$$+\frac{\omega\eta}{\Theta_K^L}\frac{(\mathcal{U}_K^{L+1} - \mathcal{U}_K^{L-1})(\Theta_{K+1}^{L+1} - \Theta_{K+1}^{L-1}) + (\mathcal{U}_{K+1}^{L+1} - \mathcal{U}_{K+1}^{L-1})(\Theta_K^{L+1} - \Theta_K^{L-1})}{8(\Delta\eta)^2} \tag{4-1}$$

$$\left. + \eta\frac{\mathcal{U}_K^{L+1} - 2\mathcal{U}_K^L + \mathcal{U}_K^{L-1} + \mathcal{U}_{K+1}^{L+1} - 2\mathcal{U}_{K+1}^L + \mathcal{U}_{K+1}^{L-1}}{2(\Delta\eta)^2}\right]$$

$$\frac{\eta \bar{P}}{\Theta_K^L}\left[U_K^L \frac{\Theta_{K+1}^L - \Theta_K^L}{\Delta x} + \frac{W_K^L}{\bar{\sigma}_w} \frac{\Theta_K^{L+1} - \Theta_K^{L-1} + \Theta_{K+1}^{L+1} - \Theta_{K+1}^{L-1}}{4\Delta\eta}\right] =$$

$$= \frac{\gamma-1}{\gamma}\eta U_K^L \frac{dP}{dx} + \frac{(\Theta_K^L)^\omega}{B\bar{\sigma}_w^2 Pr}\left[\frac{\Theta_K^{L+1} - \Theta_K^{L-1} + \Theta_{K+1}^{L+1} - \Theta_{K+1}^{L-1}}{4\Delta\eta} \right.$$

$$+ \frac{\omega\eta}{\Theta_K^L}\frac{(\Theta_K^{L+1} - \Theta_K^{L-1})(\Theta_{K+1}^{L+1} - \Theta_{K+1}^{L-1})}{4(\Delta\eta)^2} \tag{4-2}$$

$$+\eta \frac{\Theta_K^{L+1} - 2\Theta_K^L + \Theta_K^{L-1} + \Theta_{K+1}^{L+1} - 2\Theta_{K+1}^L + \Theta_{K+1}^{L-1}}{2(\Delta\eta)^2}$$

$$\left. + 2 Pr\,\eta \frac{(U_K^{L+1} - U_K^{L-1})(U_{K+1}^{L+1} - U_{K+1}^{L-1})}{4(\Delta\eta)^2}\right]$$

Note that the wall radius and pressure appearing here are evaluated at a point halfway across the step:

$$\bar{\sigma}_w = \sigma_w\left((K+\tfrac{1}{2})\Delta x\right) \quad , \quad \bar{P} = P_K + \frac{\Delta x}{2}\frac{dP}{dx}$$

The velocity boundary condition at the wall is represented by:

$$U_{K+1}^{L\max} = \frac{-\sqrt{\frac{2\gamma}{\gamma-1}\cdot\frac{\pi}{2}}\ \frac{2-\alpha_u}{\alpha_u}\ \cos\theta_w\,(\Theta_K^{L\max})^{\omega+\frac{1}{2}}}{B\,P_{END}\ \sigma_{w,K+1}} \cdot$$

$$\cdot\left\{\frac{U_K^{L\max} - U_K^{L\max-1} + U_{K+1}^{L\max} - U_{K+1}^{L\max-1}}{2\Delta\eta}\right\} \tag{4-3}$$

For an adiabatic wall, the thermal boundary condition is taken as

$$-2 Pr\, U_K^{L_{max}} \left\{ \frac{U_K^{L_{max}} - U_K^{L_{max}-1} + U_{K+1}^{L_{max}} - U_{K+1}^{L_{max}-1}}{2 \Delta \eta} \right\} = \tag{4-4}$$

$$= \frac{\Theta_K^{L_{max}} - \Theta_K^{L_{max}-1} + \Theta_{K+1}^{L_{max}} - \Theta_{K+1}^{L_{max}-1}}{2 \Delta \eta}$$

For the case where heat transfer is allowed, this is replaced by

$$\Theta_{K+1}^{L_{max}} - \Theta_W (x_{K+1}) =$$

$$= \frac{\sqrt{\frac{2\gamma}{\gamma-1} \cdot \frac{\pi}{2}}\ \frac{2-\alpha_T}{\alpha_T}\ \frac{2\gamma}{Pr\,(\gamma+1)} \cos\theta_w \left(\Theta_K^{L_{max}}\right)^{\omega + 1/2}}{B\, P_{END}\, \sigma_{w,\, K+1}} \cdot \tag{4-5}$$

$$\cdot \left\{ \frac{\Theta_K^{L_{max}} - \Theta_K^{L_{max}-1} + \Theta_{K+1}^{L_{max}} - \Theta_{K+1}^{L_{max}-1}}{2 \Delta \eta} \right\}$$

Note that in these boundary conditions the pressure and wall radius have been determined at the end of the step:

$$\sigma_{w,\, K+1} = \sigma_w \left((K+1) \Delta x \right)$$

$$P_{END} = P_K + \Delta x \cdot \frac{dP}{dx}$$

<u>Solution of the Difference Equations</u>

The solution of the finite-difference equations can be determined recursively, following the method outlined by Richtmeyer and Morton[99] (see especially Sec. 11. 5). This solution presumes that the profiles at the beginning of the step, and a value of dP/dx, are known.

The momentum and energy equations are rewritten in the form:

$$-\begin{pmatrix} a_{11}^{L} & a_{12}^{L} \\ a_{21}^{L} & a_{22}^{L} \end{pmatrix}\begin{pmatrix} \mathcal{U}_{K+1}^{L+1} \\ \Theta_{K+1}^{L+1} \end{pmatrix} + \begin{pmatrix} b_{11}^{L} & b_{12}^{L} \\ b_{21}^{L} & b_{22}^{L} \end{pmatrix}\begin{pmatrix} \mathcal{U}_{K+1}^{L} \\ \Theta_{K+1}^{L} \end{pmatrix} - \begin{pmatrix} c_{11}^{L} & c_{12}^{L} \\ c_{21}^{L} & c_{22}^{L} \end{pmatrix}\begin{pmatrix} \mathcal{U}_{K+1}^{L-1} \\ \Theta_{K+1}^{L-1} \end{pmatrix} = \tag{4-6}$$

$$= \begin{pmatrix} d_1^{L} \\ d_2^{L} \end{pmatrix} \qquad , \; L = 2, 3, 4, \ldots, L_{max} - 1$$

where the matrix coefficients (given in detail in Appendix C) depend only on known conditions at K . Richtmeyer and Morton show that the solution of these equations can be found if it is assumed that the solution follows the recursion

$$\begin{pmatrix} \mathcal{U}_{K+1}^{L} \\ \Theta_{K+1}^{L} \end{pmatrix} = \begin{pmatrix} E_{11}^{L} & E_{12}^{L} \\ E_{21}^{L} & E_{22}^{L} \end{pmatrix}\begin{pmatrix} \mathcal{U}_{K+1}^{L+1} \\ \Theta_{K+1}^{L+1} \end{pmatrix} + \begin{pmatrix} f_1^{L} \\ f_2^{L} \end{pmatrix} \tag{4-7}$$

Values of the E and f matrices on the axis are found by rewriting the symmetry conditions there as:

$$\mathcal{U}_{K+1}^{1} = \mathcal{U}_{K+1}^{2} \qquad , \; \Theta_{K+1}^{1} = \Theta_{K+1}^{2} \tag{4-8}$$

This requires that

$$E_{11}^{1} = E_{22}^{1} = 1 \;\; ; \;\; E_{12}^{1} = E_{21}^{1} = f_1^{1} = f_2^{1} = 0 \tag{4-9}$$

Values of the E and f matrices at points off the axis can now be found, in the following way: Eq. (4-7), with L replaced by $L-1$, is used to eliminate $\mathcal{U}_{K+1}^{L-1}$ and Θ_{K+1}^{L-1} from Eq. (4-6), and the result is compared with the original form of Eq. (4-7). The result is the recursion formula (here the exponent -1 denotes matrix inversion):

$$\left(E_{ij}^{L}\right) = \left(\left(b_{ij}^{L}\right) - \left(c_{ij}^{L}\right)\left(E_{ij}^{L-1}\right)\right)^{-1}\left(a_{ij}\right)$$

(4-10)

$$\left(f_{i}^{L}\right) = \left(\left(b_{ij}^{L}\right) - \left(c_{ij}^{L}\right)\left(E_{ij}^{L-1}\right)\right)^{-1}\left(\left(c_{ij}^{L}\right)\left(f_{j}^{L-1}\right) + \left(d_{j}^{L}\right)\right)$$

The explicit formula for the inverse matrix used here is

$$\left(\left(b_{ij}^{L}\right) - \left(c_{ij}^{L}\right)\left(E_{ij}^{L-1}\right)\right)^{-1} =$$

$$\frac{\begin{pmatrix} b_{22}^{L} - c_{21}^{L} E_{12}^{L-1} - c_{22}^{L} E_{22}^{L-1} & -b_{12}^{L} + c_{11}^{L} E_{12}^{L-1} + c_{12}^{L} E_{22}^{L-1} \\ -b_{21}^{L} + c_{21}^{L} E_{11}^{L-1} + c_{22}^{L} E_{21}^{L-1} & b_{11}^{L} - c_{11}^{L} E_{11}^{L-1} - c_{12}^{L} E_{21}^{L-1} \end{pmatrix}}{\left\{\left[b_{11}^{L} - c_{11}^{L} E_{11}^{L-1} - c_{12}^{L} E_{21}^{L-1}\right]\left[b_{22}^{L} - c_{21}^{L} E_{12}^{L-1} - c_{22}^{L} E_{22}^{L-1}\right] - \left[b_{21}^{L} - c_{21}^{L} E_{11}^{L-1} - c_{22}^{L} E_{21}^{L-1}\right]\left[b_{12}^{L} - c_{11}^{L} E_{12}^{L-1} - c_{12}^{L} E_{22}^{L-1}\right]\right\}} \tag{4-11}$$

Once the matrix coefficients are known for $L = 1, 2, \ldots, L_{max} - 1$, the solution for $\mathcal{U}_{K+1}^{L}$ and Θ_{K+1}^{L} can be found from Eq. (4-7) by starting with their known wall values and working down to $L = 1$. The wall values are found by writing the boundary conditions (Eqs. (4-3) - (4-5)) as

$$\begin{pmatrix} \mathcal{U}_{K+1}^{L_{max}-1} \\ \Theta_{K+1}^{L_{max}-1} \end{pmatrix} = \begin{pmatrix} M_{11} & M_{12} \\ M_{21} & M_{22} \end{pmatrix} \begin{pmatrix} \mathcal{U}_{K+1}^{L_{max}} \\ \Theta_{K+1}^{L_{max}} \end{pmatrix} + \begin{pmatrix} n_1 \\ n_2 \end{pmatrix} \tag{4-12}$$

where

$$M_{11} = \frac{2}{K_1} + 1 \quad , \quad M_{12} = 0$$

$$n_1 = \mathcal{U}_K^{L_{max}} - \mathcal{U}_K^{L_{max}-1} \tag{4-13}$$

$$K_1 = \frac{\sqrt{\frac{2\gamma}{\gamma-1} \cdot \frac{\pi}{2}} \; \frac{2-\alpha_u}{\alpha_u} \cos\theta_w \left(\Theta_K^{L_{max}}\right)^{\omega+\frac{1}{2}}}{B\, P_{END}\, \sigma_{w,K+1}\, \Delta\eta}$$

and where, for an adiabatic wall,

$$M_{21} = -\frac{4 Pr}{K_1} \mathcal{U}_K^{L_{max}} \quad , \quad M_{22} = 1 \tag{4-14}$$

$$n_2 = \Theta_K^{L_{max}} - \Theta_K^{L_{max}-1}$$

When heat transfer is allowed, these are replaced by

$$M_{21} = 0 \quad , \quad M_{22} = \frac{2}{K_2} + 1$$

$$n_2 = -\frac{2}{K_2}\Theta_w(x_{K+1}) + \Theta_K^{L_{max}} - \Theta_K^{L_{max}-1} \tag{4-15}$$

$$K_2 = \frac{\sqrt{\frac{2\gamma}{\gamma-1} \cdot \frac{\pi}{2}} \; \frac{2-\alpha_T}{\alpha_T} \; \frac{2\gamma}{Pr(\gamma+1)} \cos\theta_w \left(\Theta_K^{L_{max}}\right)^{\omega+\frac{1}{2}}}{B\, P_{END}\, \sigma_{w,K+1}\, \Delta\eta}$$

Eq. (4-12) is now equated to Eq. (4-7), evaluated at $L = L_{max} - 1$; the solution is

$$\begin{pmatrix} U_{K+1}^{L_{max}} \\ \\ \Theta_{K+1}^{L_{max}} \end{pmatrix} = \begin{pmatrix} \left[EM_{22}\,FN_1 - EM_{12}\,FN_2\right] \Big/ \left[EM_{11}\,EM_{22} - EM_{21}\,EM_{12}\right] \\ \\ \left[-EM_{21}\,FN_1 + EM_{11}\,FN_2\right] \Big/ \left[EM_{11}\,EM_{22} - EM_{21}\,EM_{12}\right] \end{pmatrix}$$

(4-16)

where the EM and FN matrices are defined as

$$(EM) = \begin{pmatrix} E_{11}^{L_{max}-1} - M_{11} & E_{12}^{L_{max}-1} - M_{12} \\ \\ E_{21}^{L_{max}-1} - M_{21} & E_{22}^{L_{max}-1} - M_{22} \end{pmatrix}$$

(4-17)

$$(FN) = \begin{pmatrix} n_1 - f_1^{L_{max}-1} \\ \\ n_2 - f_2^{L_{max}-1} \end{pmatrix}$$

Iteration Methods for Finding dP/dx

This completes the formulas required to calculate the profiles at the end of the step, for a given value of dP/dx. This parameter must be chosen so as to satisfy the three global conservation relations given above, as well as the integrated streamtube-area relation. Since the two difference equations being used are local expressions for the conservation of momentum and energy, it might be expected that the best choice would be to use the value of dP/dx that satisfies either the total mass conservation or the integrated streamtube-area relation. The computer program uses both of these options; it has been found that solutions determined with either option also satisfy the total momentum and energy conservation. Furthermore, except in the near vicinity of the saddle point, solutions found with either option also satisfy the other option. Near the saddle point, it is more accurate to use the streamtube relation; in most of the solutions described here, the pressure gradient has been determined in such a way as to enforce mass conservation up to the saddle point, and such as to satisfy the streamtube relation downstream of the saddle point. The choice of which formula to use for dP/dx is made by selecting the input parameter XIPG . The mass-conservation formula is used (IPG = 4) for X < XIPG, and the streamtube relation (IPG = 1) for X > XIPG. Downstream of the saddle point, the streamtube relation is used.

The specific procedure used in enforcing mass conservation is as follows: a value of dP/dx is chosen, and the difference equations are solved for the profiles of $\mathcal{U}$ and Θ at station $K+1$. These profiles are then used in Eq. (3-26) to calculate the pressure at the end of the step:

$$\text{PNEW} = \left(\frac{A}{\sigma_w^2 \int_0^1 \frac{\mathcal{U}\, \eta\, d\eta}{\Theta}} \right)_{K+1} \tag{4-18}$$

where the integration is done by Simpson's rule. This pressure is compared with the value that would be found by extrapolating from the beginning of the step:

$$\text{PXTRAP} = P_K + \frac{dP}{dx}\Delta x \tag{4-19}$$

and the value of dP/dx is adjusted until these two pressures are equal. The adjustment of dP/dx is accomplished by an iteration process: at the beginning of the step, an iteration counter called ITER is set equal to 1, a first trial value of dP/dx , called PG1 , is used, and the difference between PNEW and PXTRAP is calculated. A second trial value of dP/dx , called PG2 and equal to 1.01 PG1 , is then used, with ITER = 2 , and again the difference between the two pressures is calculated. A straight-line extrapolation is then used to determine a next guess at dP/dx , called PG , that should make the pressure difference zero:

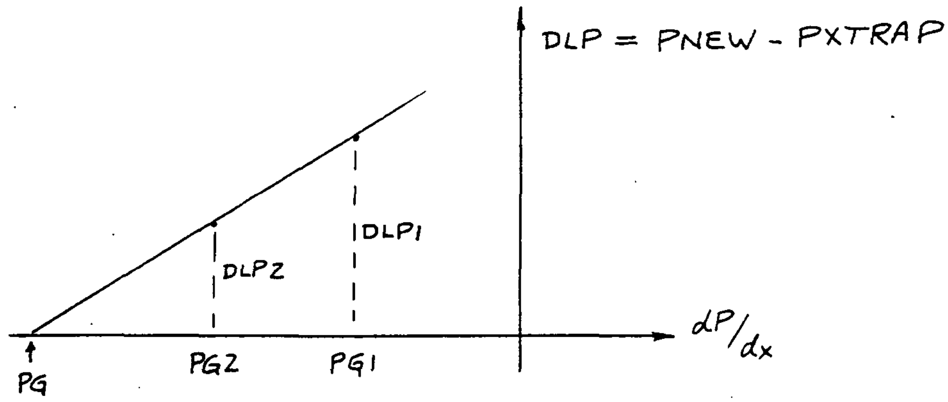

$$PG = \frac{PG1 \cdot PN2 - PG2 \cdot PN1 - P\,(PG1 - PG2)}{PN2 - PN1 + \Delta x \cdot (PG1 - PG2)} \qquad (4\text{-}20)$$

where PN1 and PN2 are the values of PNEW corresponding to the first and second iterations. A third calculation is then made, with dP/dx equal to PG , and ITER = 3 . The results of this third iteration are checked to determine whether the absolute value of PNEW - PXTRAP is less than 10^{-3} of the pressure at the beginning of the step. If it is not, the iteration counter is increased by 1, and a new trial value PG is calculated, using as base points for the straight line the iteration just completed, and the prior iteration that came closest to zeroing the quantity DLP . A maximum of ten iterations is allowed; convergence is usually attained on the third or fourth iteration.

The same procedure is followed when dP/dx is chosen so as to satisfy the streamtube-area relation. On the first two iterations, dP/dx is set equal to PG1 and PG2 , the right-hand side of Eq. (3-34) is calculated, and called PGNP1 :

$$PGNPI = {}^{DPNUM}\Big/ (AMM2AV - 0.5)\,\bar{\tau}_w \tag{4-21}$$

where

$$\bar{\tau}_w = \tau_w \Big|_{x = x_K + \frac{\Delta x}{2}} \tag{4-22}$$

$$AMM2AV = \frac{1}{2}\left\{ \left(\int_0^1 \frac{\eta\, d\eta}{M^2} \right)_K + \left(\int_0^1 \frac{\eta\, d\eta}{M^2} \right)_{K+1} \right\} \tag{4-23}$$

$$DPNUM = ARCHI - SHERI - CONDI - GENRI \tag{4-24}$$

$$ARCHI = \gamma \left(P_K + \frac{\Delta x}{2} \cdot \frac{dP}{dx} \right) \cdot \frac{d\tau_w}{dx} \Big|_{x = x_K + \frac{\Delta x}{2}} \tag{4-25}$$

$$SHERI = \frac{-2\gamma}{(\gamma - 1) B \bar{\tau}_w} \int_0^1 \frac{\Theta_{K+1} \frac{\partial u}{\partial \eta} + \eta\,\omega \left(\Theta_{K+1}\right)^{\omega - 1} \frac{\partial \Theta}{\partial \eta} + \eta \left(\Theta_{K+1}\right)^{\omega} \frac{\partial^2 u}{\partial \eta^2}}{\left(\frac{M_K + M_{K+1}}{2} \right)^2}\, d\eta \tag{4-26}$$

$$CONDI = \frac{2\gamma}{(\gamma - 1) B \bar{\tau}_w Pr} \int_0^1 \frac{\frac{u_{K+1}}{\Theta_{K+1}} \left\{ \Theta_{K+1} \frac{\partial \Theta}{\partial \eta} + \eta\,\omega \left(\Theta_{K+1}\right)^{\omega - 1} \frac{\partial \Theta}{\partial \eta} + \eta \left(\Theta_{K+1}\right)^{\omega} \frac{\partial^2 \Theta}{\partial \eta^2}}{\left(\frac{M_K + M_{K+1}}{2} \right)^2}\, d\eta \tag{4-27}$$

$$\text{GENRI} = \frac{2\gamma}{(\gamma-1)B\bar{\tau}_w}\int_0^1 \frac{2\eta\, u_{K+1}\left(\Theta_{K+1}\right)^{\omega-1}\left(\frac{\partial u}{\partial \eta}\right)^2}{\left(\frac{\mu_K + \mu_{K+1}}{2}\right)^2}\, d\eta \tag{4-28}$$

In these formulas, Simpson's rule was used, and derivatives were calculated by the formulas

$$\frac{\partial(\;)}{\partial\eta} = \frac{(\;)_K^{L+1} - (\;)_K^{L-1} + (\;)_{K+1}^{L+1} - (\;)_{K+1}^{L-1}}{4\Delta\eta} \tag{4-29}$$

$$\frac{\partial^2(\;)}{\partial\eta^2} = \frac{(\;)_K^{L+1} - 2(\;)_K^{L} + (\;)_K^{L-1} + (\;)_{K+1}^{L+1} - 2(\;)_{K+1}^{L} + (\;)_{K+1}^{L-1}}{2(\Delta\eta)^2} \tag{4-30}$$

The integrands for Simpson's rule were calculated as shown in the above formulas, except for the shear and conduction integral at the wall, where special formulas derived from the differential equations of motion were used, namely:

$$\frac{\partial}{\partial \eta}\left(\eta \Theta^{\omega} \frac{\partial \mathcal{U}}{\partial \eta}\right)\Bigg|_{\eta=1} =$$

$$B\left(\sigma_{w,K+1}\right)^2 \left\{ \frac{\gamma-1}{2\gamma}\frac{dP}{dx} + \frac{P_K + \frac{\Delta x}{2}\frac{dP}{dx}}{\Theta_K^{101}}\, \mathcal{U}_K^{101}\, \frac{\mathcal{U}_{K+1}^{101} - \mathcal{U}_K^{101}}{\Delta x} \right\}$$

$$\frac{\partial}{\partial \eta}\left(\frac{\eta \Theta^{\omega}}{P_r} \frac{\partial \Theta}{\partial \eta}\right)\Bigg|_{\eta=1} =$$

$$B\left(\sigma_{w,K+1}\right)^2 \left\{ -\frac{\gamma-1}{\gamma}\, \mathcal{U}_K^{101} \frac{dP}{dx} + \frac{P_K + \frac{\Delta x}{2}\frac{dP}{dx}}{\Theta_K^{101}}\, \mathcal{U}_K^{101}\, \frac{\Theta_{K+1}^{101} - \Theta_K^{101}}{\Delta x} \right\}$$

$$- 2\left(\Theta_K^{101}\right)^{\omega} \left\{ \frac{\mathcal{U}_K^{101} - \mathcal{U}_K^{100} + \mathcal{U}_{K+1}^{101} - \mathcal{U}_{K+1}^{100}}{2\Delta\eta} \right\}^2$$

It is clear that the averaging done in the above formulas could have been carried out in many other ways. No attempt has been made to determine the optimum choices.

After PGNP1 has been determined, the difference between PGNP1 and the value of dP/dx used in calculating it is found, and the results of the first two calculations are used as the basis for a straight-line estimate for the next iteration:

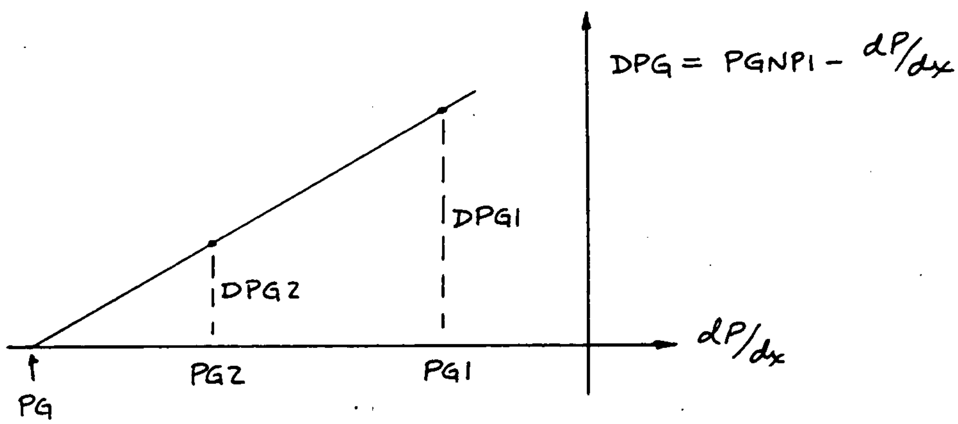

$$PG = \frac{PG1 \cdot DPG2 - PG2 \cdot DPG1}{DPG2 - DPG1} \tag{4-31}$$

The solution for this third iteration is checked to determine whether DPG is less than 10^{-3} times the value of dP/dx at the previous step. If it is not, the iteration counter is increased by one, the formula above is used to calculate a new trial value of PG, using as base points the trial just completed and the prior iteration with the least absolute value of DPG. A maximum of ten iterations is allowed.

In general, the values of dP/dx that zero the quantities DLP and DPG are different. When using either of the formulas, the mismatch in the other quantity (DLP/P_K or $DPG/(dP/dx)_K$) is typically the order of one percent, for values of $\Delta x = 0.1$.

Radial Velocity Calculation

During each iteration, with either of the pressure-gradient algorithms, the radial velocity is calculated by the finite-difference approximation of Eq. (3-25):

$$\frac{\eta W^L_{K+1}}{\sigma_{w,K+1}\, \Theta^L_{K+1} \left(\int_0^\eta \frac{U\eta\, d\eta}{\Theta} \right)_{K+1}} = \frac{1}{\Delta x} \ln \frac{\left(P\sigma_w^2 \int_0^\eta \frac{U\eta\, d\eta}{\Theta} \right)_K}{\left(P\sigma_w^2 \int_0^\eta \frac{U\eta\, d\eta}{\Theta} \right)_{K+1}} \tag{4-32}$$

The actual values of W used in advancing the solution from one step to the next were taken as the average of these values and those of the previous station:

$$W(L) = \frac{1}{2}\left(W_K^L + W_{K+1}^L\right) \tag{4-33}$$

Until the iteration on dP/dx is completed, these values are temporarily stored in the E12 array. This averaging was done in an effort to be consistent with the Crank-Nicholson averaging used in finding U ; an earlier version of the computer program which did not use this averaging for W sometimes developed divergent oscillations in dP/dx for mass flows near the critical value.

At the beginning of the iterations at each step, the initial guess (PG1) used for dP/dx was taken as the previous value of dP/dx, multiplied by the ratio of the two previous values:

$$PG1 = DPLAST \cdot PGRT$$

$$DPLAST = \left.\frac{dP}{dx}\right)_{x_{K-1} < x < x_K}, \quad PGRT = \frac{\left(\frac{dP}{dx}\right)_{x_{K-1} < x < x_K}}{\left(\frac{dP}{dx}\right)_{x_{K-2} < x < x_{K-1}}} \tag{4-34}$$

The pressure-gradient ratio PGRT is set equal to 1 at the initial station.

Determination of the Mass Flow

Once conditions at the initial station are provided, the procedure described above can be used to find the solution for a given mass flow, given Reynolds number, given nozzle geometry and wall-temperature distribution, and given gas properties. As the solution proceeds toward the throat, dP/dx becomes more and more negative; usually it reaches a minimum value very near to the throat, and subsequently increases (i. e., becomes less negative) downstream of the throat. Following this, either of two types of behavior is usually observed: in the first, dP/dx continues to increase, and eventually passes through zero, denoting a minimum in the pressure. This corresponds to a change of sign of the numerator of Eq. (3-34), and indicates that the mass flow being used is less than critical - i. e., it is associated with a generally subsonic flow.

In the second type of solution, which occurs at higher mass flows, dP/dx begins to become more and negative, until a station is reached at which there is no solution that will match PNEW and PXTRAP or the left and right sides of Eq. (3-34). This condition corresponds to a change of sign of the denominator of Eq. (3-34), and indicates that the flow has choked - i. e., the negative pressure gradient required for the specified mass flow is essentially infinite.

In general, it would be expected that some intermediate mass flow could be found, for which the numerator and denominator change sign at the same point. Of course, it is extremely unlikely that the numerical solution would pass smoothly through this saddle point, and it is necessary to force the solution through, once the mass flow has been found to a suitable accuracy. The means of carrying the solution through the saddle point is described later; for the moment, it remains to describe the logic used in determining the critical mass flow.

For this purpose, an iteration on the value of A is performed; an upper and lower bound for the mass flow (called $A1$ and $A0$ respectively) are specified as input data, and the first solution is calculated for a value of A halfway between these bounds. When this solution displays one of the two types of behavior described above - i. e., when its mass flow has been identified as either subcritical or supercritical, then its value of A is used as a new lower or upper bound, and a new solution is calculated for a value of A halfway between the (updated) lower and upper bound. This iteration process is continued until the difference between the lower and upper bounds is less than an input value called ATEST. When this condition is met, the indicator IGOTA is set equal to 1, and a final solution pass is calculated.

The symptoms that are used to detect whether a given mass flow is subcritical or supercritical are as follows: The mass flow is declared to be subcritical if dP/dx becomes positive, and supercritical if any of these four conditions occur

1. more than ten iterations are used in finding dP/dx
2. the integral $\int_0^1 \frac{\eta\, d\eta}{M^2}$ falls below 0. 5
3. if dP/dx , having passed its first minimum near the throat, turns more negative for 3 consecutive steps
4. if P falls below 0. 1 upstream of the minimum in dP/dx

The third and fourth of these conditions involve the indicator IXSTAR ; which is equal to 1 upstream of the minimum in dP/dx , and is set equal to 2 downstream of this minimum. The test to determine whether IXSTAR should be changed from 1 to 2 is not applied until after 5 steps have been taken, since occasionally some slight oscillations in dP/dx occur near the initial station.

In cases where ten iterations on dP/dx are exceeded, it usually happens that the curve of DLP versus dP/dx has no zero:

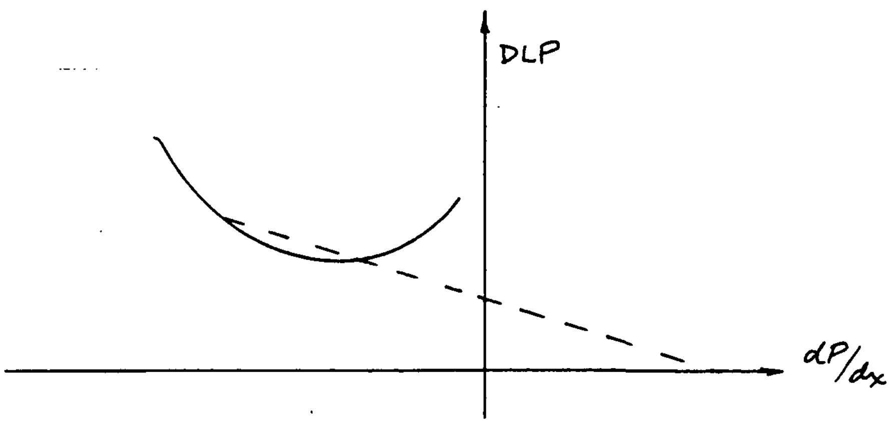

In such cases, the trial values assigned by Eq. (4-20) for some of the iterations may become large positive numbers, as indicated in the sketch above. But large positive values of dP/dx can produce reverse flow near the wall, which cannot be allowed, by the parabolic nature of the slender-channel equations. To avoid this possibility, the pressure gradient is restricted to values less than +1. If any of the trial values exceed this limit, they are reduced by a factor 10^{-3}, and are simply allowed to count as another iteration.

Passage through the Saddle Point

The procedures described above are used repetitively, until the mass-flow parameter A has been determined to within the preassigned accuracy ATEST . The indicator IGOTA is then set equal to 1, and a final pass is made. This integration is interrupted slightly upstream of the saddle point, and the pressure-gradient distribution is then chosen so as to force the solution to lie along a straight line through the saddle point, in the plane of the numerator and denominator of Eq. (3-34). As soon as this fitted portion of the solution passes through the saddle point, the iterative solution for dP/dx (satisfying the streamtube relation) is resumed.

The point at which the solution is interrupted is determined in the following way: if the solutions for various mass flows are plotted in the plane of DPNUM vs AMM2 (except for a factor $\bar{\sigma}_w$, this is essentially the plane of the numerator and denominator of the streamtube relation, and is referred to hereafter as "the saddle-point plane"), their behavior is

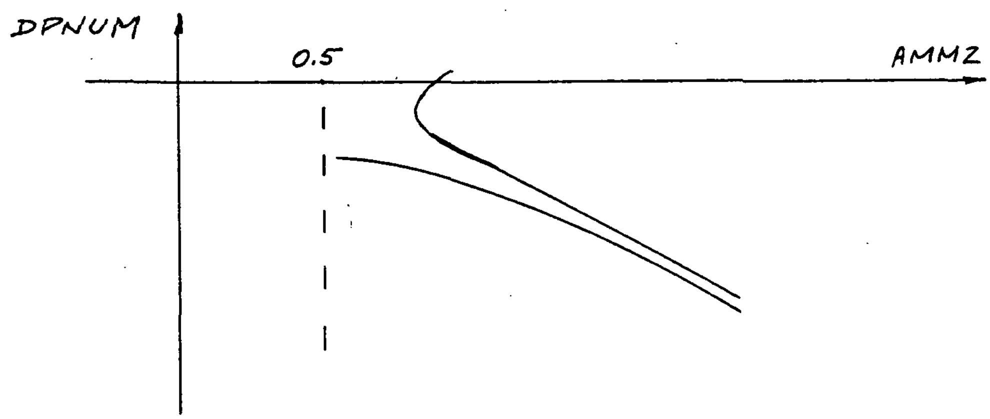

The solution for the final value of A will be one or the other of these two types. If it is supercritical, it should be interrupted at or near the point where supercritical behavior was detected on the previous pass that set the upper bound $A1$. This is accomplished by the quantity XCUT . Whenever supercritical behavior is found, XCUT is set equal to the value of x one step upstream. On the final solution, the straight-line passage through the saddle point is initiated as soon as x passes XCUT .

If the final solution is of the subcritical type, it should be interrupted when the quantity AMM2 reaches its minimum. It has been observed on runs with wall cooling (in particular, case 12 of Section 6) that local minima can occur far upstream of the saddle point. To discriminate against this possibility, the program as presently written will interpret a minimum in AMM2 as indicative of nearness to the saddle point only if it occurs for $x > -0.5$.

When either of these conditions is met, the indicator IPG is set equal to 2, and a straight line is fitted between the point just calculated (AMM21, DPNM1) and the saddle point (0.5, 0)

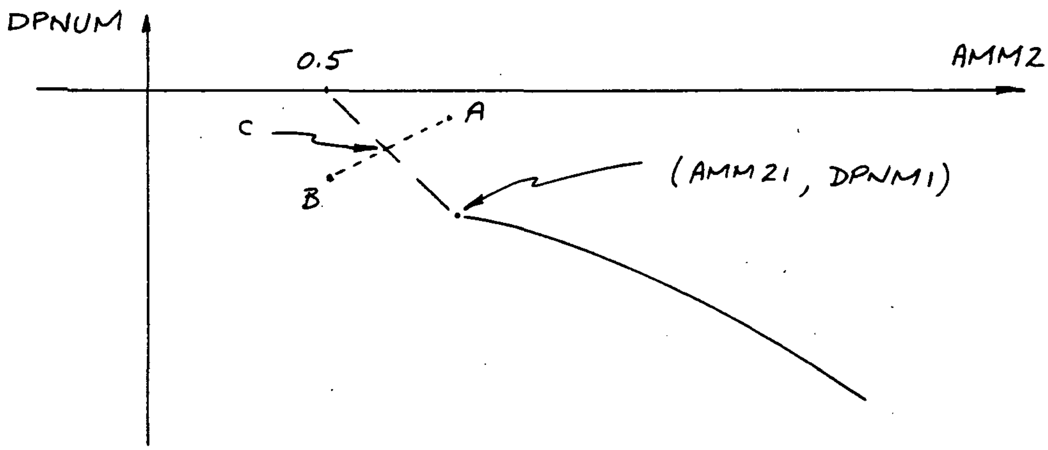

$$\frac{DPNUM - DPNM1}{-DPNM1} = \frac{AMM2 - AMM21}{0.5 - AMM21} \tag{4-35}$$

At a given value of x, it is true to a good approximation that DPNUM and AMM2 are linear functions of the trial values of dP/dx, and hence of each other. If point A locates the coordinates of the first iteration (DPDX = PG1) and point B the second (DPDX = PG2), then a straight line connecting these points is

$$\frac{DPNUM - DPNUMA}{DPNUMB - DPNUMA} = \frac{AMM2 - AMM2A}{AMM2B - AMM2A} \tag{4-36}$$

The intersection of this line with the straight line through the saddle point occurs at point C, where the value of AMM2 is

$$AMM2C =$$

$$= \frac{DPNM1 - DPNUMA + \dfrac{DPNM1 \cdot AMM21}{0.5 - AMM21} + \dfrac{(DPNUMB - DPNUMA) \cdot AMM2A}{AMM2B - AMM2A}}{\dfrac{DPNUMB - DPNUMA}{AMM2B - AMM2A} + \dfrac{DPNM1}{0.5 - AMM21}} \quad (4\text{-}37)$$

To the extent that these quantities are linear with dP/dx, the value of dP/dx associated with point C would be

$$DPDXC = \frac{PG1 \cdot (AMM2B - AMM2C) + PG2 \cdot (AMM2C - AMM2A)}{AMM2B - AMM2A} \quad (4\text{-}38)$$

This value is used for the third iteration, and it has been found that the resulting solution lies sufficiently close to the straight line through the saddle point that no further iterations are necessary.

This three-step placement of the solution is continued until it passes through the saddle point, after which an iterative solution of the streamtube relation is resumed. This could be accomplished by setting IPG equal to 3; however, it has been found that the rate of convergence of the iterations at this first station downstream of the saddle point is improved if the following procedure is followed: the indicator ISW is set equal to 2, and the first two iterations (points A and B) are calculated. Then IPG is set equal to 3, and the value of dP/dx to be used on the third iteration is found by solving the quadratic equation that follows from the (roughly) linear dependence of AMM2 and DPNUM on dP/dx - i. e., since

$$DPNUM = BR11 \cdot DPDX + BR12$$

(4-39)

and

$$AMM2 = BR21 \cdot DPDX + BR22$$

where

$$BR11 = \frac{DPNUMB - DPNUMA}{PG2 - PG1}, \quad BR12 = -BR11 \cdot PG1 + DPNUMA$$

$$BR21 = \frac{AMM2B - AMM2A}{PG2 - PG1}, \quad BR22 = -BR21 \cdot PG1 + AMM2A \tag{4-40}$$

it follows that the streamtube relation can be approximated by

$$\frac{dP}{dx} = \frac{BR11 \cdot \frac{dP}{dx} + BR12}{\bar{\sigma}_w \left[\frac{AM2LST}{2} + \frac{BR21}{2}\frac{dP}{dx} + \frac{BR22}{2} - \frac{1}{2} \right]}$$

The solution of this equation is

$$\frac{dP}{dx} = \frac{-BRB - \sqrt{(BRB)^2 + 8 \cdot BR21 \cdot BR12 \cdot \bar{\sigma}_w}}{2\bar{\sigma}_w \cdot BR21} \tag{4-41}$$

where

$$BRB = \bar{\sigma}_w \left(AM2LST + BR22 - 1 \right) - 2\, BR11 \tag{4-42}$$

This quadratic solution could in fact be used throughout the program, in place of the straight-line extrapolation presently incorporated. It is not clear how much of a saving in time could be achieved by doing so; however, at the first station downstream of the saddle point, there are instances where ten iterations would not be enough for convergence of the solution if the more nearly correct location of the solution were not determined by the quadratic formula very early in the iterations.

Once the solution has converged downstream of the saddle point, the integration continues until the maximum X -location (XMAX) is passed.

5. INITIAL CONDITIONS

In order to start the calculation method described in the previous section, it is necessary to specify a value of P, and profiles of $\mathcal{U}$ and Θ, at some initial station. In applications of thin-boundary-layer theory to the present problem, this initial station is usually taken at the geometric throat of the nozzle; there the boundary layer is assumed to have zero thickness, and the pressure, velocity, and enthalpy are assumed equal to the values they would have in an isentropic, inviscid, one-dimensional channel flow.

In the present study, where results are sought at very low Reynolds numbers, this approximation is not acceptable; instead, the solution must be started far upstream of the throat. Asymptotic solutions of the slender-channel equations for slow flow in a converging cone were derived for this purpose. Analogous solutions of the Navier-Stokes equations for incompressible flow have been presented by Ackerberg.[100]

The initial solution was derived by expanding all of the dependent variables in inverse powers of the nozzle radius:

$$P = 1 + \sum_{N=3} \frac{\pi_N}{\sigma_w^{\,N}} \quad , \quad \Theta = 1 + \sum_{N=4} \frac{T_N(\eta)}{\sigma_w^{\,N}}$$

$$\mathcal{U} = \sum_{N=2} \frac{\mathcal{U}_N(\eta)}{\sigma_w^{\,N}} \quad , \quad W = \sum_{N=3} \frac{W_N(\eta)}{\sigma_w^{\,N}} \qquad (5\text{-}1)$$

The expansion for $\mathcal{U}$ begins with $N = 2$, since any contributions from lower values of N would not satisfy mass conservation (see Eq. (3-26)). If this term is then substituted into the continuity and momentum equations, it is found that the first nonzero coefficients in the expansions of P and W are π_3 and $W_3(\eta)$. The fact that $W_2(\eta) = 0$ implies that the flow resembles a conical sink flow in the leading approximation:

$$\frac{V_2(\eta)}{\mathcal{U}_2(\eta)} = \eta \frac{d\sigma_w}{dx} + O(\sigma_w^{-3})$$

Finally, substitution of these expressions into the energy equation reveals that $T_4(\eta)$ is the first nonzero coefficient in the enthalpy expansion.

When the boundary conditions are expanded in powers of σ_w^{-1}, the first few velocity terms are found to satisfy:

$$\mathcal{U}_2(1) = 0 \, , \quad \mathcal{U}_{N+1}(1) = -K_u \, \mathcal{U}_N'(1) \, , \; N = 2, 3, 4.$$

where

$$K_u = \sqrt{\frac{2\gamma}{\gamma - 1} \cdot \frac{\pi}{2}} \; \frac{2 - \alpha_u}{\alpha_u} \; \frac{\cos\theta_w}{B} \qquad (5\text{-}2)$$

The first term in the expansion of the enthalpy profile must satisfy either $T_4(1) = 0$ if heat transfer is allowed, or $T_4'(1) = 0$ if there is no heat transfer.

The ordinary differential equations for $\mathcal{U}_N(\eta)$ and $T_N(\eta)$ can be integrated explicitly.* The resulting expressions contain as parameters the coefficients π_N ; these latter quantities are found in terms of the given mass flow from the expansion of Eq. (3-26), i. e.:

$$A\left(1 - \frac{\pi_3}{\sigma_w^{3}} + \cdots\right) = \qquad (5\text{-}3)$$

$$= \sigma_w^{2} \int_0^1 \left(\frac{\mathcal{U}_2}{\sigma_w^{2}} + \frac{\mathcal{U}_3}{\sigma_w^{3}} + \cdots\right) \eta \, d\eta$$

*These equations are presented in detail in Appendix D.

or

$$\int_0^1 \mathcal{U}_2\, \eta \, d\eta = A \qquad , \int_0^1 \mathcal{U}_3\, \eta \, d\eta = 0$$

$$\int_0^1 \mathcal{U}_4\, \eta \, d\eta = 0 \qquad , \int_0^1 \mathcal{U}_5\, \eta \, d\eta = -A\pi_3$$

The results for the first few terms are

$$\mathcal{U}_2(\eta) = 4A(1-\eta^2)$$

$$\mathcal{U}_3(\eta) = A^2 B \tan\theta_w \left[4(\eta^4-\eta^2) + \frac{8}{9}(1-\eta^6)\right]$$

$$+ 8AK_u(2\eta^2-1)$$

$$W_3(\eta) = A^2 B \tan^2\theta_w \left[\frac{4}{9}\eta - \eta^3 + \frac{2}{3}\eta^5 - \frac{\eta^7}{9}\right] \tag{5-4}$$

$$+ 4A\tan\theta_w K_u(\eta^3-\eta)$$

$$T_4(\eta) = -16A^2 Br (1-\eta^2)^2$$

$$\pi_3 = \frac{32\gamma}{3(\gamma-1)} \cdot \frac{A}{B\tan\theta_w}$$

$$\pi_4 = \frac{-8\gamma}{(\gamma-1)B\tan\theta_w}\left[A^2 B\tan\theta_w + 4AK_u\right]$$

Further terms are given in Appendix D. The above result for $T_4(\eta)$ is valid for either thermal condition of the wall.

Simplified Initial Conditions

It is desirable to specify the initial conditions to a level of accuracy that is commensurate with the accuracy of the finite-difference scheme. From an inspection of Eq. (5-3), the indication is that mass conservation requires the $\mathcal{U}$ -profile to be specified through order σ_w^{-5} and the pressure through order σ_w^{-3}. When this was done in an early version of the computer program, however, it was found that the higher-order contributions were masked by the truncation error in the finite-difference results - i. e., if dP/dx is specified through order σ_w^{-3}, a Simpson's-rule integration of the resulting $\mathcal{U}$ -profile at $x + \Delta x$ is in general different from the right side of Eq. (5-3) by an amount of order greater than σ_w^{-5}. For this reason, the iterative method of finding dP/dx, described in Section 4, was chosen. This has the effect of doing numerically to dP/dx what the series coefficients π_ν would do analytically. In this method, the series solution is used only to give the starting profiles, and an initial guess at dP/dx.

To be consistent with this procedure, the starting conditions were simplified to

$$\mathcal{U} = \frac{\mathcal{U}_2(\eta)}{\sigma_w^2} + \frac{\mathcal{U}_3(1)}{\sigma_w^3} = \frac{4A(1-\eta^2)}{\sigma_w^2} + \frac{8AK_u}{\sigma_w^3}$$

$$\Theta = 1 + \frac{T_4(\eta)}{\sigma_w^4} \quad , \quad P = \frac{1}{1 - \dfrac{\pi_3}{\sigma_w^3}} \tag{5-5}$$

$$\frac{dP}{dx} = - \frac{3\pi_3 \, \sigma_w'}{\sigma_w^4}$$

This approximate velocity profile fails to conserve mass at the initial station; the error introduced is typically less than one percent.

For all of the solutions presented in this paper, the initial station was chosen as $X_o = -5$.

6. RESULTS

In the subsections that follow, the nozzle geometry used is described first; following this, the general features of the flow fields found by changing various parameters are described. Results that relate specifically to performance characteristics (mass flow, thrust, specific impulse) are deferred to the end of this section.

Geometry

The particular geometrical configuration used in the present study consisted of a convergent cone and a divergent cone, connected by a constant radius-of-curvature-section:

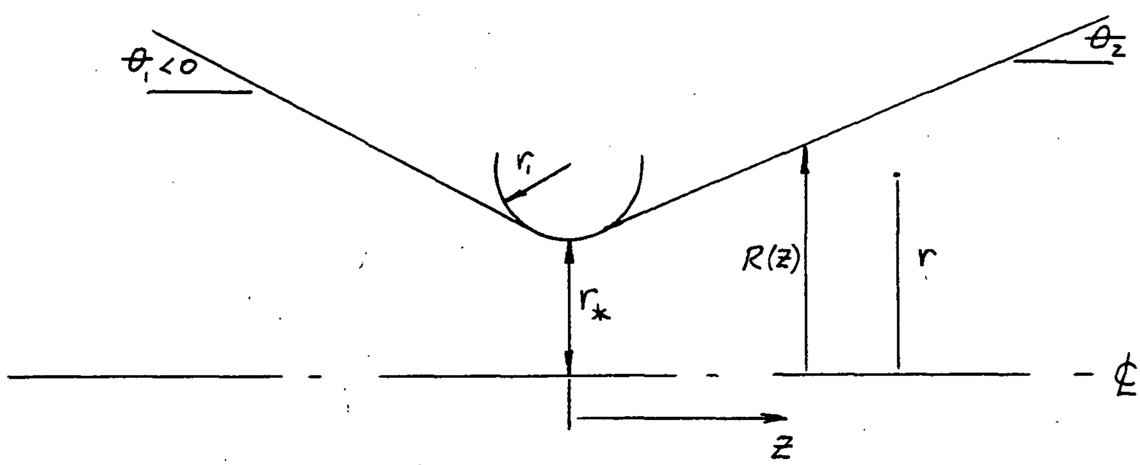

The coordinates are given by

$$x \leq R_1 \sin \theta_1 :$$

$$\sigma_w = x \tan \theta_1 + 1 + R_1 (1 - \cos \theta_1 - \sin \theta_1 \tan \theta_1)$$

$$\sigma_w' = \tan \theta_1$$

$R_1 \sin\theta_1 \leqslant x \leqslant R_1 \sin\theta_2$:

$$\sigma_w = 1 + R_1 - \sqrt{R_1^2 - x^2}$$

$$\sigma_w' = x \Big/ \sqrt{R_1^2 - x^2} \qquad (6\text{-}1)$$

$x \geqslant R_1 \sin\theta_2$:

$$\sigma_w = x \tan\theta_2 + 1 + R_1 \left(1 - \cos\theta_2 - \sin\theta_2 \tan\theta_2\right)$$

$$\sigma_w' = \tan\theta_2$$

where

$$R_1 \equiv r_1 / r_*$$

This geometry is built into the program as a subroutine. Other geometrical configurations could be studied without difficulty.

Cases Studied

The computer program described earlier has been used to investigate the effects of varying some of the parameters of the problem. Table 1 lists the values used for the various parameters. For all cases, the values $\gamma = 1.4$, $Pr = 0.75$, $\omega = 0.9$, $\alpha_u = \alpha_T = 1.0$ were used. In general, a step size of $\Delta x = 0.1$ was used; however, for runs with the sharp throat ($R_1 = 0.5$), it was reduced to $\Delta x = 0.01$ in the region $-0.3 \leqslant x \leqslant +0.3$. The calculations were performed on an IBM 360, Model 65, in double precision. The program listed below is written in single precision, and check runs have shown that the results are essentially unchanged. A typical case, where the mass flow is unknown to plus or minus

20 percent (i. e., ΔA originally is the order of 0.04) takes between 5 and 10 minutes, depending on the step size and the amount of output desired.

Comparison with Experiment

Case 1 provides a direct comparison with the experimental data reported by Yevseyev,[68] who carried out a very detailed probing of the low-density flow in a conical nozzle. Results for the centerline Mach number (taken from Yevseyev's Fig. 8) are presented in Fig. 1; the present calculation is 6 percent high at $X = 6$, and about 3 percent low at $X = 15$. A more stringent test of the calculational method is shown in Fig. 2 where the measured and calculated velocity profiles at $X = 11.1$ (see Yevseyev's Fig. 7) show excellent agreement.

It should be emphasized that the calculations shown contain no approximations beyond those implicit in the use of the slender-channel equations; they constitute the solution of the direct problem, for a specified nozzle geometry and a specified set of reservoir conditions. No attempt has been made to improve the agreement by varying the gas-property parameters.

Effects of Upstream Geometry

Cases 2 and 3 are identical except for the value of the inlet angle; the results of these two runs are indistinguishable for $X \geq 0$, and were taken as evidence that the upstream geometry has little effect on the flow. Obviously, much more evidence is needed before the quantitative limitations of this statement are clear, but it was felt that exploration of this effect could be deferred until after the variation of other parameters had been studied; all of the other cases described here used $\theta_1 = -20°$.

Effect of Reynolds Number

Cases 2, 4, and 5 show the effect of the Reynolds number. Before discussing this effect specifically, it is well to examine how the iteration process led to determination of the eigensolution. For case 2, Fig. 3 shows the variation of P with X at various values of the mass flow; these exhibit the two types of behavior described earlier. This behavior is shown more clearly in Fig. 4, which is the saddle-point plane. After the iterations shown had been completed, the value $A = 0.121$ was selected as the eigenvalue of A, and this solution was interrupted at $x = 0$; it was then placed on a straight line through the saddle point, as shown in Fig. 4. The result of this fitting is shown in the P, x plane in Fig. 3. Note that the saddle point is crossed about one radius downstream of the throat; thereafter, the iterative method of finding dP/dx is resumed, and continues to run stably.

An isometric view of the velocity and enthalpy profiles at various positions along the nozzle is shown in Fig. 5.

Lowering the Reynolds number B to 800 has the effect of moving the saddle point slightly farther downstream (case 4), and a further reduction to $B = 400$ moves it out beyond twenty radii (case 5). For this case, the solution in the plane of Fig. 4 moves along the straight-line segment toward the saddle point, but never reaches it.

Effect of Exit-Cone Angle

Cases 4, 6, 7, 8, and 9 show the effect of changing the angle θ_2, at a constant Reynolds number $B = 800$. Reducing this angle inhibits the expansion to supersonic conditions, and so has the same effect as lowering B. As θ_2 becomes smaller, the saddle point moves farther down the nozzle, passing beyond twenty radii for $\theta_2 \leq 18°$. There is obviously a range of expansion angles and Reynolds numbers for which there is no unique supersonic solution of the problem determined by passage through the singular point.

Extended Study of the Nonsingular-Solution Region

The conditions of case 10 lie well within the region where there is no saddle point. A large number of computer runs was made for this case, and the resulting pressure distributions along the nozzle are shown in Fig. 6. At the lowest value of the mass flow ($A = 0.04$), dP/dx is negative out to forty radii; at somewhat higher mass flows, the pressure reaches a minimum, and then rises slightly as the flow continues to decelerate. Ultimately a pressure maximum is reached, and the final state of the flow is a Poiseuille velocity profile, with the static enthalpy uniformly equal to its wall value.

For sufficiently high mass flows, a choking condition is encountered; however, in contrast to the higher Reynolds number, higher θ_z cases, the locus of zero pressure gradients does not intersect with the locus of infinite pressure gradients. The solution for A = 0.08764252 extends all the way to forty radii with dP/dx negative. Figure 6 shows this solution passing between the loci of the zero- and infinite-slope points.

For values of A greater than about 0.086, these solutions exhibit a zone of supersonic flow near the axis, and slightly downstream of the throat. Contours of constant Mach number are shown in Fig. 7 for the case A = 0.08764252. A smooth transition from supersonic back to subsonic conditions is predicted. This type of transition is possible within the framework of the slender-channel equations, where the axial gradients in the stress tensor (which could give rise to a shock-wave type of transition) have been neglected in comparison with transverse shear stresses. The Mach number distribution along these streamlines is analogous to that of a streamline entering the boundary layer on a flat plate in a supersonic flow; the Mach number decays below one as the streamline is carried deeper into the slower part of the boundary layer.

Figure 7 also shows the locus where the axial velocity reaches 99 percent of its centerline value. This locus shows how the boundary layer essentially closes on this flow. In all of these flows, the decreasing pressure generates two opposing effects: the first, appearing in the inviscid terms of the streamtube relation, is to accelerate the flow to a supersonic state. The opposing effect, appearing in the viscous terms, is to thicken the boundary layer. The conditions of case 10 lie in a region where the latter effect dominates the former; no acceleration to a permanent supersonic state is possible within the framework of the slender-channnel equations, and the flow undergoes a transition back to subsonic conditions.

Whether a smooth transition of this type is realized experimentally is, to the author's knowledge, an open question. Measurements aimed at resolving this problem are needed; in addition, further analysis in which the longitudinal stress contributions are retained would be very useful.

The precise boundary above which a unique supersonic solution can be found has not yet been adequately determined; the present results suggest that this will be the state of the flow if $\mathcal{B}$ is greater than 800 and $-\theta_2$ is greater than about 20°. This value of $\mathcal{B}$ corresponds to a throat Reynolds number around 300; using Sutherland and Maes' rule of thumb (see Ref. 1, p. 1160), this corresponds to a thrust level in the vicinity of 10^{-4} lbf for a typical nozzle size.

It is interesting to note that the range of $\mathcal{B}$ below which no supersonic solution was found corresponds roughly with Smetana's estimate[20] of the Reynolds number at which the boundary layer fills the throat. Assuming that the displacement thickness is 0.27 times the velocity boundary-layer thickness when this occurs, Smetana derives the following formula for the Reynolds number at which the boundary layer closes

$$\frac{\rho_* u_* \cdot 2 r_*}{\mu_o} = \left(\mathcal{B}_{SM} \frac{0.65}{0.35} \right)^2$$

For the constant $\mathcal{B}_{SM}$, he recommends a value on the order of 4. In the present notation, his result is

$$\frac{\rho_o \sqrt{2H_o}\; r_*}{\mu_o} = \frac{\rho_o}{\rho_*} \cdot \frac{\sqrt{2H_o}}{u_*} \cdot \frac{1}{2} \left(\mathcal{B}_{SM} \frac{0.65}{0.35} \right)^2$$

Approximating the density and velocity ratios by their isentropic-flow values for $\gamma = 1.4$, this becomes

$$\frac{\rho_o \sqrt{2H_o}\; r_*}{\mu_o} = \frac{1}{0.634} \cdot \frac{1}{0.408} \cdot \frac{1}{2} \left(\mathcal{B}_{SM} \frac{0.65}{0.35} \right)^2 = 6.67\, \mathcal{B}_{SM}^2$$

Smetana's value of $\mathcal{B}_{SM} = 4$ corresponds to $\mathcal{B} \approx 110$, while a value $\mathcal{B}_{SM} \approx 9$ would recover the present result $\mathcal{B} \approx 600$. A larger value of $\mathcal{B}_{SM}$ is probably more correct for the present configuration, which has a longer entrance than the one used in Smetana's analysis.

Even if these predictions of an imbedded supersonic zone are accepted as having physical significance, there still remains a problem of predicting nozzle performance when the pressure imposed at the exit plane is extremely low. Figure 8 shows the slender-channel prediction of mass flow as a function of exit-plane pressure, if the nozzle is cut off at $x = 40$. The point to be noted is that no solutions were found for which p_e/p_o was less than around 0.09. It seems probable that for values of A between 0.08764252 and 0.08764343, solutions could be found in which choking occurs arbitrarily far downstream. However, it may be that some mechanisms which are not included in the slender-channel equations must be invoked in order to predict how the flow adjusts to the exit conditions encountered in the space environment.

Effect of Exit-Plane Pressure

The fact that large subsonic regions are predicted suggests that a strong upstream influence of the exit-plane conditions may exist under certain conditions. In an earlier publication of the present results,[101] the speculation was advanced that this mechanism might explain the anomalous effect of the exit-plane pressure reported by several authors.[57, 58, 102] Further evidence has since suggested that this mechanism does not explain the observations when the flow has a supersonic core; whether it plays a role at the lower Reynolds numbers, where the slender-channel equations have no solutions with a supersonic core, remains to be determined.

The principal item of new evidence is the observation, by the group at AVCO,* that experimental arrangements in the test cell can affect the measured thrust if the cell pressure is greater than 10^{-4} torr. Values in

---

*Private communication from R. R. John and Walter Davis, July 8, 1969.

this range have previously been recommended as the maximum desirable cell pressure in all three of the references cited above; the more recent AVCO observations appear to be the first in which it is clearly shown that different arrangements of the same equipment will indicate different thrust levels at cell pressures in excess of 10^{-4} torr.

A second item of new evidence is that calculations made with the present computer program for one of the experiments reported in Ref. 102 show good agreement with the measured performance at low cell pressure. The calculations were done for the parameter values listed in Table 1 as case 13, and were intended to duplicate the conditions of Fig. 9 of Ref. 102. The mass-flow result $\mathcal{A} = 0.118$ corresponds to 1.577×10^{-5} lbm/sec. The thrust coefficient (with no correction due to ambient pressure) was calculated as 1.437 at $x = 11.0$ (A/A_* = 34.10). This corresponds to a thrust level of 11.12×10^{-3} lbf, and a specific impulse of 705 sec. The latter result agrees quite well with the line marked "theoretical performance" in Fig. 9 of Ref. 102. Apparently, this performance prediction is based on experimental data, and includes the effect of viscosity.

Effects of Heat Transfer and Variable Wall Temperature

Operation of a rocket device at low density implies that the thermal condition of the wall can exert a strong influence. Two cases were run in order to explore the effect of heat transfer on the flow. In the first of these (case 11) the wall temperature was equal to the reservoir temperature all along the nozzle. In the second (case 12), the wall temperature was dropped from T_o to $T_o/5$ between -4 and -2 radii, and was held constant thereafter:

$$
\begin{aligned}
\Theta_w &= 1.0 && , \quad -5 \leq x \leq -4 \\
&= 0.6 + 0.4 \cos\left[(x+4)\frac{\pi}{2}\right] && , \quad -4 \leq x \leq -2 \\
&= 0.2 && , \quad x \geq -2
\end{aligned}
$$

This latter case was an attempt to simulate the thermal environment that might be encountered when gas flows out of a hot reservoir and into a relatively cold channel. Cases 11 and 12 were the same as case 2 in all other respects.

The wall-temperature and heat-transfer distributions, and the variations of the total-enthalpy flux (which are related by Eq. (3-31)) are shown in Fig. 9, and typical profiles are given in Fig. 10. Profiles for the hot-wall case are practically identical to those of the adiabatic-wall case, but the cold-wall case shows marked differences. In particular, in the cold-wall case, about 20 percent of the enthalpy flux is lost in heat transfer to the wall. Also, the discharge coefficient is greater than one -- the nozzle can pass more mass flow than an isentropic, one-dimensional nozzle would, due to the elevated density level near the walls. The enthalpy profile in Fig. 10d has a slight bulge near the wall, typically of what happens in high Mach number flows due to viscous heating.

The computer program described in Appendix A permits a more general wall-temperature variation of this type, where the end-points of the cosine variation and the lower temperature level can be specified as inputs:

$$\begin{aligned}\Theta_w &= 1 \qquad\qquad , \; x \leq XTW1 \\ &= \frac{1+TW2}{2} + \frac{1-TW2}{2}\cos\left(\pi \cdot \frac{x - XTW1}{XTW2 - XTW1}\right), \; XTW1 \leq x \leq XTW2 \\ &= TW2 \qquad\qquad , \; x \geq XTW2 \qquad\qquad (6\text{-}2)\end{aligned}$$

A noticeable thinning of the boundary layer is apparent with the cold wall. Figure 11 shows the variation of the displacement thickness with distance along the nozzle, compared to the constant-wall-temperature case. The displacement thickness used here is defined by

$$\int_0^R \rho u r\,dr = \rho_{\mathfrak{c}} u_{\mathfrak{c}} \int_0^{R-\delta_1} r\,dr$$

or

$$\frac{\delta_1}{r_*} = \sigma_w \left[1 - \sqrt{2 \int_0^1 \frac{DU}{(DU)_{\mathfrak{c}}} \eta \, d\eta} \right] \tag{6-3}$$

Conditions on the axis can be calculated with an error of a few percent, by using the isentropic, one-dimensional flow results at an effective area ratio found by subtracting the displacement thickness:

$$\frac{A_{EFF}}{A_*} = \left(\sigma_w - \frac{\delta_1}{r_*} \right)^2 \tag{6-4}$$

Thus the present results provide a corroboration, without a priori assumptions, that the displacement thickness is indeed the correct scale to use in making boundary-layer corrections to the core flow.

Performance Characteristics

The thrust coefficients obtained from these calculations are shown in Fig. 12, as a function of geometric area ratio. (No correction has been made for any effects that might accompany the transition from conditions at the given area ratio to zero-pressure ambient conditions.) For comparison, the ideal value at the same area ratio is shown. These were calculated without any correction for divergence loss (see, for example, Ref. 103, p. 446):

$$\bar{\bar{F}} = \left\{ \frac{2\gamma^2}{\gamma-1}\left(\frac{2}{\gamma+1}\right)^{\frac{\gamma+1}{\gamma-1}} (1-P)^{\frac{\gamma-1}{\gamma}} \right\}^{1/2} + P\sigma_w^2 \tag{6-5}$$

The effect of increasing Reynolds number is to increase the thrust coefficient, as might be expected (cases 2 and 4). Increasing θ_{ξ} produced a slight increase in $\bar{\bar{F}}$ (cases 4, 6, and 7), indicating that thrust losses due to divergence were not yet dominant in the range shown here. Decreasing the longitudinal radius of curvature of the throat (cases 1 and 2) and cooling the wall (cases 12, 1 and 2) both increased the thrust markedly.

One interesting feature of the sharp-throat results is the rapid rise toward the maximum. For these configurations, the nozzle can be cut off at 5 radii with less than a five percent loss in thrust. These results illustrate the importance, in these calculations, of establishing the correct initial state of the flow at the throat.

In Fig. 12, the higher thrust coefficients are obtained at the expense of higher mass flows. The quantity $\bar{F}/A$ is shown in Fig. 13. This quantity is proportional to the specific impulse:

$$\frac{F}{\dot{m}} = \frac{\gamma-1}{4\gamma}\sqrt{2H_0}\,\frac{\bar{F}}{A}$$

If $F/\dot{m}$ is expressed in lbf/lbm/sec, and $\sqrt{2H_0}$ in ft/sec, this becomes (for γ = 1.4):

$$\frac{F}{\dot{m}}\left[\text{SECONDS}\right] = 0.0222\ \frac{\bar{F}}{A}\cdot\sqrt{2H_0}\left[\text{FT/SEC}\right]$$

The results in Fig. 13 indicate that the specific impulse is a relatively weak function of Reynolds number and nozzle geometry, for the range investigated here. The strongest influence was that associated with strong cooling of the nozzle walls.

One indication for design practice is that performance is increased by using a sharp throat, and by cutting the nozzle off at a rather modest exit-area ratio. This indication must be used with some caution, however, until more extensive calculations and further comparisons with experiment are made.

7. CONCLUDING REMARKS

The net result of the studies reported here is a computational method for finding a solution of the direct problem of low-density flow from given reservoir conditions through a nozzle of given shape. Results found by this method show good agreement with experiment. The equations used become identical with the thin-boundary-layer approximation at high Reynolds number, and can be used well down into the lower Reynolds number region where the importance of the state of the flow at the throat makes the conventional thin-boundary-layer model of limited value.

Within the limits of the calculations made, it appears that sharp throats lead to better performance, and that exit area ratios as low as 10 can be employed without serious loss in specific impulse.

At sufficiently low Reynolds number and small divergence angles, the slender-channel equations do not have a solution in which the flow expands to supersonic conditions. Instead, the boundary layer completely fills the channel, and the solution takes on the character of a viscous, subsonic pipe flow. One implication of this result is that a relatively strong upstream effect of the exit-plane conditions is likely to be felt in these flows. Further clarification of this regime awaits experimental probing of the flow structure and the application of more complex analyses which retain some of the effects discarded in the slender-channel approximation.

REFERENCES

1. Sutherland, G. S. and Maes, M. E., Review of Microrocket Technology: 10^{-6} to 1 lbf Thrust. J. Spacecraft and Rockets 3, 1153-1165 (1966).

2. Anon, NASA Literature Search No. 6324 (May 24, 1968).

3. Anon, Rocket-Nozzle Thrust; A Report Bibliography. Defense Documentation Center, Search Control No. 093325 (May 1968).

4. Bennett, S., Connors, J. F., and Clark, K. E., Development of a 3-Kilowatt Resistojet. AIAA Paper 64-672 (1964).

5. Durand, J. A. and Potter, J. L., Calculation of Thickness of Laminar Boundary Layers in Axisymmetric Nozzles with Low-Density, Hypervelocity Flows. AEDC-TN-61-146 (Dec. 1961).

6. Henshall, B. D. and Zlotnic, M., Design Study for a Hypersonic Low Density Wind Tunnel. AVCO RAD Tech. Rept. RAD-TR-9-60-37 (Jan. 31, 1961).

7. Johnson, A. F., A Method of Calculating Boundary-Layer Thickness in Axisymmetric Nozzles with Laminar Hypersonic Flow. Sandia Corp. Rept. SC-4370 (RR) (Oct. 1959).

8. Johnson, R. H., Hypersonic Viscous Effects in Wind Tunnels. ARS J. 31, 1022-1024 (1961).

9. Lam, S. H., Interactions of Heat Transfer and Hypersonic Boundary Layers under Highly Favorable Pressure Gradients. Proc. of the 1963 Heat Transfer and Fluid Mechanics Institute, ed. by A. Roshko, B. Sturtevant, and D. R. Bartz (Stanford Univ. Press, 1963).

10. Luce, R. G., Gregorek, G. M., and Lee, J. D., The Laminar Boundary Layer in Axisymmetric Hypersonic Nozzles with Wall Cooling. Ohio State Univ., ARL-65-112 (June 1965).

11. Maslach, G. J. and Sherman, F. S., Design and Testing of an Axisymmetric Hypersonic Nozzle for a Low Density Wind Tunnel. Univ. Calif. Rept. 150-134 (WADC-TR-56-341) (Aug. 1966).

12. Michel, R., Developpement de la Couche Limite dans une Tuyere Hypersonique. AGARD Specialists' Meeting, High Temperature Aspects of Hypersonic Flow (held at Rhode-St. Genese, Belgium) (Pergamon Press, London, 1963).

13. Murch, C. K., Broadwell, J. E., Silver, A. H., and Marcisz, T. J., Low-Thrust Nozzle Performance. AIAA Paper 68-91 (Jan. 1968); also J. Spacecraft and Rockets 5, 9, 1090-1094 (Sept. 1968).

14. Owen, J. M. and Sherman, F. S., Fluid Flow and Heat Transfer - Design and Testing of a Mach 4 Axially Symmetric Nozzle for Rarefied Gas Flows. Univ. Calif. Rept. HE-150-104 (July 1952).

15. Potter, J. L. and Carden, W. H., Design of Axisymmetric Contoured Nozzles for Laminar Hypersonic Flow. AIAA Paper 68-372 (April 1968); also J. Spacecraft and Rockets 5, 9, 1095-1100 (Sept. 1968).

16. Potter, J. L. and Durand, J. A., Analysis of Very Thick Laminar Boundary Layers in Axisymmetric High-Speed Fluid Flow, Developments in Theoretical and Applied Mechanics (Plenum Press, 1963), Vol. 1, pp. 341-360.

17. Rasmussen, M. L. and Karamcheti, K., Viscous Effects far Downstream in a Slowly Expanding Hypersonic Nozzle. AIAA J. 4, 807-815 (1966).

18. Sichel, M., The Effect of the Boundary Layer upon the Flow in a Conical Hypersonic Wind Tunnel Nozzle. Univ. Mich., Office of Research Administration Rept. 02953-2-F (July 1963).

19. Sichel, M., Integral Equations for Viscous Hypersonic Nozzle Flow. AIAA J. 2, 148-150 (1964).

20. Smetana, F. O., A Semi-Empirical Description of the Discharge Characteristics of the Converging Section of a Low-Density Hypersonic Nozzle. J. Aerospace Sci. 28, 988-989 (1961).

21. Spisz, E. W., Brinich, P. F., and Jack, J. R., Thrust Coefficients of Low-Thrust Nozzles. NASA TN D-3056 (Oct. 1965).

22. Touryan, K. J., Experimental and Analytical Investigations of Supersonic Flows in Very Low Density Wind Tunnels. Princeton Univ. Mech. Engng. Dept. Rept. FLD-6 (1962).

23. Touryan, K. J. and Drake, R. M., Flow Investigation in DeLaval Supersonic Nozzles at Very Low Pressures. 3rd RGD Symposium, ed. by J. A. Laurmann (Academic Press, New York, 1963), pp. 402-434.

24. Viventi, R., Analytical Methods for Resistance Jet Design. Supplementary Rept. No. 1, Gen. Elec. Co., Space Power & Propulsion Section, Cincinnati, Ohio, R64SD3008, NASA CR-84823 (Aug. 1964).

25. Whitfield, D. L., Theoretical and Experimental Investigation of Boundary Layers in Low Density Hypersonic Axisymmetric Nozzles. AEDC-TR-68-193 (Sept. 1968).

26. Agafonov, V. P., Interaction between the Boundary Layer and the Hypersonic Flow in a Conical Nozzle. Aerospace Technology Div., Library of Congress ATD Rept. 66-54 (16 May 1966).

27. Bolotina, K. S., On the Calculation of Flows through a Laval Nozzle with Viscosity and Heat Exchange Taken into Account, and on the Transition through the Velocity of Sound. Izv. AN SSSR, OTN, 5 (1956).

28. Burke, A. F. and Bird, K. D., The Use of Conical and Contoured Expansion Nozzles in Hypervelocity Facilities. Proc. of the Second Symposium on Hypervelocity Techniques; Advances in Hypervelocity Techniques (Plenum Press, New York, 1962), pp. 373-424.

29. Buschulte, W. and Hartung, W., Loss of Thrust in Nozzles of Rocket Engines Caused by Skin Friction and Non-Axial Discharge at a High Expansion Ratio. (In German) Deutsche Forschungsanstalt fur Luft- und Raumfahrt, Braunschweig, W. Germany, DLR-FB-65-58 (Nov. 1965).

30. Polianskii, A. F., Method of Integral Relations for the Case of Gas Flow in a Slender Channel. (In Russian) Leningrad Univ., Vestnik, Matematika, Mekhanika, Astronomiia, 23, 117-120 (July 1968).

31. Shang, J. -S. and Bloom, M. H., Compressible Viscous Flow in a Two-Dimensional Adiabatic Channel. Polytech. Inst. Brooklyn, PIBAL Rept. 749 (May 1962).

32. Anon, Development of the Subliming Solid Control Rocket, Phase II. Rocket Research Corp. Rept., NASA CR-712 (March 1967).

33. Ferrera, J. D. and McKown, P. M., A Method for Calculating Steady-State Thrust and Flow-Rate Levels for Mariner IV Type Attitude Control Nitrogen Gas Jets. JPL Tech. Rept. 32-1353 (Dec. 1, 1968).

34. Jeffries, N. P. and Cumbers, L. L., Computer Program for Calculation of Laminar Boundary Layer in a Supersonic Nozzle. Gen. Elec. Co., Missile and Space Div., Cincinnati, Ohio, Rept. R65SD3007 (June 9, 1965).

35. Geropp, D., Eine Ahnliche Losung der Kompressiblen Laminaren Grenzschichtgleichungen fur Eine Dusenstromung. ZAMM 46 Sonderheft, T195-T198 (1966).

36. Abbott, M. R., Axially Symmetric Steady Motion of Viscous Incompressible Fluid. Computer J. 7, 1, 47-53 (April 1964).

37. Bodoia, J. R., The Finite Difference Analysis of Confined Viscous Flows. Ph. D. Thesis, Carnegie Inst. Tech. (1959).

38. Milligan, M. W., Low Density Gas Flow through Varying Area Passages. Ph. D. Thesis, Univ. Tenn. (Dec. 1963).

39. Myers, William A., A Numerical Solution of Viscous Compressible Flow in Slender Channels. M. S. Thesis, Univ. Tenn. (Knoxville) (June 1964).

40. Quarmby, A., A Finite-Difference Analysis of Developing Slip Flow. Appl. Sci. Res. 19, 18-33 (April 1968).

41. Staiano, E. F., A General Numerical Procedure for Solutions of Viscous Compressible Flows with Shock Waves. Ph. D. Thesis, Univ. New Mexico (1967).

42. Adams, J. C., Jr., Similar Solutions for Viscous Compressible Laminar Flow in Slender Axisymmetric Channels. Ph. D. Thesis, North Carolina State College, Raleigh (1966).

43. Williams, J. C., A Study of Compressible and Incompressible Viscous Flow in Slender Channels. Univ. So. Calif., Engng. Center Rept. 83-213 (June 1962).

44. Williams, J. C., Viscous Compressible and Incompressible Flow in Slender Channels. AIAA J. 1, 186-195 (1963).

45. Williams, J. C., Conical Nozzle Flow with Velocity Slip and Temperature Jump. AIAA J. 5, 2128-2134 (1967); See Errata, AIAA J. 7, 2, 384 (1969).

46. Williams, J. C., Conical Nozzle Flow of a Viscous Compressible Gas with Energy Extraction. Appl. Sci. Res. 19, 285-301 (1968).

47. Williams, J. C. and Oliver, R. E., Slender Channel Approximation in Low Reynolds Number Channel Flow. AIAA J. 7, 2, 375-377 (Feb. 1969).

48. Bennett, S., Huss, W., John, R. R., and Tuchman, A., Experimental Propulsion Performance of a Low Power Pulsed Resistojet. AIAA Paper 65-97 (1965).

49. Berkopec, F. D., Performance of Two Subliming-Solid-Propellant Thrustor Systems for Attitude Control of Spacecraft. NASA TN D-3841 (Feb. 1967).

50. Cygnarowicz, T. A. and Gibson, R. N., Design and Performance of a Thermal Storage Resistojet. J. Spacecraft and Rockets 5, 686-689 (1968).

51. Ferguson, H. and Sovey, J. S., Performance Tests of a 1/2-Millipound (2.2 mN) Ammonia Resistojet Thrustor System. NASA TN D-4249 (Nov. 1967).

52. Ferguson, H., Sovey, J. S., and Hunczak, H. R., Preliminary Tests of a Single-Axis Ammonia-Resistojet Attitude Control System. NASA TM X-1677 (Oct. 1968).

53. Forsythe, R. W., Impulse and Thrust Test of a Sublimating-Solid Micropropulsion System. NASA TN D-3245 (March 1966).

54. Goldstein, R. and Mastrup, F. N., Performance Measurements on a Pulsed Ablating Thruster. AIAA J. 4, 99-102 (1966).

55. Grant, Daniel J., Precision Flow Measurement Techniques for Low Thrust Auxiliary Propulsion Liquid Rockets. NASA TM X-55967 (Aug. 1967); Same title, NASA TN D-4785 (Jan. 1969).

56. Greco, R. V. and Stoner, W. A., Research and Development of a 1-kw Plasmajet Thruster. AIAA J. 1, 320-324 (1963).

57. John, R. R., Resistojet Research and Development Phase II: Design, Development and Fabrication of an Ammonia-Fueled Resistojet Thrustor System. AVCO Corp. Rept. AVSSD-0356-66-CR, NASA CR-54688 (Dec. 1966).

58. Kanning, G., Measured Performance of Water Vapor Jets for Space Vehicle Attitude Control Systems. NASA TN D-3561 (Aug. 1966).

59. MacDermott, W. N., Preliminary Experimental Results of the Reduction of Viscous Effects in a Low-Density Supersonic Nozzle by Wall Cryopumping. AEDC-TN-61-71 (Oct. 1961).

60. Mikami, H. and Takashima, Y., Critical Mass Flow of Rarefied Gas Mixture through a Slit Nozzle. Bull. Tokyo Inst. Tech., No. 83, 103-114 (1968).

61. Milligan, M. W., Nozzle Characteristics in the Transition Regime between Continuum and Free Molecular Flow. AIAA J. 2, 1088-1092 (1964).

62. Page, R. J., Buhler, R. D., Stoner, W. A., and Masser, P. S., Arc Plasma Thrustor Studies. ARS Preprint 1508-60 (1960); Plasmadyne Corp. Rept. PLR-90 (Dec. 1, 1960).

63. Rollbuhler, R. J., Performance Investigation of Bipropellant Fractional-Pound Thrusters. NASA TM X-1699 (Dec. 1968).

64. Rollbuhler, R. J., Experimental Performance of a Water-Electrolysis Rocket. NASA TM X-1737 (Feb. 1969).

65. Smetana, F. O., Convergent-Divergent Nozzle Discharge Characteristics in the Transition Regime between Free Molecule and Continuum Flow. ASME Paper 63-WA-94 (1963).

66. Sreekanth, A. K., Performance of a Mach 4 Axially Symmetric Nozzle Designed to Operate at 40 Microns Hg in the UTIA Low Density Wind Tunnel. Univ. Toronto Tech. Note 10 (AFOSR-TN-57-94) (Sept. 1956).

67. Sreekanth, A. K., An Experimental Investigation of Mass Flow through Short Circular Tubes in the Transition Flow Regime. Boeing Scientific Res. Labs. Rept. DI-0427 (April 1965).

68. Yevseyev, G. A., Experimental Investigation of Flow of Rarefied Gas. AN SSSR, Izvestiya. Mekhanika, 3, 165-172 (1965); Transl. in AF, FTD, MT-67-22 (March 31, 1967).

69. Owens, W. L., Design Aspects of Subliming Solid Reaction Control Systems. AIAA Paper 68-516 (June 1968).

70. Price, T. W. and Evans, D. D., The Status of Monopropellant Hydrazine Technology. Calif. Inst. Tech., JPL Tech. Rept. 32-1227 (Feb. 15, 1968).

71. Grant, A. F., Jr., and Lee, D. H., Evolution of the Small Rocket Engine. AIAA Paper 67-982 (Oct. 1967).

72. Jonath, A. D., Gasdynamic Problems in Low Pressure Microthrust Engines. AIAA Paper 65-616 (June 1965), Astronautica Acta 11, 5, 348-354 (1965).

73. Greer, H., Analytical Investigation of Nitrogen Jet Reaction Control System. Aerospace Corp., Rept. SSD-TDR-64-242 (30 Nov. 1964).

74. Greer, H., Propulsive Performance of a Cold Gas Attitude Control Reaction Jet System. J. Spacecraft and Rockets 3, 429-431 (1966).

75. Greer, H. and Griep, D. J., Low Thrust Reaction Jet Performance. Aerospace Corp., Rept. SSD-TR-65-122 (Aug. 1965).

76. Greer, H. and Griep, D. J., Dynamic Performance of Low Thrust Cold Gas Reaction Jets in a Vacuum. Aerospace Corp., Rept. SSD-TR-66-180 (Aug. 1966).

77. Greer, H. and Griep, D. J., Dynamic Performance of a Subliming Solid Reaction Jet. Aerospace Corp. Rept. TR-1001 (2230-33)-1 (Dec. 1966).

78. Greer, H. and Griep, D. J., Pulsed Performance of a Steam Reaction Jet. Aerospace Corp. Rept. TR-1001 (2230-33)-2 (July 1967).

79. Griep, D. J., Experimental Performance of Anhydrous Ammonia. Aerospace Corp. Rept. TDR-469 (5230-33)-1 (Oct. 1964).

80. Bruschi, A. T. and Kibbe, R. K., Microthrust Measurement Systems. pp. 533-543 of the Bull. 7th Liquid Propulsion Symp. (unclassified title, volume confidential) JHU, Chem. Prop. Inf. Agency, CPIA Publication No. 72, Vol. II (Nov. 1967).

81. Cutler, W., Direct Microthrust Measurement on 'Swinging Gate' Test Stand. Space/Aeronautics 47, 115, 116, 119 (March 1967).

82. John, R. R., Chen, M. M., Connors, J. F., and Megrue, J. F., Arc Jet Engine Performance - Experiment and Theory IV. pp. 43-68 of Electric Propulsion Development, ed. by E. Stuhlinger. Progress in Astronautics and Aeronautics, Vol. 9 (Academic Press, 1963).

83. Roberts, S. L. and Peterson, D. D., Small Rocket Engine Testing Techniques. McDonnell Co., Engng. Labs. Rept., No no.; Paper presented at the 14th Annual Institute of Environmental Sciences Technical Meeting, St. Louis, Mo. (29 April - 1 May 1968).

84. Sinnette, J. T. and Stoner, W. A., Some Innovations in Thrust Balance Design. AIAA Paper 66-228 (March 1966).

85. Steger, R., Measurement of Very Low Thrust Associated with Reaction Control Systems. Instrument Soc. Am., Preprint No. 17 (June 19, 1965).

86. Zafran, S. and Kemp, R. F., Colloid Microthruster Test Stand. AIAA Paper 69-314 (March 1969).

87. Flugge-Lotz, I. and Baxter, D. C., The Solution of Compressible Laminar Boundary-Layer Problems by a Finite-Difference Method. Part I, Stanford Univ. Rept. TR-103 (Sept. 1956), Part II, TR-110 (Oct. 1957).

88. Wu, J. C., The Solution of Laminar Boundary-Layer Equations by the Finite-Difference Method. Proc. of the 1961 Heat Transfer and Fluid Mechanics Institute (Stanford Univ. Press, Stanford, Calif., 1961).

89. Zeiberg, S. L. and Bleich, G. D., Finite-Difference Calculation of Hypersonic Wakes. AIAA J. 2, 1396-1402 (1964).

90. Langan, W. T., Cresswell, J. D., and Browne, W. G., Effects of Ablation Products on Ionization in Hypersonic Wakes. AIAA J. 3, 2211-2218 (1965).

91. Chen, T. and Wen, K. S., FORTRAN Computer Code for the Axisymmetric Viscous Wake Analysis of a Hypersonic Reentry Body. General Motors Corp., AC DRL Tech. Rept. 66-66 (1966).

92. Baum, E. and Denison, M. R., Interacting Supersonic Laminar Wake Calculations by a Finite-Difference Method. AIAA J. 5, 1124-1230 (1967).

93. Pan, Y. S. and Probstein, R. F., Rarefied Flow Transition at a Leading Edge. pp. 259-306 of Fundamental Phenomena in Hypersonic Flow, ed. by J. G. Hall (Cornell Univ. Press, Ithaca, N. Y., 1965).

94. Anon, Equations, Tables, and Charts for Compressible Flow. NACA Rept. 1135 (1953).

95. Weinbaum, S. and Garvine, R. W., An Exact Treatment of the Boundary Layer Equations Describing the Two-Dimensional Viscous Analog of the One-Dimensional Inviscid Throat. AIAA Paper 68-102 (Jan. 1968).

96. Garvine, R. W. and Weinbaum, S., The Axially Symmetric Throat Phenomenon in Interacting Viscous-Inviscid Flows. Proc. of a Symp. on Viscous Interaction Phenomena in Supersonic and Hypersonic Flow. Wright-Patterson AFB, Ohio, May 7-8, 1969 (to be published).

97. Shapiro, A. H., The Dynamics and Thermodynamics of Compressible Fluid Flow (Ronald Press, New York, 1953), Vol. 1, Chap. 8.

98. Lighthill, M. J., On Boundary Layers and Upstream Influence, II. Supersonic Flows without Separation. Proc. Roy. Soc. (A) 217, 478-507 (1953).

99. Richtmeyer, R. D. and Morton, K. W., Difference Method for Initial-Value Problems. 2nd Ed. (Interscience Publishers, New York, 1967).

100. Ackerberg, R. C., The Viscous Incompressible Flow inside a Cone. J. Fluid Mech. 21, 47-81 (1965).

101. Rae, W. J., Some Numerical Results on Viscous Low-Density Nozzle Flows in the Slender-Channel Approximation. AIAA Paper 69-654 (June 1969).

102. Page, R. J., Halbach, C. R., Ownby, M. L., and Short, R. A., Life Test of Six High Temperature Resistojets. AIAA Paper 69-294 (March 1969).

103. Summerfield, M., The Liquid Propellant Rocket Engine. Section G of Jet Propulsion Engines, ed. by O. E. Lancaster (Princeton Univ. Press, Princeton, New Jersey, 1959).

APPENDIX A

COMPUTER PROGRAM DETAILS

The program was coded in FORTRAN IV, and the G compiler was used. Execution was done on an IBM 360/65, Release 14. The amount of core used is approximately 45K bytes. A typical run may take between two and ten minutes, depending on how good the initial guesses at the mass flow are, how many axial stations are specified, and how much output is specified.

The required input data are described in comment cards in the listing (Appendix E). Most of these need no further explanation, but some of the restrictions on their magnitudes are given below:

IBC: If this is read in as 2, then XTW1 must be greater than XTW2.

IETAPR: The value 2 gives a convenient one-page output, with enough detail (51 values) to adequately define the profiles.

R1, THETA1, THETA2: The only nozzle geometry that can be handled by the present version is a converging cone joined to a diverging cone by a constant-radius-of-curvature section. The angles must be read in degrees, and should be restricted to values small enough for the slender-channel equations to apply. Angles up to 30 degrees have been used, but the magnitude of the error made is unknown at present.

TW2: For cases where heat transfer is allowed (IBC = 1), the wall-temperature distribution must be specified. The only distribution allowed in the present program consists of two constant values connected by a cosine variation:

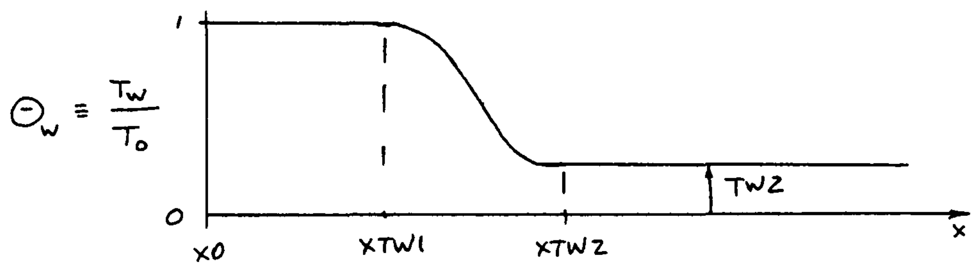

The second level TW2 can be greater or less than one.

B: This is a Reynolds number based on reservoir conditions and the throat radius. It can be expressed in the alternate forms:

$$\mathcal{B} = \frac{\rho_0 \sqrt{2H_0}\, r_*}{\mu_0} = \sqrt{\frac{2\gamma}{\gamma-1}\,\frac{\mathcal{M}}{\mathcal{R}}}\;\frac{p_0\, r_*}{\mu_0 \sqrt{T_0}} \qquad \text{(A-1)}$$

Consistent units for the latter form are

p_0	r_*	μ_0	T_0	$\mathcal{R}$
lbf/ft^2	ft	slug/ft-sec	°R	4.97×10^4 ft-lbf/slug-°R
nt/m^2	m	kg/m-sec*	°K	$8.32 \times 10^3\ m^2/sec^2$-°K

* 1 poise = 1 gm/cm-sec = 10^{-1} kg/m-sec

If the value of $\mathcal{B}$ is less than about 600, it is probable that no solution with a supersonic core will be found. There is also an upper limit beyond which accuracy is lost, but its value is unknown at present. Runs have been made with $\mathcal{B}$ as large as 3000, and it is probable that values at least to 10,000 can be used. The loss in accuracy occurs for two reasons: first, as the boundary layer thins, it is described by fewer of the 101 equally spaced radial grid points. Secondly, the slip velocity at the wall decreases, and the integrals which are inversely proportional to this velocity are not calculated accurately by Simpson's rule over the equally spaced grid.

Actually, for values of $\mathcal{B}$ greater than 10,000, a more conventional thin-boundary-layer program with no slip at the walls may be a preferable calculational method.

XIPG: It is recommended that XIPG be greater than XMAX, so that mass conservation is enforced up to the saddle point.

ATEST: Present experience suggests that three significant figures are adequate; this means ATEST = 10^{-4} for $\gamma \leq 1.3$, 10^{-3} for $\gamma \geq 1.4$, and perhaps 3×10^{-4} for $1.3 \leq \gamma \leq 1.4$. If the mass flow is known exactly, in advance of the run, set ATEST = 1.0, and A0 = A1.

A0, A1: If the discharge coefficient is known, Eq. (3-27) can be used to make these initial guesses. If it is not, it is usually safe to assume $C_D = 0.5$ for a lower bound. The upper bound can be taken as $C_D = 1.0$ for an adiabatic wall or a heated wall (TW2 > 1) and should be set at $C_D = 1.2$ for a cooled wall (TW2 < 1). The corresponding values of A can be quickly estimated from the table following Eq. (3-27). If the mass flow is known exactly, set A0 = A1, and ATEST = 1.0. Then the program will proceed immediately to the final solution, with no iteration on A.

XCUT: An input is required here if the mass flow is known in advance, i. e., if A0 = A1; set XCUT = 0 unless some previous runs have shown that it would be preferable to start the extrapolation through the saddle point at some other location.

XPRINT: Subtract .001 from the desired print interval -- i. e., if profile output is desired at intervals of 0.5 in Δx, read this number in as 0.499.

DELX: The value 0.1 has been found acceptable. It is not known how much larger this can be without loss of accuracy; smaller values can be used at the expense of longer calculation times.

X0: A value of -5 is recommended, although smaller values can perhaps be used for $B < 10^3$.

X1, X2: If the throat is very sharp (i. e., if R1 < 1), the transition from entrance to exit cones occurs over an axial distance equal to approximately one throat radius. In such cases, it is well to set X1 and X2 equal to about -.5 and +.5, in order to follow some of the rapid changes that occur in this region. If R1 is greater than about 1.0, set X1 > X2, and the small step-size region is omitted.

XMAX: This choice is dictated by the desired exit-area ratio. The present program has been run successfully at exit-area ratios up to 150. In some cases, an oscillation in dP/dx may occur at X > 10. Even when this does occur, however, the integrated quantities (such as the thrust coefficient) appear to be relatively unaffected.

ALPHU, ALPHT: Set these equal to one for perfect accommodation.

XTW1, XTW2: These are the stations that enclose the cosine variation in wall-to-stagnation temperature ratio. XTW1 must be greater than X0 (preferably no less than X0+1, so that the initial profiles have time to stabilize). XTW2 can be either greater or less than zero. No computational difficulties were encountered when the difference XTW2 - XTW1 was made as small as 1.0, with a temperature change $\Delta\Theta_w = 0.5$ in that distance.

The output begins with a printing of all the input values. Following this, the iterations on A begin. For each value of A, for each x, and for each of the iterations on dP/dx, a large number of quantities are printed. These quantities serve a dual purpose: some of the information they contain (such as the displacement-thickness variation) is often desired at more stations than those at which the profiles are printed, and, in addition, this output is useful as a diagnostic when the case fails to run to completion. Many users may wish to omit this output when making routine runs. A definition of all the program variables is given in Appendix F. This output is continued for each of the iterations on A, until A has been determined to the prescribed accuracy, ATEST. The final solution is then calculated; on this pass, the output is augmented by a listing of the profiles at intervals of XPRINT.

Some excerpts from the output of a sample case are given in Table 2. The first two pages of the output are shown, giving the input data, and the iterations used on the first two steps with the first A-value. Next is shown the page at which this first A-pass was terminated. The second A-value, 0.095, was found to have too little mass flow, and the page of output showing this determination is shown. The subsequent values of used were

$$
\begin{aligned}
A = \ & 0.1025 \\
& 0.10625 \\
& 0.108125 \\
& 0.1090625 \\
& 0.10859375
\end{aligned}
$$

The last of these values is the one used for the final solution. Its first output page is shown, giving the initial profiles. The next page shown is that giving the iterations at $X = -.10$. The indicator IPG is set equal to 2, beginning with $X = .0$, since XCUT had been set equal to $-.10$ on the A-pass with $A = 0.1090625$. The next page shown is that beginning with $X = 1.0$. The saddle point is crossed between $X = 1.0$ and 1.1, and six iterations are required to converge to the solution at $X = 1.2$. Finally, the profiles at $X = 2$ are shown.

The quantities appearing in the columns of profile output are η, U, Θ, W, V, D, Ψ, M, and the five terms that enter the differential form of the streamtube-area relation, written in the form:

$$
\underbrace{\gamma P \frac{\partial}{\partial \eta}\left(\eta \frac{V}{U}\right)}_{DA/DX} = \underbrace{\frac{1-M^2}{M^2}\,\eta\,\sigma_w \frac{dP}{dx}}_{PGT} - \underbrace{\frac{2\gamma}{(\gamma-1)B\sigma_w M^2}\frac{\partial}{\partial \eta}\left(\eta\,\Theta^{\omega}\frac{\partial U}{\partial \eta}\right)}_{SHEAR} \qquad \text{(A-2)}
$$

$$
+ \underbrace{\frac{2\gamma}{(\gamma-1)B\sigma_w M^2}\,\frac{U}{\Theta}\frac{\partial}{\partial \eta}\left(\frac{\eta\,\Theta^{\omega}}{P_r}\frac{\partial \Theta}{\partial \eta}\right)}_{COND'N} - \underbrace{\frac{2\gamma}{(\gamma-1)B\sigma_w M^2}\cdot 2\eta\,\Theta^{\omega}\left(\frac{\partial U}{\partial \eta}\right)^2}_{GEN}
$$

The last four terms should add up to a number equal to the first; these quantities are useful for studying the relative contributions that these different effects make along the various streamtubes.

APPENDIX B

DERIVATION OF THE GLOBAL CONSERVATION RELATIONS

Continuity:

Equation (3-15) is divided by P, and the result is integrated from zero to η:

$$\frac{\eta W}{\Theta} + \frac{\sigma_w}{P}\int_0^\eta \eta \frac{\partial}{\partial x}\left(\frac{PU}{\Theta}\right) d\eta + 2\sigma_w' \int_0^\eta \frac{\eta U}{\Theta} d\eta = 0 \quad \text{(B-1)}$$

The middle term is then expanded, noting that $P = P(x)$

$$\frac{\eta W}{\Theta} + \frac{\sigma_w}{P}\left\{\frac{dP}{dx}\int_0^\eta \frac{\eta U\, d\eta}{\Theta} + P\frac{\partial}{\partial x}\int_0^\eta \frac{\eta U}{\Theta} d\eta\right\} \quad \text{(B-2)}$$

$$+ 2\sigma_w' \int_0^\eta \frac{\eta U}{\Theta} d\eta = 0$$

Division by $\sigma_w \int_0^\eta \frac{\eta U}{\Theta} d\eta$ then gives the result shown in Eq. (3-25).

Momentum:

In deriving this integral, it is simpler to replace P/Θ by D. Integrating the momentum equation from zero to one gives:

$$\int_0^1 \eta D\left[U\frac{\partial U}{\partial x} + \frac{W}{\sigma_w}\frac{\partial U}{\partial \eta}\right] d\eta = \quad \text{(B-3)}$$

$$= -\frac{\gamma-1}{2\gamma}\frac{dP}{dx}\cdot\frac{1}{2} + \frac{1}{B\sigma_w^2}\left[\Theta(1)\right]^\omega \left.\frac{\partial U}{\partial \eta}\right|_{\eta=1}$$

The left side of this expression can be recast, as follows: note that

$$\mathcal{J} \equiv \frac{\partial}{\partial x}\int_0^1 \eta D U^2 \, d\eta = \int_0^1 \eta D U \frac{\partial U}{\partial x}\, d\eta + \int_0^1 \eta U \frac{\partial}{\partial x}(DU)\, d\eta \tag{B-4}$$

Use continuity to rewrite the last term:

$$\mathcal{J} = \int_0^1 \eta D U \frac{\partial U}{\partial x}\, d\eta + \int_0^1 \eta U \left\{ \frac{\sigma_w'}{\sigma_w}\, \eta \frac{\partial}{\partial \eta}(DU) - \frac{1}{\eta \sigma_w} \frac{\partial}{\partial \eta}(DV\eta) \right\} d\eta$$

Integrate by parts:

$$\mathcal{J} = \int_0^1 \eta D U \frac{\partial U}{\partial x}\, d\eta + \frac{\sigma_w'}{\sigma_w} \left\{ \Big[U \eta^2 D U \Big]_0^1 - \int_0^1 D U \frac{\partial}{\partial \eta}(\eta^2 U)\, d\eta \right\}$$

$$- \frac{1}{\sigma_w} \left\{ \Big[U D V \eta \Big]_0^1 - \int_0^1 D V \eta \frac{\partial U}{\partial \eta}\, d\eta \right\}$$

Expand these terms, and collect:

$$\mathcal{J} = \int_0^1 \eta D \left[U \frac{\partial U}{\partial x} + \frac{V}{\sigma_w} \frac{\partial U}{\partial \eta} - \frac{\sigma_w'}{\sigma_w} U \eta \frac{\partial U}{\partial \eta} \right] d\eta$$

$$- 2 \frac{\sigma_w'}{\sigma_w} \int_0^1 D U^2 \eta \, d\eta + \frac{\Big[D U (U \sigma_w' - V) \Big]_{\eta = 1}}{\sigma_w} \tag{B-5}$$

The last term here is zero, with or without slip at the wall. Using this result in Eq. (B-3) gives

$$\frac{\partial}{\partial x}\int_0^1 \eta D\mathcal{U}^2\,d\eta + 2\frac{\sigma_w'}{\sigma_w}\int_0^1 D\mathcal{U}^2\eta\,d\eta =$$

$$= -\frac{\gamma-1}{4\gamma}\frac{dP}{dx} + \frac{[\Theta(1)]^{\omega}\left.\frac{\partial\mathcal{U}}{\partial\eta}\right|_{\eta=1}}{B\sigma_w^2} \qquad \text{(B-6)}$$

Equation (3-29) is then obtained by multiplying through by $\frac{4\gamma\sigma_w^2}{(\gamma-1)}$, and collecting terms.

Energy:

Note first that

$$\frac{\partial}{\partial x}\int_0^1 D\mathcal{U}\Theta\eta\,d\eta =$$

$$= \int_0^1 \eta\Theta\frac{\partial}{\partial x}(D\mathcal{U})\,d\eta + \int_0^1 D\mathcal{U}\eta\frac{\partial\Theta}{\partial x}\,d\eta \qquad \text{(B-7)}$$

As before, the continuity equation is then used to rewrite the last term, and an integration by parts is applied to the result. This leads to

$$\frac{\partial}{\partial x}\int_0^1 D\mathcal{U}\eta\Theta\,d\eta = \int_0^1 D\mathcal{U}\eta\frac{\partial\Theta}{\partial x}\,d\eta + \int_0^1 \frac{DW}{\sigma_w}\eta\frac{\partial\Theta}{\partial\eta}\,d\eta \qquad \text{(B-8)}$$

$$- \frac{2\sigma_w'}{\sigma_w}\int_0^1 D\Theta\mathcal{U}\eta\,d\eta$$

Thus the energy equation, integrated from zero to one, can be written as:

$$\frac{\partial}{\partial x}\int_0^1 D\mathcal{U}\Theta\eta\,d\eta + \frac{2\sigma_w'}{\sigma_w}\int_0^1 D\mathcal{U}\Theta\eta\,d\eta - \frac{\gamma-1}{\gamma}\frac{dP}{dx}\int_0^1 \eta\mathcal{U}\,d\eta =$$

$$= \frac{1}{B\sigma_w^2}\left\{\frac{\Theta^{\omega}}{Pr}\frac{\partial\Theta}{\partial\eta}\right\}_{\eta=1} + \frac{2}{B\sigma_w^2}\int_0^1 \eta\Theta^{\omega}\left(\frac{\partial\mathcal{U}}{\partial\eta}\right)^2 d\eta \qquad \text{(B-9)}$$

In order to obtain an expression for the total enthalpy flux, multiply the momentum equation by $\mathcal{U}$ and integrate from zero to one:

$$\int_0^1 \eta D \mathcal{U} \left(\mathcal{U} \frac{\partial \mathcal{U}}{\partial x} + \frac{W}{\sigma_w} \frac{\partial \mathcal{U}}{\partial \eta} \right) d\eta =$$

$$= - \frac{\gamma - 1}{2\gamma} \frac{dP}{dx} \int_0^1 \eta \mathcal{U} \, d\eta + \frac{1}{B \sigma_w^2} \int_0^1 \mathcal{U} \frac{\partial}{\partial \eta} \left(\eta \Theta^\omega \frac{\partial \mathcal{U}}{\partial \eta} \right) d\eta \tag{B-10}$$

Note that

$$\frac{\partial}{\partial x} \int_0^1 \eta D \mathcal{U}^3 \, d\eta = \int_0^1 \eta D \mathcal{U}^2 \frac{\partial \mathcal{U}}{\partial x} \, d\eta + \int_0^1 \eta \mathcal{U} \frac{\partial}{\partial x} (D \mathcal{U}^2) \, d\eta$$

Again, the last term here is expanded, rewritten with the aid of the continuity equation, and the result is integrated by parts. This gives

$$\frac{\partial}{\partial x} \int_0^1 \eta D \mathcal{U}^3 \, d\eta = 2 \int_0^1 \eta D \mathcal{U} \left(\mathcal{U} \frac{\partial \mathcal{U}}{\partial x} + \frac{W}{\sigma_w} \frac{\partial \mathcal{U}}{\partial \eta} \right) d\eta$$

$$- 2 \frac{\sigma_w'}{\sigma_w} \int_0^1 D \mathcal{U}^3 \eta \, d\eta$$

If this is now used in Eq. (B-10) above (multiplied by 2) and the result is added to Eq. (B-9), the result is Eq. (3-31).

APPENDIX C

MATRIX - COEFFICIENT EXPRESSIONS

The matrix coefficients appearing in Eq. (4-6) are:

$$a_{11}^{L} = -\frac{\eta \bar{P} W_K^L}{T_K^L \bar{\nu}_w \cdot 4\Delta\eta} + \frac{(T_K^L)^{\omega}}{B\bar{\nu}_w^{2}} \left\{ \frac{1}{4\Delta\eta} + \frac{\omega\eta}{T_K^L} \cdot \frac{(T_K^{L+1} - T_K^{L-1})}{8(\Delta\eta)^2} + \frac{\eta}{2(\Delta\eta)^2} \right\}$$

$$a_{12}^{L} = \frac{(T_K^L)^{\omega}}{B\bar{\nu}_w^{2}} \cdot \frac{\omega\eta}{T_K^L} \, \frac{(u_K^{L+1} - u_K^{L-1})}{8(\Delta\eta)^2}$$

$$a_{21}^{L} = \frac{(T_K^L)^{\omega}}{B\bar{\nu}_w^{2}\cancel{Pr}} \cdot \frac{\cancel{Pr}\,\eta}{2(\Delta\eta)^2} \left(u_K^{L+1} - u_K^{L-1} \right)$$

$$a_{22}^{L} = -\frac{\eta \bar{P} W_K^L}{T_K^L \bar{\nu}_w \cdot 4\Delta\eta} + \frac{(T_K^L)^{\omega}}{B\bar{\nu}_w^{2} Pr} \left\{ \frac{1}{4\Delta\eta} + \frac{\omega\eta}{T_K^L} \, \frac{(T_K^{L+1} - T_K^{L-1})}{4(\Delta\eta)^2} + \frac{\eta}{2(\Delta\eta)^2} \right\}$$

$$b_{11}^{L} = \frac{\eta\bar{P}}{T_K^L} \cdot \frac{u_K^L}{\Delta x} + \frac{(T_K^L)^{\omega}}{B\bar{\nu}_w^{2}} \cdot \frac{\eta}{(\Delta\eta)^2}$$

$$b_{12}^{L} = 0$$

$$b_{21}^{L} = 0$$

$$b_{22}^{L} = \frac{\eta\bar{P}}{T_K^L} \cdot \frac{u_K^L}{\Delta x} + \frac{(T_K^L)^{\omega}}{B\bar{\nu}_w^{2} Pr} \cdot \frac{\eta}{(\Delta\eta)^2}$$

$$c_{11}^L = \frac{\eta \bar{P} W_K^L}{T_K^L \bar{\sigma}_w 4\Delta\eta} - \frac{(T_K^L)^\omega}{B\bar{\sigma}_w^2}\left\{\frac{1}{4\Delta\eta} + \frac{\omega\eta}{T_K^L}\cdot\frac{(T_K^{L+1} - T_K^{L-1})}{8(\Delta\eta)^2} - \frac{\eta}{2(\Delta\eta)^2}\right\}$$

$$c_{12}^L = -\frac{(T_K^L)^\omega}{B\bar{\sigma}_w^2}\left\{\frac{\omega\eta}{T_K^L}\;\frac{U_K^{L+1} - U_K^{L-1}}{8(\Delta\eta)^2}\right\}$$

$$c_{21}^L = -\frac{(T_K^L)^\omega}{B\bar{\sigma}_w^2 \cancel{P_r}}\cdot\frac{\cancel{P_r}\,\eta}{2(\Delta\eta)^2}\left(U_K^{L+1} - U_K^{L-1}\right)$$

$$c_{22}^L = \frac{\eta \bar{P} W_K^L}{T_K^L \bar{\sigma}_w 4\Delta\eta} - \frac{(T_K^L)^\omega}{B\bar{\sigma}_w^2 P_r}\left\{\frac{1}{4\Delta\eta} + \frac{\omega\eta}{T_K^L}\cdot\frac{(T_K^{L+1} - T_K^{L-1})}{4(\Delta\eta)^2} - \frac{\eta}{2(\Delta\eta)^2}\right\}$$

$$d_1 = \frac{\eta\bar{P}}{T_K^L}\left\{\frac{(U_K^L)^2}{\Delta x} - \frac{W_K^L}{\bar{\sigma}_w}\,\frac{(U_K^{L+1} - U_K^{L-1})}{4\Delta\eta}\right\} - \frac{\gamma-1}{2\gamma}\,\eta\,\frac{dP}{dx}$$
$$+ \frac{(T_K^L)^\omega}{B\bar{\sigma}_w^2}\left\{\frac{U_K^{L+1} - U_K^{L-1}}{4\Delta\eta} + \frac{\eta}{2(\Delta\eta)^2}\left(U_K^{L+1} - 2U_K^L + U_K^{L-1}\right)\right\}$$

$$d_2 = \frac{\eta\bar{P}}{T_K^L}\left\{\frac{U_K^L\,T_K^L}{\Delta x} - \frac{W_K^L}{\bar{\sigma}_w}\,\frac{(T_K^{L+1} - T_K^{L-1})}{4\Delta\eta}\right\} + \frac{\gamma-1}{\gamma}\,\eta\,U_K^L\,\frac{dP}{dx}$$
$$+ \frac{(T_K^L)^\omega}{B\bar{\sigma}_w^2 P_r}\left\{\frac{T_K^{L+1} - T_K^{L-1}}{4\Delta\eta} + \frac{\eta}{2(\Delta\eta)^2}\left(T_K^{L+1} - 2T_K^L + T_K^{L-1}\right)\right\}$$

APPENDIX D

SERIES EXPANSION OF THE INITIAL CONDITIONS

If the series expansions of $\mathcal{U}$, Θ, P, and W are substituted into the partial differential equations of motion, and coefficients of like powers of σ_W are equated, the results are, for the momentum equation:

$$\frac{\gamma-1}{2\gamma}\sigma_w' \cdot 3\pi_3 B\eta + (\eta\mathcal{U}_2')' = 0$$

$$\frac{\gamma-1}{2\gamma}\sigma_w' B\eta \cdot 4\pi_4 + (\eta\mathcal{U}_3')' = B\eta\left\{-2\sigma_w'\mathcal{U}_2^2 + w_2\mathcal{U}_2'\right\}$$

$$\frac{\gamma-1}{2\gamma}\sigma_w' B\eta \cdot 5\pi_5 + (\eta\mathcal{U}_4')' = B\eta\left\{-5\sigma_w'\mathcal{U}_2\mathcal{U}_3 + W_2\mathcal{U}_3' + W_3\mathcal{U}_2'\right\}$$

$$\frac{\gamma-1}{2\gamma}\sigma_w' B\eta \cdot 6\pi_6 + (\eta\mathcal{U}_5')' = B\eta\left\{-\sigma_w'\left(6\mathcal{U}_2\mathcal{U}_4 + 3\mathcal{U}_3^2\right)\right.$$

$$\left. + W_2\mathcal{U}_4' + W_3\mathcal{U}_3' + W_4\mathcal{U}_2'\right\} \tag{D-1}$$

$$\frac{\gamma-1}{2\gamma}\sigma_w' B\eta \cdot 7\pi_7 + (\eta\mathcal{U}_6')' + (\eta\omega T_4\mathcal{U}_2')' =$$

$$= B\eta\left\{-\sigma_w'\left(7\mathcal{U}_2\mathcal{U}_5 + 7\mathcal{U}_3\mathcal{U}_4\right) - \sigma_w'\pi_3 \cdot 2\mathcal{U}_2^2 + W_2\mathcal{U}_5'\right.$$

$$\left. + W_3\mathcal{U}_4' + W_4\mathcal{U}_3' + W_5\mathcal{U}_2' + \pi_3 W_2\mathcal{U}_2'\right\}$$

For the energy equation, only the leading term has been worked out:

$$-\frac{\gamma-1}{\gamma}\,\sigma_w'\,B\eta\,\mathcal{U}_2\cdot 3\pi_3+\frac{1}{Pr}\left(\eta T_4'\right)'+2\eta\left(\mathcal{U}_2'\right)^2 \qquad \text{(D-2)}$$

The continuity equation is used to find W directly from $\mathcal{U}$, Θ, and P:

$$\eta W_N=\sigma_w'\,(N-2)\int_0^\eta \eta\,\mathcal{U}_N\,d\eta \quad , \quad N=2,3,4.$$

$$\eta W_5=3\sigma_w'\int_0^\eta \eta\,\mathcal{U}_5\,d\eta+3\sigma_w'\,\pi_3\int_0^\eta \mathcal{U}_2\,\eta\,d\eta \qquad \text{(D-3)}$$

As noted in Section 5, the coefficients π_N are found by enforcing the global conservation of mass.

Results for the first few terms are given in Section 5; the remaining terms that have been worked out are

$$\mathcal{U}_4(\eta)=(\sigma_w')^2B^2A^3\left\{\frac{479}{135}(1-\eta^2)-\frac{53}{9}(1-\eta^4)+\frac{76}{18}(1-\eta^6)-\frac{13}{9}(1-\eta^8)+\frac{152}{900}(1-\eta^{10})\right\}$$

$$+\sigma_w'A^2BK_u\left\{-\frac{8}{3}-20(1-\eta^2)+28(1-\eta^4)-8(1-\eta^6)\right\}+32AK_u^2(1-2\eta^2)$$

$$W_4(\eta)=(\sigma_w')^3A^3B^2\left\{\frac{409}{675}\eta-\frac{479}{270}\eta^3+\frac{53}{27}\eta^5-\frac{19}{18}\eta^7+\frac{13}{45}\eta^9-\frac{152}{5400}\eta^{11}\right\}$$

$$+(\sigma_w')^2A^2BK_u\left\{-\frac{8}{3}\eta+10\eta^3-\frac{28}{3}\eta^5+2\eta^7\right\}+32\,\sigma_w'\,AK_u^2\left(\eta-\eta^3\right)$$

$$\frac{\gamma-1}{2\gamma}\pi_5=-\frac{1936}{2700}\sigma_w'BA^3+16A^2K_u+\frac{256}{5}\frac{AK_u^2}{\sigma_w'B}$$

$$
\begin{aligned}
u_5(\eta) = (\sigma_w')^3 A^4 B^3 \Big\{ & \frac{2854}{675}(1-\eta^2) - \frac{9503}{1350}(1-\eta^4) + \frac{3598}{486}(1-\eta^6) - \frac{19}{4}(1-\eta^8) \\
& + \frac{9}{5}(1-\eta^{10}) - \frac{2948}{8100}(1-\eta^{12}) + \frac{1892}{66150}(1-\eta^{14}) \Big\} \\
& + (\sigma_w')^2 A^3 B^2 K_u \Big\{ -\frac{80}{3}(1-\eta^2) + \frac{424}{9}(1-\eta^4) - \frac{380}{9}(1-\eta^6) + \frac{52}{3}(1-\eta^8) - \frac{532}{225}(1-\eta^{10}) \Big\} \\
& + \sigma_w' A^2 B K_u^2 \Big\{ 240(1-\eta^2) - 168(1-\eta^4) + \frac{160}{3}(1-\eta^6) \Big\} \\
& + (1-\eta^2) \Big\{ -\frac{128}{3(\gamma-1)} \frac{A^2}{\sigma_w' B} - \frac{138159}{178605}(\sigma_w')^3 A^4 B^3 + \frac{242}{45}(\sigma_w')^2 A^3 B^2 K_u \\
& \qquad - 144\, \sigma_w' A^2 B K_u^2 - 256 A K_u^3 \Big\} \\
& - \frac{134}{135}(\sigma_w')^2 A^3 B^2 K_u + 24\, \sigma_w' A^2 B K_u^2 + 128 A K_u^3
\end{aligned}
$$

$$
\begin{aligned}
\frac{3}{8} \frac{\gamma-1}{2\gamma} \sigma_w' B \pi_6 = & - \frac{32\gamma}{3(\gamma-1)} \frac{A^2}{\sigma_w' B} - \frac{138159}{714420}(\sigma_w')^3 A^4 B^3 \\
& + \frac{121}{90}(\sigma_w')^2 A^3 B^2 K_u - 36\, \sigma_w' A^2 B K_u^2 - 64 A K_u^3
\end{aligned}
$$

APPENDIX E

PROGRAM LISTING AND FLOW CHART

```
CCCC
      REAL DAY(3)
      COMMON A,ABDLP1,ABDLP2,ABDPG1,ABDPG2,AEFF,ALPHT,ALPHU,AMACH,
     *AMACH2,AMM2,AMM2A,AMM2AV,AMM2B,AMM2C,AMM2MN,AMM21,AMSC,AM2LST,
     *ARCHI,ATEST,A0,A1,A11,A12,A21,A22
      COMMON B,BOTTOM,BRB,BR1,BR11,BR12,BR2,BR21,BR22,B11,B12,B21,B22
      COMMON C,CFBOT,CONDI,CPKU,C11,C12,C21,C22
      COMMON D,DELETA,DELX,DELXS,DENOM,DFBRDX,DLP1,DLP2,DLSTR,DPDX,DPG1,
     *DPG2,DPLAST,DPNM1,DPNUM,DPNUMA,DPNUMB,DTDN,DUDN,DUDNSQ,DVDN,D1,D2,
     *D2TDN2,D2UDN2,DAY
      COMMON EM11,EM12,EM21,EM22,ETTBU2,E11MAX
      COMMON FACT,FN1,FN2
      COMMON GAMMA,GAMMAP,GENRI,G1,G10,G11,G12,G13,G14,G15,G16,G17,G18,
     *G19,G2,G20,G21,G3,G4,G4BGM1,G5,G6,G7,G8,G9
      COMMON HDELX,HFLUX,HTR
      COMMON IBC,IETAPR,IGOTA,IPG,ISW,ITER,ITERA,IX,IXSTAR,IXTHW
      COMMON K,K1,KP1,KX,KX0,KX1
      COMMON LC,MORE,NPRO,NRUN
      COMMON OHMPH,OMEGA,O1,O2,O3,O4,O5
      COMMON P,PART1,PART2,PDA,PG,PGNP1,PGRT,PG1,PG2,PHW,PI3,PNEW,PN1,
     *PN2,PR,PSCW2,PSI,PXTRAP
      COMMON Q,QQ11,QQ12,QQ21,QQ22,Q11,Q12,Q21,Q22
      COMMON RADDEG,RTPB2,RT2827,RT2GM1,R1,R1ST1,R1ST2,R12
      COMMON SAME,SA1,SC1,SGDX,SHERI,SIGBAR,SIGDP,SIGMAW,SW2,SW3,SW4
      COMMON TANBAR,TANTHP,TAU,TCF,TCFTOP,THCOEF,THETAP,THETAW,THETA1,
     *THETA2,TOMF,TOP,TTERM,TW2
      COMMON UCF,UCFTOP,UTERM,U2HTAT,V
      COMMON X,XCUT,XHW,XIPG,XMAX,XPLAST,XPRINT,XTW1,XTW2,X0,X1,X2
      COMMON Y1,Y2,Y3,Y4,Y5,Y6,Y7,Y8,Y9
      COMMON Z1,Z10,Z11,Z12,Z13,Z15,Z16,Z2,Z23,Z31,Z32,Z33,Z34,Z35,Z41,
     *Z42,Z43,Z5,Z7,Z8
      COMMON ETA(101),E11(101),E12(101),E21(101),E22(101),F1(101),
     *F2(101),S3(101),S4(101),W(101)
      COMMON T(101,2),U(101,2)
      DIMENSION ARCH(101),PGRO(101),COND(101),SHER(101),GENR(101)
      EQUIVALENCE (ARCH,E21),(PGRO,E22),(COND,F1),(SHER,F2),(GENR,S4)
      COMMON/ERRLIM/ CHECKS(4)
      INTEGER*2 CHECKS
      CHECKS(1)=1
      CHECKS(2)=1
      CHECKS(3)=-10
      CHECKS(4)=1
      CALL OVDCHK
  500 CALL CLEAR(A,U(101,2))
      CALL INPUT
      CALL INIT
C
C     BEGINNING OF A ITERATION LOOP
C
    1 CALL START
```

```
C
C      BEGINNING OF X INTEGRATION LOOP
C
      PGRT=1.0
      IPG=4
      IF(X.GT.XIPG) IPG=1
      KXI=0
      IXSTAR=1
      ISW=1
    5 DO 4 L=1,101
      U(L,1)=U(L,2)
    4 T(L,1)=T(L,2)
      ITER=1
      PG1=DPDX*PGRT
      PG2=1.01  *PG1
      GO TO (301,305), IXSTAR
  301 IF(KX.LE.5) GO TO 305
      IF(DPDX.GT.DPLAST) IXSTAR=2
  305 GO TO (21,22,23,23), IX
   21 IF(X.LT.X1) GO TO 23
      IX=2
      KI=KI*10
      DELX=DELX/10.0
      Z41=Z34*DELX
      PGRT=PGRT**0.2
      GO TO 23
   22 IF(MOD(KI,10).NE.0) GO TO 23
      IF(X.LT.X2) GO TO 23
      IX=3
      KI=KI/10
      DELX=DELXS
      Z41=Z34*DELX
      PGRT=PGRT**5
      PG1=DPDX*PGRT
      PG2=1.01  *PG1
   23 KI=KI+1
      DPLAST=DPDX
      AM2LST=AMM2
      DPDX=PG1
      X=XO+ FLOAT(KI)*DELX
      KX=KX+1
C
C      BEGINNING OF P ITERATION LOOP
C
      HDELX=0.5  *DELX
      XHW=X-HDELX
      GO TO (41,42,14), IXTHW
   41 IF(X.LE.XTW1) GO TO 14
      IXTHW=2
   42 IF(X.GT.XTW2) GO TO 43
```

```
      THETAW=U3+U4*COS(U5*(X-XTW1))
      GO TO 14
   43 IXTEW=3
      THETAW=TW2
   14 CALL GEOM(XHW)
      SIGBAR=SIGMAW
      TANBAR=TANTHP
      PHW=P+DPDX*HDELX
      E11(1)=1.0
      E12(1)=0
      E21(1)=0
      E22(1)=1.0
      F1(1)=0
      F2(1)=0
      Y1=Z35*SIGMAW**2
      Y2=2.0   *Y1
      Y3=4.0   *Y1
      Y4=8.0   *Y1
      Y5=Z34*SIGMAW
      Y6=Z41*SIGMAW
      Y7=Y1*PR
      Y8=4.0   *Y7
      Y9=Z7*DPDX
      DO 6 L=2,100
      G1=PHW*ETA(L)
      G2=G1*W(L)
      G3=Y5*T(L,1)
      G4=T(L,1)**Z32
      G5=Z33*T(L,1)
      G6=OMEGA*ETA(L)
      G7=T(L+1,1)-T(L-1,1)
      G8=G6*G7
      G9=4.0   *ETA(L)
      G10=G9*T(L,1)
      G11=U(L+1,1)-U(L-1,1)
      G12=T(L,1)**OMEGA
      G13=ETA(L)*G12
      G14=DELETA*T(L,1)
      G15=2.0   *ETA(L)
      G16=G15*T(L,1)
      G17=DELX*T(L,1)
      G18=G1*U(L,1)
      G19=DELX*W(L)
      G20=Y6*T(L,1)
      G21=Y9*ETA(L)
C
C     CALCULATION OF THE MATRIX ELEMENTS.
C
      A11=-G2/G3+G4*(G5+G8+G10)/Y4
      A12=G6*G4*G11/Y4
```

```
      A21=G13*G11/Y2
      A22=-G2/G3+G4*(G14+G8+G16)/Y8
C
      B11=G18/G17+G13/Y1
      B12=0
      B21=0
      B22=G18/G17+G13/Y7
C
      C11=G2/G3-G4*(G5+G8-G10)/Y4
      C12=-A12
      C21=-A21
      C22=G2/G3-G4*(G14+G8-G16)/Y8
C
      D1=G1*(Y5*U(L,1)**2-G19*G11)/G20-G21/Z8
     *  +G12*(DELETA*G11+G15*(U(L+1,1)-2.0D0*U(L,1)+U(L-1,1)))/Y3
      D2=G1*(Y5*U(L,1)*T(L,1)-G19*G7)/G20+G21*U(L,1)/GAMMA
     *  +G12*(DELETA*G7+G15*(T(L+1,1)-2.0D0*T(L,1)+T(L-1,1)))/Y8
      QQ11= B22-C21*E12(L-1)-C22*E22(L-1)
      QQ12=-B12+C11*E12(L-1)+C12*E22(L-1)
      QQ21=-B21+C21*E11(L-1)+C22*E21(L-1)
      QQ22= B11-C11*E11(L-1)-C12*E21(L-1)
      DENOM=QQ11*QQ22-QQ21*QQ12
      Q11=QQ11/DENOM
      Q12=QQ12/DENOM
      Q21=QQ21/DENOM
      Q22=QQ22/DENOM
      PART1=C11*F1(L-1)+C12*F2(L-1)+D1
      PART2=C21*F1(L-1)+C22*F2(L-1)+D2
      E11(L)=Q11*A11+Q12*A21
      E12(L)=Q11*A12+Q12*A22
      E21(L)=Q21*A11+Q22*A21
      E22(L)=Q21*A12+Q22*A22
      F1(L) =Q11*PART1+Q12*PART2
      F2(L) =Q21*PART1+Q22*PART2
      CALL GEOM(X)
      SW2=SIGMAW**2
      TOP= COS(THETAP)*T(101 ,1)**CHMPH
      BOTTOM=CFBOT*(P+DPDX*DELX)*SIGMAW
      UCF=TOP*UCFTOP/BOTTOM
      TCF=TOP*TCFTOP/BOTTOM
      FN1=U(101 ,1)-U(100  ,1)-F1(100   )
      EM11=E11(100   )-(2.0  +UCF)/UCF
      EM12=E12(100   )
      IF(IBC.NE.1) GO TO 7
      FN2=-(2.0  *THETAW/TCF)+T(101 ,1)-T(100   ,1)-F2(100   )
      EM21=E21(100   )
      EM22=E22(100   )-(2.0  +TCF)/TCF
      GO TO 8
    7 FN2=T(101 ,1)-T(100   ,1)-F2(100   )
      EM21=E21(100   )+4.0  *PR*U(101 ,1)/UCF
```

```
      EM22=E22(100   )-1.0
    8 DENOM=EM11*EM22-EM21*EM12
      U(101 ,2  )=(EM22*FN1-EM12*FN2)/DENOM
      T(101 ,2  )=(EM11*FN2-EM21*FN1)/DENOM
      UI=U(101,2)
      TI=T(101,2)
      E11(101)=UI/TI
      E12(101)=UI*E11(101)
      E22(101)=TI/UI**2
      DO 9 I=1,100
      U(101-I,2)  =E11(101-I)*UI+E12(101-I)*TI+F1(101-I)
      UI=U(101-I,2)
      IF(UI.LE.0.0.AND.X.GT.0.0) GO TO 85
      T(101-I,2)  =E21(101-I)*UI+E22(101-I)*TI+F2(101-I)
      TI=T(101-I,2)
      E11(101-I)=UI*ETA(101-I)/TI
      E22(101-I)=ETA(101-I)*TI/UI**2
    9 E12(101-I)=UI*E11(101-I)
      ETTBU2=4.0  *E22(2)
      S4(1)=0
      HFLUX=U(2,2)  *(ETA(2)+E12(2))*4.0
      S4(2)=Z23*(8.0  *E11(2)-E11(3))
      U2ETAT=4.0  *E12(2)
      DO 10 L=3,101
      SCALE=4-2*MOD(L,2)
      IF(L.EQ.101 ) SCALE=1
      ETTBU2=ETTBU2+SCALE*E22(L)
      U2ETAT=U2ETAT+SCALE*E12(L)
      HFLUX=HFLUX+U(L,2)  *(ETA(L)+E12(L))*SCALE
   10 S4(L)=S4(L-2)+Z13*(E11(L-2)+4.0  *E11(L-1)+E11(L))
      AMSC=Z43*U2ETAT
      AMM2=0.5  *Z7*Z13*ETTBU2
      AMM2AV=0.5  *(AMM2+AM2LST)
      IF(IGETA.EQ.0.AND.AMM2.LT.0.5) GO TO 302
      PNEW=A/(S4(101 )*SW2)
      PXTRAP=P+DPDX*DELX
      ARCHI=0
      SHERI=0
      CONDI=0
      GENRI=0
      PSGW2=PNEW*SW2
      SGDX=SIGMAW/DELX
      HFLUX=PSGW2*Z13*HFLUX
      THCOEF=PSGW2*(1.0  +Z8*AMSC)
      UTERM=(U(101,2)-U(100,2)+U(101,1)-U(100,1))
      TTERM=(0.5*(T(101,2)+T(101,1)))**OMEGA
      Q=(TTERM*((T(101,2)-T(100,2)+T(101,1)-T(100,1))/PR
     *  +UTERM* (U(101,2)+U(101,1))))/(8*Z33)
      E11(101 )=PSGW2*S4(101 )
      E12(101 )=0
```

```
      E12(1)=0
      DO 2 L=2,100
      E11(L)=PSGW2*S4(L)
    2 E12(L)=0.5*(SGDX*(T(L,2)  *S4(L)/ETA(L))*ALOG(S3(L)/E11(L))+W(L))
      GAMMAP=GAMMA*PHW
      FACT=Z8/(Z7*B*SIGBAR)
      SIGDP=SIGMAW*DPDX
      ARCH(1)=0
      COND(1)=0
      SHER(1)=0
      GENR(1)=0
      PGRD(1)=0
      DO 3 L=2,100
      DUDN=(U(L+1,2)  -U(L-1,2)  +U(L+1,1)-U(L-1,1))/Z34
      DVDN=(E12(L+1)-E12(L-1))/Z33+TANBAR*(0.5  *(U(L,2)  +U(L,1))
     *     +ETA(L)*DUDN)
      DTDN=(T(L+1,2)  -T(L-1,2)  +T(L+1,1)-T(L-1,1))/Z34
      D2UDN2=(U(L+1,2)  -2.0  *U(L,2)  +U(L-1,2)
     *     +U(L+1,1)-2.0  *U(L,1)+U(L-1,1))/Z42
      D2TDN2=(T(L+1,2)  -2.0  *T(L,2)  +T(L-1,2)
     *     +T(L+1,1)-2.0  *T(L,1)+T(L-1,1))/Z42
      AMACH=0.5  *RT2GM1*(U(    L,2)  / SQRT(T(    L,2)  )
     *                   +U(    L,  1)/ SQRT(T(    L,  1)))
      AMACH2= AMACH**2
      SAME=T(L,2)  +ETA(L)*OMEGA*DTDN
      V=E12(L)+TANTHP*ETA(L)*U(L,2)
      ARCH(L)=GAMMAP*       (V*(1.0  -ETA(L)*DUDN/U(L,2)  )+ETA(L)*DVDN)
     *     /U(L,2)
      TOMF=FACT*T(L,2)  **Z32
      SHER(L)=-TOMF*(DUDN*SAME+T(L,2)  *ETA(L)*D2UDN2)/AMACH2
      COND(L)=(TOMF*(DTDN*SAME+T(L,2)  *ETA(L)*D2TDN2)*U(L,2)  /
     *     (T(L,2)  *PR))/AMACH2
      GENR(L)=2.0  *TOMF*U(L,2)  *ETA(L)*DUDN**2/AMACH2
      PGRD(L)=(1.0  -AMACH2)*ETA(L)*SIGDP/AMACH2
      SCALE=4-2*MOD(L,2)
      ARCHI=ARCHI+SCALE*ARCH(L)
      SHERI=SHERI+SCALE*SHER(L)
      CONDI=CONDI+SCALE*COND(L)
    3 GENRI=GENRI+SCALE*GENR(L)
      ARCH(101 )=0
      AMACH=0.5  *RT2GM1*(U(101 ,2)  / SQRT(T(101 ,2))
     *                   +U(101 ,  1)/ SQRT(T(101 ,  1)))
      AMACH2=AMACH**2
      PGRD(101)=SIGDP*(1.0-AMACH2)/AMACH2
      ARCHI = GAMMAP*TANBAR
      SHER(101 )=      -FACT*B*SW2*(Z7*DPDX/Z8+PHW*U(101 ,1)*
     *     (U(101 ,2)  -U(101 ,1))/(T(101 ,1)*DELX))/AMACH2
      DUDNSQ=((U(101 ,1)-U(100    ,1)+U(101 ,2)  -U(100    ,2)  )/Z33)**2
      COND(101 )=      FACT*(U(101 ,2)  /T(101 ,2)  )*(-2.0  *T(101 ,1)
     *     **OMEGA*DUDNSQ+B*SW2*(-Z7*U(101 ,1)*DPDX/GAMMA+PHW*U(101 ,1)
```

```
     *      *(T(101 ,2)  -T(101 ,1))/(T(101 ,1)*DELX)))/AMACH2
      GENR(101 )=FACT*U(101 ,2)  *2.0  *T(101 ,2)  **Z32*DUDNSQ/AMACH2
      SHERI=Z13*(SHERI+SHER(101 ))
      CONDI=Z13*(CONDI+COND(101 ))
      GENRI=Z13*(GENRI+GENR(101 ))
      DPNUM=ARCHI-SHERI-CONDI-GENRI
      PGNP1=DPNUM/(SIGBAR*(AMM2AV-0.5  ))
C     THE FOLLOWING STATEMENT IS USED TO SUPPRESS OSCILLATIONS IN DPDX
      IF(X.GT.10.0)  PGNP1= (PGNP1+DPLAST)*0.5
      AEFF=2.0  *A*T(1,2)  /(PNEW*U(1,2))
      DLSTR=SIGMAW- SQRT(AEFF)
      IF(MOD(LC,48).EQ.0) WRITE(6,217) A
      WRITE(6,223)    X,DPDX,PGNP1,PXTRAP,PNEW,U(1,2 )  ,T(1,2),
     *                        ARCHI,SHERI,CONDI,GENRI,DPNUM,AMSQ,
     *                        HFLUX,SIGBAR,SIGMAW,TANBAR,TANTHP,AMM2,
     *                        U(101 ,2)  ,T(101 ,2)  ,AEFF,DLSTR,C
      LC=LC+4
      GO TO (51,600,51,620), IPG
  600 GO TO (601,602,19),ITER
  601 AMM2A=AMM2
      DPNUMA=DPNUM
      DPG1=PGNP1-PG1
      ITER=2
      DPDX=PG2
      GO TO 14
  602 AMM2B=AMM2
      DPNUMB=DPNUM
      ITER=3
      IF(ISW.EQ.2) GO TO 599
      BR1=(DPNUMB-DPNUMA)/(AMM2B-AMM2A)+DPNM1/(0.5  -AMM21)
      BR2=DPNM1-DPNUMA+DPNM1*AMM21/(0.5  -AMM21)+(DPNUMB-DPNUMA)*AMM2A/(
     *AMM2B-AMM2A)
      AMM2C=BR2/BR1
      DPDX=(PG1*(AMM2B-AMM2C)+PG2*(AMM2C-AMM2A))/(AMM2B-AMM2A)
      GO TO 14
  620 IF(ITER.GT.2) GO TO 628
      IF(ITER.EQ.2) GO TO 625
      ITER=2
      PN1=PNEW
      DLP1=PN1-(P+PG1*DELX)
      DPDX=PG2
      GO TO 14
  625 PN2=PNEW
      ITER=3
      DLP2=PN2-(P+PG2*DELX)
  626 PG=((PG1*PN2-PG2*PN1)-P*(PG1-PG2))/
     *    ((PN2-PN1)+DELX*(PG1-PG2))
      IF(PG.GT.1.0   ) PG=1.0E-03*PG
      ABDLP1= ABS(DLP1)
      ABDLP2= ABS(DLP2)
```

```
      IF(AMIN1(ABDLP1,ABDLP2).EQ.ABDLP1) GO TO 627
      DLP1=DLP2
      PG1=PG2
      PN1=PN2
  627 PG2=PG
      DPDX=PG2
      GO TO 14
  628 PN2=PNEW
      DLP2=PN2-(P+PG2*DELX)
      IF( ABS(DLP2)/P.LE.1.0E-03) GO TO 629
      ITER=ITER+1
      IF(ITER.LE.10) GO TO 626
      WRITE(6,210)
      IF(IGOTA.EQ.0) GO TO 304
      GO TO 13
  629 IF(X.GT.XIPG ) IPG=1
      GO TO 19
   51 IF( ITER.GT.2) GO TO 18
      IF(ITER.EQ.2) GO TO 15
      ITER=2
      DPG1=PGNP1-PG1
      DPDX=PG2
      GO TO 14
   15 DPG2=PGNP1-PG2
      ITER=3
   16 PG=(PG1*DPG2-PG2*DPG1)/(DPG2-DPG1)
      IF(PG.GT.1.0  ) PG=1.0E-03*PG
      ABDPG1= ABS(DPG1)
      ABDPG2= ABS(DPG2)
      IF(AMIN1(ABDPG1,ABDPG2).EQ.ABDPG1) GO TO 17
      DPG1=DPG2
      PG1=PG2
   17 PG2=PG
      DPDX=PG2
      GO TO 14
   18 DPG2=PGNP1-PG2
      IF( ABS(DPG2/DPLAST).LE.1.0E-03) GO TO 19
      ITER=ITER+1
      IF(ITER.LE.10) GO TO 16
      WRITE(6,210)
      IF(IGOTA.EQ.0) GO TO 304
      GO TO 13
   19 P=PXTRAP
      WRITE(6,224)
      PGRT=DPDX/DPLAST
      IF(AMM2.LT.AMM2MN) AMM2MN=AMM2
      DO 11 L=1,101
      W(L)=E12(L)
   11 S3(L)=E11(L)
      IF(IGOTA.NE.0) GO TO 90
```

```
      IF(DPDX.GT.0.0) GO TO 27
      GO TO (91,92), IXSTAR
   91 IF(P.GT.0.1) GO TO 5
      GO TO 304
   92 IF(DPDX.GT.DPLAST) GO TO 5
      IF(KX-KX1.NE.1) GO TO 303
      KX1=KX
      IF(KX-KXC.GE.3) GO TO 300
      GO TO 5
  303 KX1=KX
      KXC=KX
      XCUT=X
      GO TO 5
  300 WRITE(6,203)
      GO TO 304
  302 WRITE(6,204) AMM2
  304 A1=A
      XCUT=X-1.01   *DELX
      GO TO 28
   27 A0=A
      WRITE(6,207)
   28 IF( ABS(A0-A1).LE.ATEST) IGOTA=1
      GO TO 1
C
C     END OF A ITERATION LOOP
C
   13 IF(MORE.NE.0) GO TO 500
      STOP
   90 IF(DPDX.GT.0.0) GO TO 99
      ETR=ETR+C*DELX
      IF(NPRO.EQ.0) CALL OUTPUT
      GO TO (93,94,98,93), IPG
   93 IF(X.GE.XMAX) GO TO 13
      IF(X.GE.XCUT) GO TO 931
      IF((AMM2-AMM2MN).GT.0.0.AND.X.GT.-0.5  ) GO TO 931
      GO TO 5
  931 IPG=2
      AMM21=AMM2
      DPNM1=DPNUM
      GO TO 5
   94 IF(AMM2.LT.0.49999.AND.DPNUM.GT.0.0 ) GO TO 95
      IF(X.GE.XMAX) GO TO 13
      GO TO 5
   95 ISW=2
      GO TO 5
  999 IPG=3
      BR11=(DPNUMB-DPNUMA)/(PG2-PG1)
      BR12=-BR11*PG1+DPNUMA
      BR21=(AMM2B-AMM2A)/(PG2-PG1)
      BR22=-BR21*PG1+AMM2A
      BRB=SIGBAR*(AM2LST+BR22-1.0   )-2.0   *BR11
      DPDX=-(BRB+ SQRT(BRB**2+8.0   *BR21*BR12*SIGBAR))/(2.0   *BR21*SIGBAR)
      PG2=DPDX
      GO TO 14
   98 IF(X.LT.XMAX) GO TO 5
      GO TO 13
   99 WRITE(6,205)
      GO TO 13
   85 J=ICI-1
      WRITE(6,206) J,U(J,2)
      GO TO 13
  203 FORMAT(' DPDX IS DECREASING FOR TOO MANY STEPS')
  204 FORMAT(' AMM2=',1PE14.6)
  205 FORMAT(' DPDX.GT.0.0 ON PROFILE PASS')
  206 FORMAT(' NEGATIVE VELOCITY ENCOUNTERED AT U(',I3,',K+1)=',1PE13.6)
  207 FORMAT(' TOO LITTLE MASS FLOW')
  210 FORMAT(' TOO MANY ITERATIONS ON P')
  217 FORMAT('1A=',1PE16.6//)
  223 FORMAT(0PF12.2,4X,1P6E16.6,3(/16X,6E16.6))
  224 FORMAT(1X)
      END
```

```
CCCC
      SUBROUTINE GEOM(Y)
      REAL DAY(3)
      COMMON A,ABDLP1,ABDLP2,ABDPG1,ABDPG2,AEFF,ALPHT,ALPHU,AMACH,
     *AMACH2,AMM2,AMM2A,AMM2AV,AMM2B,AMM2C,AMM2MN,AMM21,AMSQ,AM2LST,
     *ARCHI,ATEST,A0,A1,A11,A12,A21,A22
      COMMON B,BOTTOM,BRB,BR1,BR11,BR12,BR2,BR21,BR22,B11,B12,B21,B22
      COMMON C,CFBOT,CONDI,CPRO,C11,C12,C21,C22
      COMMON D,DELETA,DELX,DELXS,DENOM,DFBRDX,DLP1,DLP2,DLSTR,DPDX,DPG1,
     *DPG2,DPLAST,DPNM1,DPNUM,DPNUMA,DPNUMB,DTON,DUDN,DUDNSQ,DVDN,D1,D2,
     *D2TDN2,D2UDN2,DAY
      COMMON EM11,EM12,EM21,EM22,ETTBU2,E11MAX
      COMMON FACT,FN1,FN2
      COMMON GAMMA,GAMMAP,GENRI,G1,G10,G11,G12,G13,G14,G15,G16,G17,G18,
     *G19,G2,G20,G21,G3,G4,G4BGM1,G5,G6,G7,G8,G9
      COMMON HDELX,HFLUX,HTR
      COMMON IBC,IETAPR,IGOTA,IPG,ISW,ITER,ITERA,IX,IXSTAR,IXTHW
      COMMON K,KI,KP1,KX,KX0,KX1
      COMMON LC,MORE,NPRO,NRUN
      COMMON OHMPH,OMEGA,O1,O2,O3,O4,O5
      COMMON P,PART1,PART2,PDA,PG,PGNP1,PGRT,PG1,PG2,PHW,PI3,PNEW,PN1,
     *PN2,PR,PSGW2,PSI,PXTRAP
      COMMON Q,QQ11,QQ12,QQ21,QQ22,Q11,Q12,Q21,Q22
      COMMON RADDEG,RTPB2,RT2BZ7,RT2GM1,R1,RIST1,RIST2,R12
      COMMON SAME,SA1,SC1,SGDX,SHERI,SIGBAR,SIGDP,SIGMAW,SW2,SW3,SW4
      COMMON TANBAR,TANTHP,TAU,TCF,TCFTOP,TFCOEF,THETAP,THETAW,THETA1,
     *THETA2,TOMF,TOP,TTERM,TW2
      COMMON UCF,UCFTOP,UTERM,U2ETAT,V
      COMMON X,XCUT,XHW,XIPG,XMAX,XPLAST,XPRINT,XTW1,XTW2,X0,X1,X2
      COMMON Y1,Y2,Y3,Y4,Y5,Y6,Y7,Y8,Y9
      COMMON Z1,Z10,Z11,Z12,Z13,Z15,Z16,Z2,Z23,Z31,Z32,Z33,Z34,Z35,Z41,
     *Z42,Z43,Z5,Z7,Z8
      COMMON ETA(101),E11(101),E12(101),E21(101),E22(101),F1(101),
     *F2(101),S3(101),S4(101),W(101)
      COMMON T(101,2),U(101,2)
      DIMENSION ARCH(101),PGRD(101),COND(101),SHER(101),GENR(101)
      EQUIVALENCE (ARCH,E21),(PGRD,E22),(COND,F1),(SHER,F2),(GENR,S4)
      IF(Y.GT.RIST1) GO TO 1
      SIGMAW=Y*Z1+Z10
      THETAP=THETA1
      GO TO 3
    1 IF(Y.GE.RIST2) GO TO 2
      C= SQRT(R12-Y**2)
      SIGMAW=Z11-C
      THETAP= ATAN(Y/C)
      GO TO 3
    2 SIGMAW=Y*Z2+Z12
      THETAP=THETA2
    3 TANTHP= TAN(THETAP)
      RETURN

      END
```

```
CCCC
      SUBROUTINE INPUT
      REAL CAY(3)
      COMMON A,ABDLP1,ABDLP2,ABDPG1,ABDPG2,AEFF,ALPHT,ALPHU,AMACH,
     *AMACH2,AMM2,AMM2A,AMM2AV,AMM2B,AMM2C,AMM2MN,AMM21,AMSC,AM2LST,
     *ARCHI,ATEST,A0,A1,A11,A12,A21,A22
      COMMON B,BOTTOM,BRB,BR1,BR11,BR12,BR2,BR21,BR22,B11,B12,B21,B22
      COMMON C,CFBOT,CONDI,CPKU,C11,C12,C21,C22
      COMMON D,DELETA,DELX,DELXS,DENOM,DFBRCX,DLP1,DLP2,DLSTR,DPDX,DPG1,
     *DPG2,DPLAST,DPNMI,DPNUM,DPNUMA,DPNUMB,DTDN,DUDN,DUDNSC,DVDN,D1,D2,
     *D2TDN2,D2UDN2,DAY
      COMMON EM11,EM12,EM21,EM22,ETTEG2,E11MAX
      COMMON FACT,FN1,FN2
      COMMON GAMMA,GAMMAP,GENRI,G1,G10,G11,G12,G13,G14,G15,G16,G17,G18,
     *G19,G2,G20,G21,G3,G4,G4BGM1,G5,G6,G7,G8,G9
      COMMON HDELX,HFLUX,HTR
      COMMON IBC,IETAPR,IGOTA,IPG,ISW,ITER,ITERA,IX,IXSTAR,IXTHW
      COMMON K,KI,KP1,KX,KXO,KX1
      COMMON LC,MORE,NPRO,NRUN
      COMMON OHMPH,OMEGA,O1,O2,O3,O4,O5
      COMMON P,PART1,PART2,PDA,PG,PGNP1,PGRT,PG1,PG2,PHW,P13,PNEW,PN1,
     *PN2,PR,PSGW2,PSI,PXTRAP
      COMMON Q,QQ11,QQ12,QQ21,QQ22,Q11,Q12,Q21,Q22
      COMMON RADDEG,RTPB2,RTZBZ7,RT2GM1,R1,R1ST1,R1ST2,R12
      COMMON SAME,SA1,SC1,SGDX,SHERI,SIGBAR,SIGDP,SIGMAW,SW2,SW3,SW4
      COMMON TANBAR,TANTHP,TAU,TCF,TCFTOP,THCOEF,THETAP,THETAW,THETA1,
     *THETA2,TOME,TOP,TTERM,TW2
      COMMON UCF,UCFTOP,UTERM,U2ETAT,V
      COMMON X,XCUT,XHW,XIPG,XMAX,XPLAST,XPRINT,XTW1,XTW2,X0,X1,X2
      COMMON Y1,Y2,Y3,Y4,Y5,Y6,Y7,Y8,Y9
      COMMON Z1,Z10,Z11,Z12,Z13,Z15,Z16,Z2,Z23,Z31,Z32,Z33,Z34,Z35,Z41,
     *Z42,Z43,Z5,Z7,Z8
      COMMON ETA(101),E11(101),E12(101),E21(101),E22(101),F1(101),
     *F2(101),S3(101),S4(101),W(101)
      COMMON T(101,2),U(101,2)
      DIMENSION ARCH(101),PGRD(101),COND(101),SHER(101),GENR(101)
      EQUIVALENCE (ARCH,E21),(PGRD,E22),(COND,F1),(SHER,F2),(GENR,S4)
      DIMENSION HTRSFR(6,2)
      DATA HTRSFR/48HHEAT TRANSFER IS ALLOWEDADIABATIC-WALL CASE      /
      READ(5,100) NRUN,IBC,MORE,NPRO,IETAPR
      IF(IETAPR.LE.0) IETAPR=1
C     NRUN  -- RUN NUMBER
C     IBC   -- =1, HEAT TRANSFER IS ALLOWED; =2, ADIABATIC-WALL CASE
C     MORE  -- ANOTHER RUN TO FOLLOW IF NONZERO
C     NPRO  -- PROFILES ARE NOT PRINTED IF NONZERO
C     IETAPR-- PRINT PROFILES AT ETA(1), ETA(1+IETAPR), ETA(1+2*IETAPR), ETC.
      READ(5,101) R1,THETA1,THETA2,TW2,GAMMA,
     *              OMEGA,PR,B,XIPG,ATEST,
     *              A0,A1,XCUT,XPRINT,DELX,
     *              X0,X1,X2,XMAX,ALPHU,
```

```
     *              ALPHT,XTW1,XTW2
C      R1     -- LONGITUDINAL RADIUS OF CURVATURE OF THE THROAT EXPRESSED IN UNITS
C                OF THE TRANSVERSE THROAT RADIUS
C      THETA1-- HALF-ANGLE OF THE CONVERGENT CONE (NEGATIVE)
C      THETA2-- HALF-ANGLE OF THE DIVERGENT CONE
C      TW2    -- WALL-TO-STAGNATION TEMPERATURE RATIO DOWNSTREAM OF XTW2
C      GAMMA -- SPECIFIC-HEAT RATIO
C      OMEGA -- TEMPERATURE EXPONENT IN VISCOSITY LAW
C      PR     -- PRANDTL NUMBER
C      B      -- RESERVOIR REYNOLDS NUMBER
C      XIPG   -- IF XO.LE.XIPG, IPG=4 AND DP/DX BETWEEN XO AND XIPG IS
C                FOUND BY CONSERVING MASS
C                IF X .GT.XIPG, IPG=1 AND DP/DX IS FOUND BY USING THE STREAMTUBE
C                ALGORITHM
C                DOWNSTREAM OF THE SADDLE POINT THE STREAMTUBE ALGORITHM IS ALWAYS
C                USED -- IPG=3 IN THAT CASE
      IF(THETA1.GT.0.0) THETA1=-THETA1
C      ATEST  -- TOLERANCE ALLOWED FOR A
C      AO     -- INITIAL LOWER BOUND OF A
C      A1     -- INITIAL UPPER BOUND OF A
C      XCUT   -- SWITCH POINT FOR STRAIGHT LINE EXTRAPOLATION THROUGH THE
C                SADDLE POINT (USED ONLY FOR RUNS WHERE AO=A1)
C      XPRINT-- PROFILES PRINTED IN INTERVALS OF XPRINT
C      DELX   -- INITIAL DELTA X
C      XO     -- INITIAL X VALUE (NEGATIVE)
C      X1     -- CUT STEP SIZE BY 10 WHEN X.GE.X1
C      X2     -- RESTORE ORIGINAL STEP SIZE WHEN X.GE.X2
C                IF X1.GE.X2, THE INITIAL STEP SIZE IS ALWAYS USED
C      XMAX   -- CALCULATION STOPS FOR X.GE.XMAX
C      ALPHU -- VELOCITY ACCOMMODATION COEFFICIENT
C      ALPHT -- TEMPERATURE ACCOMMODATION COEFFICIENT
C      XTW1   -- IF X.LT.XTW1, THETAW=1
C      XTW2   -- IF X.GT.XTW2, THETAW=TW2
C                THETAW FOLLOWS A COSINE BEHAVIOR BETWEEN XTW1 AND XTW2
      CALL DATE3(DAY)
C     DATE3 IS A ROUTINE WHICH RETURNS THE DAY, MONTH AND YEAR
      WRITE(6,200) DAY,NRUN,IBC,MCRE,NPRO,IETAPR
      WRITE(6,201)
      WRITE(6,202) R1,THETA1,THETA2,TW2,GAMMA,
     *                OMEGA,PR,B,XIPG,ATEST,
     *                AO,A1,XCUT,XPRINT,DELX,
     *                XO,X1,X2,XMAX,ALPHU,
     *                ALPHT,XTW1,XTW2
      WRITE(6,203) (HTRSFR(I,IBC),I=1,6)
      WRITE(6,204)
      RETURN
  100 FORMAT(A4,19I4)
  101 FORMAT(5E14.8)
  200 FORMAT(1H1,3A4//1X,'NRUN=',A5,4X,'IBC=',I2,4X,'MCRE=',I2,4X,
     *'NPRO=',I2,4X,'IETAPR=',I3//)
  201 FORMAT(13X,'R1',16X,'THETA1',14X,'THETA2',16X,'TW2',15X,'GAMMA'
     */11X,'OMEGA',17X,'PR',18X,'B',18X,'XIPG',15X,'ATEST'
     */13X,'AO',18X,'A1',17X,'XCUT',15X,'XPRINT',15X,'DELX'
     */13X,'XO',18X,'X1',18X,'X2',17X,'XMAX',15X,'ALPHU'
     */11X,'ALPHT',16X,'XTW1',16X,'XTW2'/)
  202 FORMAT(1P5E20.6)
  203 FORMAT(//1X,6A4//)
  204 FORMAT(' THE OUTPUT FORMAT OF THE P ITERATION PRINTOUT FOLLOWS'//
     *9X,'X',14X,'DPDX',11X,'PGNP1',11X,'PXTRAP',11X,'PNEW',10X,
     *'U(1,KP1)',8X,'T(1,KP1)'/
     *23X,'ARCH1',11X,'SHER1',11X,'COND1',11X,'GENR1',11X,'DPNUM',12X,
     *'AMSQ'/
     *23X,'FFLUX',11X,'SIGBAR',10X,'SIGMAW',10X,'TANBAR',10X,'TANTHP',
     *11X,'AMM2'/
     *21X,'U(101,KP1)',6X,'T(101,KP1)',5X,'AEFF',11X,'DLSTR',13X,'Q'//
     *' A DESCRIPTION OF THE VARIABLES PRINTED ABOVE IS CONTAINED IN THE
     * PROGRAM REPORT'/)
      END
```

```
CCCC
      SUBROUTINE INIT
      REAL CAY(3)
      COMMON A,ABCLP1,ABCLP2,ABDPG1,ABDPG2,AEFF,ALPHT,ALPHU,AMACH,
     *AMACH2,AMM2,AMM2A,AMM2AV,AMM2B,AMM2C,AMM2MN,AMM21,AMSQ,AM2LST,
     *ARCHI,ATEST,A0,A1,A11,A12,A21,A22
      COMMON B,BOTTOM,BRB,BR1,BR11,BR12,BR2,BR21,BR22,B11,B12,B21,B22
      COMMON C,CFBOT,CONDI,CPKU,C11,C12,C21,C22
      COMMON D,DELETA,DELX,DELXS,DENOM,DFBRDX,DLP1,DLP2,DLSTR,DPDX,DPG1,
     *DPG2,DPLAST,DPNM1,DPNUM,DPNUMA,DPNUMB,DTDN,DUDN,DUDNSQ,DVDN,D1,D2,
     *D2TDN2,D2UDN2,DAY
      COMMON EM11,EM12,EM21,EM22,ETTBU2,E11MAX
      COMMON FACT,FN1,FN2
      COMMON GAMMA,GAMMAP,GENR1,G1,G10,G11,G12,G13,G14,G15,G16,G17,G18,
     *G19,G2,G20,G21,G3,G4,G4BGM1,G5,G6,G7,G8,G9
      COMMON HDELX,HFLUX,HTR
      COMMON IBC,IETAPR,IGOTA,IPG,ISW,ITER,ITERA,IX,IXSTAR,IXTHW
      COMMON K,KI,KP1,KX,KX0,KX1
      COMMON LC,MORE,NPRG,NRUN
      COMMON OMMPH,OMEGA,O1,O2,O3,O4,O5
      COMMON P,PART1,PART2,PDA,PG,PGMP1,PGRT,PG1,PG2,PHW,PI3,PNEW,PN1,
     *PN2,PR,PSQW2,PSI,PXTRAP
      COMMON Q,QQ11,QQ12,QQ21,QQ22,Q11,Q12,Q21,Q22
      COMMON RADDEG,RTPB2,RT2BZ7,RT2GM1,R1,R1ST1,R1ST2,R12
      COMMON SAME,SA1,SC1,SGDX,SHER1,SIGBAR,SIGDP,SIGMAW,SW2,SW3,SW4
      COMMON TANBAR,TANTHP,TAU,TCF,TCFTOP,THCOEF,THETAP,THETAW,THETA1,
     *THETA2,TOMF,TOP,TTERM,TW2
      COMMON UCF,UCFTOP,UTERM,U2ETAT,V
      COMMON X,XCL1,XHW,XIPG,XMAX,XPLAST,XPRINT,XTW1,XTW2,X0,X1,X2
      COMMON Y1,Y2,Y3,Y4,Y5,Y6,Y7,Y8,Y9
      COMMON Z1,Z10,Z11,Z12,Z13,Z15,Z16,Z2,Z23,Z31,Z32,Z33,Z34,Z35,Z41,
     *Z42,Z43,Z5,Z7,Z8
      COMMON ETA(101),E11(101),E12(101),E21(101),E22(101),F1(101),
     *F2(101),S3(101),S4(101),W(101)
      COMMON T(101,2),U(101,2)
      DIMENSION ARCH(101),PGRD(101),COND(101),SHER(101),GENR(101)
      EQUIVALENCE (ARCH,E21),(PGRD,E22),(COND,F1),(SHER,F2),(GENR,S4)
C     INITIALIZATION OF CONSTANTS.
      IF(XTW1.GE.XTW2) GO TO 1
      O3=(1.0+TW2)*0.5
      O4=(1.0-TW2)*0.5
      O5=3.141593/(XTW2-XTW1)
    1 RADDEG=57.29578
      RTPB2=1.253314
      X1=X1-1.0E-05
      X2=X2-1.0E-05
      IGOTA=0
      ITERA=0
      XPLAST=X0
      R12=R1**2
```

```
      THETA1=THETA1/RADDEG
      THETA2=THETA2/RADDEG
      DELETA=1.0E-02
      Z1= TAN(THETA1)
      Z2= TAN(THETA2)
      Z5= COS(THETA1)
      Z7=GAMMA-1.0
      Z8=2.0  *GAMMA
      IF( ABS(A0-A1).LE.ATEST) IGOTA=1
      RT2GM1= SQRT(2.0  /Z7)
      G4BGM1=4.0  *GAMMA/Z7
      R1ST1=R1* SIN(THETA1)
      R1ST2=R1* SIN(THETA2)
      Z10=1.0  +R1*(1.0  -Z5)-Z1*R1ST1
      Z11=1.0  +R1
      Z12=1.0  +R1*(1.0  - COS(THETA2))-Z2*R1ST2
      DELXS=DELX
      Z13=DELETA/3.0
      RTZ8Z7= SQRT(Z8/Z7)
      Z15=RTZ8Z7*Z5/B
      Z23=DELETA/12.0
      SA1=((2.0  -ALPHU)*RTPB2)/ALPHL
      SC1=((2.0  -ALPHT)*RTPB2*Z8)/(ALPHT*PR*(GAMMA+1.0  ))
      CPKL=SA1*Z15
      HCFTOP=RTZ8Z7*SA1
      CFBCT=B*DELETA
      TCFTOP=RTZ8Z7*SC1
      OHMPH=OMEGA+0.5
      Z31=DELETA**2
      Z32=OMEGA-1.0
      Z33=2.0  *DELETA
      Z34=4.0  *DELETA
      Z35=8*Z31
      Z42=2.0  *Z31
      Z43=Z33/(3.0  *Z7)
      RETURN
      END
```

```
CCCC
      SUBROUTINE START
      REAL DAY(3)
      COMMON A,ABDLP1,ABDLP2,ABDPG1,ABDPG2,AEFF,ALPHT,ALPHU,AMACH,
     *AMACH2,AMM2,AMM2A,AMM2AV,AMM2B,AMM2C,AMM2MN,AMM21,AMSQ,AM2LST,
     *ARCHI,ATEST,A0,A1,A11,A12,A21,A22
      COMMON B,BOTTOM,BRB,BR1,BR11,BR12,BR2,BR21,BR22,B11,B12,B21,B22
      COMMON C,CFBOT,COND1,CPKU,C11,C12,C21,C22
      COMMON D,DELETA,DELX,DELXS,DENOM,DFBRDX,DLP1,DLP2,DLSTR,DPDX,DPG1,
     *DPG2,DPLAST,DPNM1,DPNUM,DPNUMA,DPNUMB,DTDN,DUDN,DUDNSQ,DVDN,D1,D2,
     *D2TDN2,D2UDN2,DAY
      COMMON EM11,EM12,EM21,EM22,ETTBU2,E11MAX
      COMMON FACT,FN1,FN2
      COMMON GAMMA,GAMMAP,GENRI,G1,G10,G11,G12,G13,G14,G15,G16,G17,G18,
     *G19,G2,G20,G21,G3,G4,G4BGM1,G5,G6,G7,G8,G9
      COMMON HDELX,HFLUX,HTR
      COMMON IBC,IETAPR,IGOTA,IPG,ISW,ITER,ITERA,IX,IXSTAR,IXTHW
      COMMON K,KI,KP1,KX,KX0,KX1
      COMMON LC,MORE,NPRC,NRUN
      COMMON OHMPH,OMEGA,O1,O2,O3,O4,O5
      COMMON P,PART1,PART2,PDA,PG,PGNP1,PGRI,PG1,PG2,PHW,PI3,PNEW,PN1,
     *PN2,PR,PSGW2,PSI,PXTRAP
      COMMON Q,QQ11,QQ12,QQ21,QQ22,Q11,Q12,Q21,Q22
      COMMON RADDEG,RTPB2,RTZ8Z7,RT2GM1,R1,R1ST1,R1ST2,R12
      COMMON SAME,SA1,SC1,SGDX,SHERI,SIGBAR,SIGDP,SIGMAW,SW2,SW3,SW4
      COMMON TANBAR,TANTHP,TAU,TCF,TCFTOP,TFCOEF,THETAP,THETAW,THETA1,
     *THETA2,TCMF,TOP,TTERM,TW2
      COMMON UCF,UCFTOP,UTERM,U2ETAT,V
      COMMON X,XCUT,XHW,XIPG,XMAX,XPLAST,XPRINT,XTW1,XTW2,X0,X1,X2
      COMMON Y1,Y2,Y3,Y4,Y5,Y6,Y7,Y8,Y9
      COMMON Z1,Z10,Z11,Z12,Z13,Z15,Z16,Z2,Z23,Z31,Z32,Z33,Z34,Z35,Z41,
     *Z42,Z43,Z5,Z7,Z8
      COMMON ETA(101),E11(101),E12(101),E21(101),E22(101),F1(101),
     *F2(101),S3(101),S4(101),W(101)
      COMMON T(101,2),U(101,2)
      DIMENSION ARCH(101),PGRD(101),COND(101),SHER(101),GENR(101)
      EQUIVALENCE (ARCH,E21),(PGRD,E22),(COND,F1),(SHER,F2),(GENR,S4)
C     CALCULATION OF STARTING CONDITIONS.
      A=0.5  *(A0+A1)
      DELX=DELXS
      Z16=4.0  *A
      Z41=Z34*DELX
      CALL GEOM(X0)
      SW2=SIGMAW**2
      SW3=SIGMAW*SW2
      SW4=SIGMAW*SW3
      X=X0
C     THE STATION AT WHICH U AND T ARE CALCULATED IS K+1 (=2)
C     AT THE END OF EACH STEP THE U AND T ARE TRANSFERRED TO K (=1)
      K=1
```

```
      KP1=K+1
      KX=1
      KI=0
      IX=1
      IF(X1.GE.X2) IX=4
      D1=Z16**2*PR
      D2=6.0*CPRO*A/SW3
      PI3=(32.0*A*GAMMA)/(3.0*Z7*Z1*B)
      P=SW3/(SW3-PI3)
      DPDX=-3.0*TANTHP*PI3/SW4
      AMP2=0
      AMP2MN=1.0E+10
      DO 1 L=1,101
      ETA(L)= FLOAT(L-1)/100.0
      S=ETA(L)**2
      T(L,2)=(SW4+D1 *(S*(2.0  -S)-1.0  ))/SW4
      U(L,2)=D2+Z16*(1.0  -S)/SW2
      W(L)=0
      ARCH(L)=0
      GENR(L)=0
      COND(L)=0
      SHER(L)=0
    1 PGRD(L)=0
      HFLUX=A
      HTR=0
      THETAW=1.0
      IXTHW=1
      IF(XTW1.GE.XTW2) IXTHW=3
      LC=0
      IF(IGOTA.NE.0.AND.NPRO.EQ.0) CALL OUTPUT
      S4(1)=0
      S4(2)=(U(2,2)*ETA(2))/T(2,2)
      S4(3)=(U(3,2)*ETA(3))/T(3,2)
      S3(1)=0
      S3(2)=Z23*(8.0  *S4(2)-S4(3))
      DO 2 L=3,101
      S4(L)=(U(L,2)*ETA(L))/T(L,2)
    2 S3(L)=S3(L-2)+Z13*(S4(L-2)+4.0  *S4(L-1)+S4(L))
      PSGW2=P*SW2
      DO 3 L=1,101
    3 S3(L)=S3(L)*PSGW2
      RETURN
      END
```

```
CCCC
      SUBROUTINE OUTPUT
      REAL DAY(3)
      COMMON A,ABDLP1,ABDLP2,ABDPG1,ABDPG2,AEFF,ALPHT,ALPHU,AMACH,
     *AMACH2,AMM2,AMM2A,AMM2AV,AMM2B,AMM2C,AMM2MN,AMM21,AMSQ,AM2LST,
     *ARCHI,ATEST,A0,A1,A11,A12,A21,A22
      COMMON B,BOTTOM,BRB,BR1,BR11,BR12,BR2,BR21,BR22,B11,B12,B21,B22
      COMMON C,CFBOT,CONDI,CPKU,C11,C12,C21,C22
      COMMON D,DELETA,DELX,DELXS,DENOM,DFBRDX,DLP1,DLP2,DLSTR,DPDX,DPG1,
     *DPG2,DPLAST,DPNM1,DPNUM,DPNUMA,DPNUMB,DTDN,DUDN,DUDNSQ,DVDN,D1,D2,
     *D2TDN2,D2UDN2,DAY
      COMMON EM11,EM12,EM21,EM22,ETTBU2,E11MAX
      COMMON FACT,FN1,FN2
      COMMON GAMMA,GAMMAP,GENRI,G1,G10,G11,G12,G13,G14,G15,G16,G17,G18,
     *G19,G2,G20,G21,G3,G4,G4BGM1,G5,G6,G7,G8,G9
      COMMON HDELX,HFLUX,HTR
      COMMON IBC,IETAPR,IGOTA,IPG,ISW,ITER,ITERA,IX,IXSTAR,IXTHW
      COMMON K,KI,KP1,KX,KX0,KX1
      COMMON LC,MORE,NPRO,NRUN
      COMMON OMMPH,OMEGA,O1,O2,O3,O4,O5
      COMMON P,PART1,PART2,PDA,PG,PGNP1,PGRT,PG1,PG2,PHW,PI3,PNEW,PN1,
     *PN2,PR,PSGW2,PSI,PXTRAP
      COMMON Q,QQ11,QQ12,QQ21,QQ22,Q11,Q12,Q21,Q22
      COMMON RADDEG,RTPB2,RTZ8Z7,RT2GM1,R1,R1ST1,R1ST2,R12
      COMMON SAME,SA1,SC1,SGDX,SHER1,SIGBAR,SIGDP,SIGMAW,SW2,SW3,SW4
      COMMON TANBAR,TANTHP,TAU,TCF,TCFTOP,THCOEF,THETAP,THETAW,THETA1,
     *THETA2,TCMF,TOP,TTERM,TW2
      COMMON UCF,UCFTOP,UTERM,U2ETAT,V
      COMMON X,XCUT,XHW,XIPG,XMAX,XPLAST,XPRINT,XTW1,XTW2,X0,X1,X2
      COMMON Y1,Y2,Y3,Y4,Y5,Y6,Y7,Y8,Y9
      COMMON Z1,Z10,Z11,Z12,Z13,Z15,Z16,Z2,Z23,Z31,Z32,Z33,Z34,Z35,Z41,
     *Z42,Z43,Z5,Z7,Z8
      COMMON ETA(101),E11(101),E12(101),E21(101),E22(101),F1(101),
     *F2(101),S3(101),S4(101),W(101)
      COMMON T(101,2),U(101,2)
      DIMENSION ARCH(101),PGRD(101),COND(101),SHER(101),GENR(101)
      EQUIVALENCE (ARCH,E21),(PGRD,E22),(COND,F1),(SHER,F2),(GENR,S4)
      IF(X.EQ.X0) GO TO 1
      IF(X-XPLAST.LT.XPRINT) RETURN
      XPLAST=X
      PDA=2.0   *SIGBAR*P*TANBAR
      TAU=G4BGM1*TTERM*UTERM/(B*Z33)
      DFBRDX=PDA+TAU
      E11MAX=1.0/E11(101)
      GO TO 2
    1 E11MAX=0
      AMSQ=0
      THCOEF=0
      ARCHI=0
      CONDI=0
```

```
      SHERI=0
      GENRI=0
      PDA=0
      TAU=0
      DFBRDX=0
      Q=0
    2 WRITE(6,200) DAY,NRUN,X,A,SIGMAW,
     *             SW2,TANTHP,P,DPDX,ARCHI,CONDI,SHERI,GENRI,
     *             AMSQ,THCOEF,PDA,TAU,DFBRDX,HFLUX,HTR,Q
      LC=0
      DO 3 L=1,101,IETAPR
      V=W(L)+TANTHP*ETA(L)*U(L,2)
      D=P/T(L,2)
      PSI=E11(L)*E11MAX
      AMACH=RT2GM1*U(L,2)   / SQRT(T(L,2))
    3 WRITE(6,201) ETA(L),U(L,2)  ,T(L,2)   ,W(L),V,D,PSI,AMACH,
     *             ARCH(L),PGRD(L),SHER(L),COND(L),GENR(L)
      RETURN
  200 FORMAT(1H1,3A4//
     *' RUN',A5,4X,'X=',F6.2,4X,'A=',F9.6,4X,'SIGMAW=',F7.3,4X,'SW2=',
     *F8.2,4X,'TANTHP=',F6.3,4X,'P=',1PE11.4,4X,'DPDX=',E11.4//
     *' ARCHI=',E11.4,4X,'CONDI=',E11.4,4X,'SHERI=',E11.4,4X,'GENRI=',
     *E11.4,4X,'AMSQ=',E11.4,4X,'THCOEF=',E11.4//
     *' PDA=',E11.4,4X,'TAU=',E11.4,4X,'DFBRDX=',E11.4,4X,'HFLUX=',
     *E11.4,4X,'HTR=',E11.4,4X,'Q=',E11.4//
     *' ETA',6X,'U',8X,'T',9X,'W',8X,'V',8X,'D',7X,'PSI',5X,'M',7X,
     *'DA/DX',7X,'PGT',7X,'SHEAR',5X,6HCOND'N,7X,'GEN')
  201 FORMAT(F5.2,2F9.5,1PE11.3,0PF8.4,1PE11.3,0PF7.3,F8.3,1P5E11.3)
      END
```

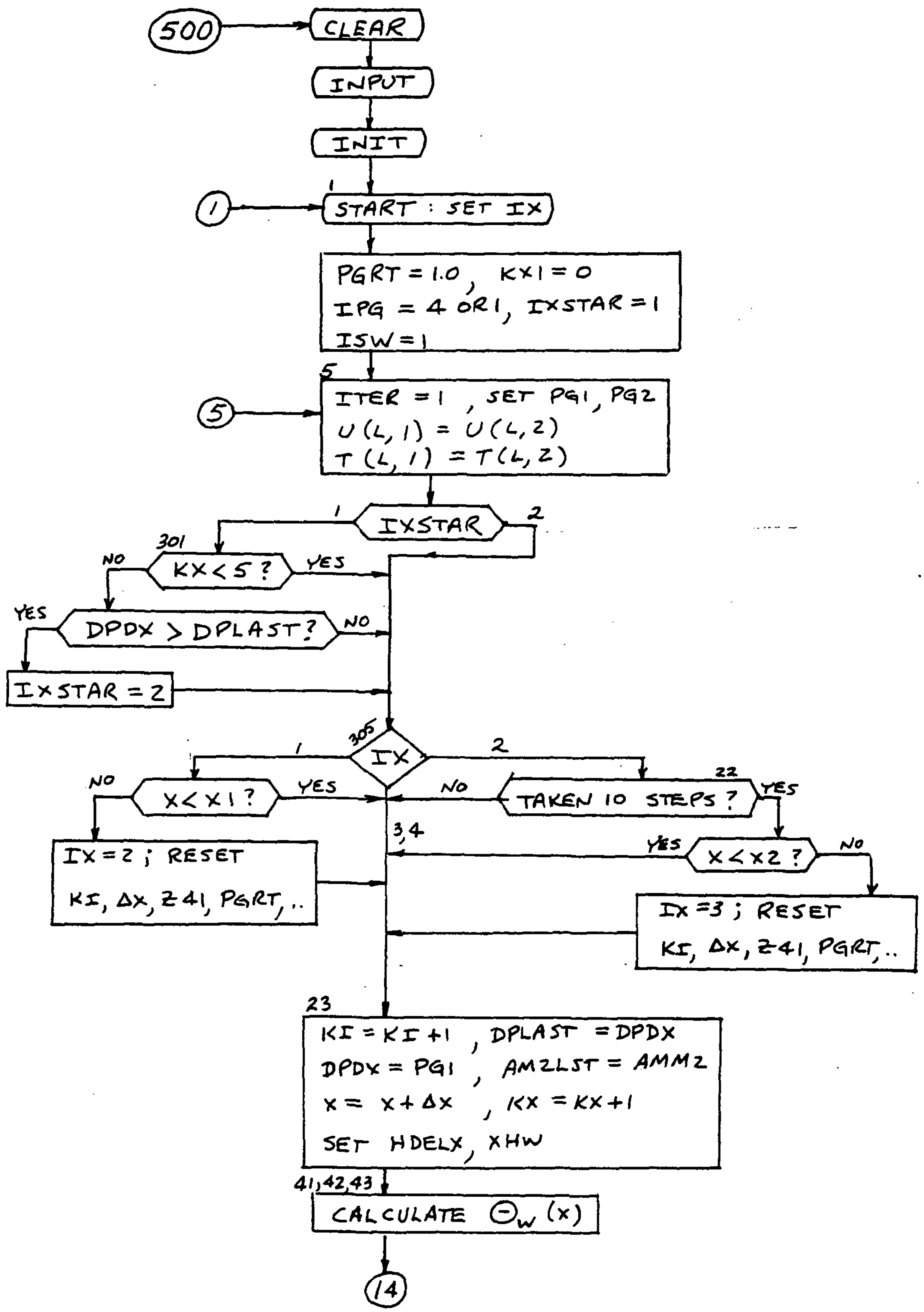
500
CLEAR
INPUT
INIT
1
START : SET IX
PGRT = 1.0, KX1 = 0
IPG = 4 OR 1, IXSTAR = 1
ISW = 1
5
ITER = 1, SET PG1, PG2
U(L,1) = U(L,2)
T(L,1) = T(L,2)
IXSTAR
1
2
301
KX < 5 ?
NO
YES
DPDX > DPLAST ?
YES
NO
IXSTAR = 2
305
IX
1
2
X < X1 ?
NO
YES
22
TAKEN 10 STEPS ?
NO
YES
3,4
X < X2 ?
YES
NO
IX = 2 ; RESET
KI, ΔX, Z41, PGRT, ..
IX = 3 ; RESET
KI, ΔX, Z41, PGRT, ..
23
KI = KI + 1, DPLAST = DPDX
DPDX = PG1, AM2LST = AMM2
X = X + ΔX, KX = KX + 1
SET HDELX, XHW
41,42,43
CALCULATE Θw (x)
14

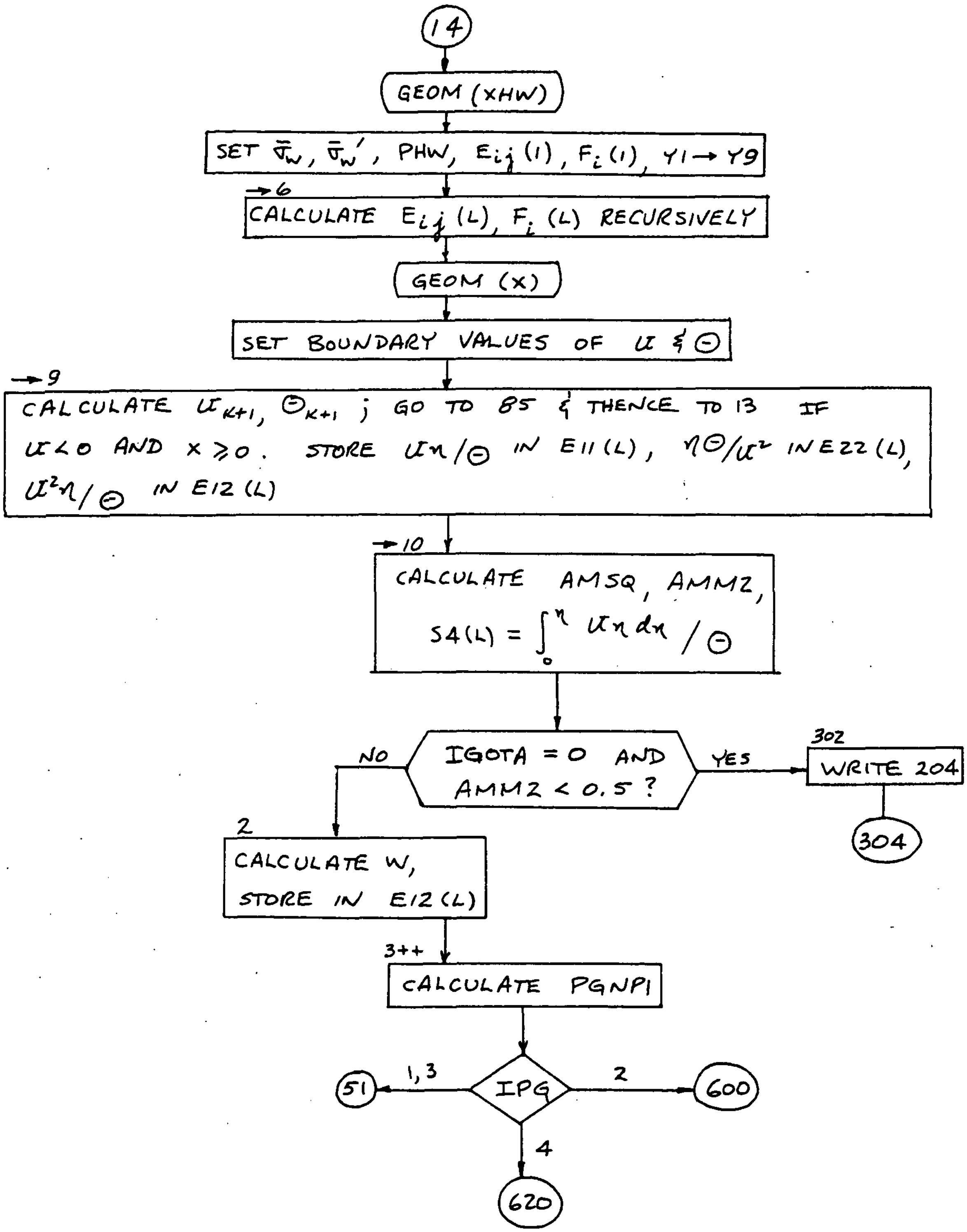
14
GEOM (XHW)
SET $\bar{\tau}_w$, $\bar{\tau}_w'$, PHW, $E_{ij}(1)$, $F_i(1)$, Y1 → Y9
→6
CALCULATE $E_{ij}(L)$, $F_i(L)$ RECURSIVELY
GEOM (X)
SET BOUNDARY VALUES OF $\mathcal{U}$ & Θ
→9
CALCULATE $\mathcal{U}_{K+1}$, Θ_{K+1} ; GO TO 85 & THENCE TO 13 IF $\mathcal{U}<0$ AND $x \geq 0$. STORE $\mathcal{U}\eta/\Theta$ IN E11(L), $\eta\Theta/\mathcal{U}^2$ IN E22(L), $\mathcal{U}^2\eta/\Theta$ IN E12(L)
→10
CALCULATE AMSQ, AMMZ, $S4(L) = \int_0^\eta \mathcal{U}\eta\, d\eta / \Theta$
IGOTA = 0 AND AMMZ < 0.5 ?
NO
YES
302
WRITE 204
304
2
CALCULATE W, STORE IN E12(L)
3++
CALCULATE PGNP1
IPG
1, 3
51
2
600
4
620

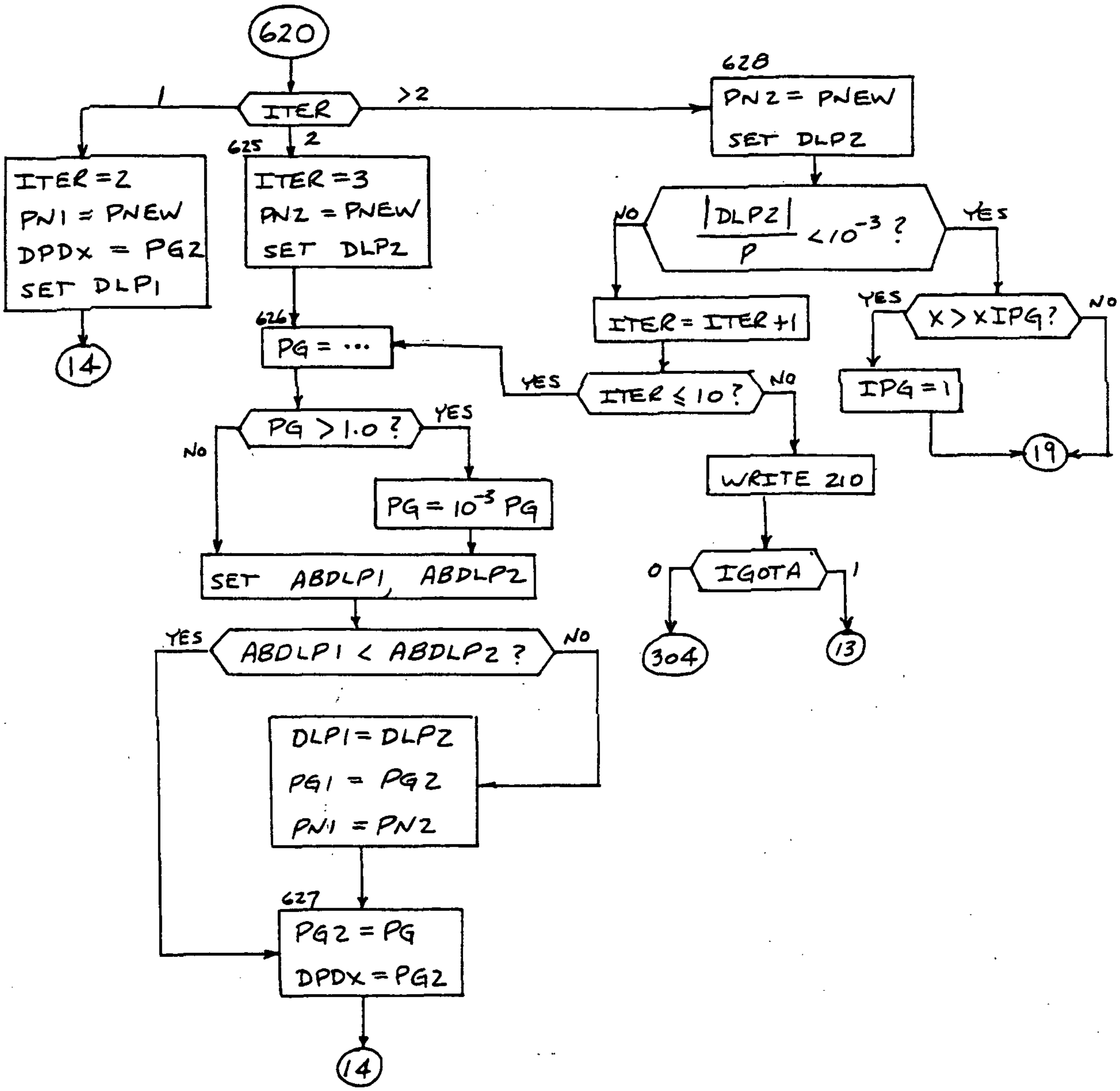

620
ITER
1
>2
2
625
ITER=2
PN1 = PNEW
DPDX = PG2
SET DLP1
14
ITER=3
PN2 = PNEW
SET DLP2
628
PN2 = PNEW
SET DLP2
NO
YES
|DLP2| / P < 10^-3 ?
ITER = ITER+1
YES
X > XIPG?
NO
IPG = 1
19
626
PG = ···
YES
ITER ≤ 10 ?
NO
WRITE 210
PG > 1.0 ?
YES
NO
PG = 10^-3 PG
SET ABDLP1, ABDLP2
0
IGOTA
1
304
13
YES
ABDLP1 < ABDLP2 ?
NO
DLP1 = DLP2
PG1 = PG2
PN1 = PN2
627
PG2 = PG
DPDX = PG2
14

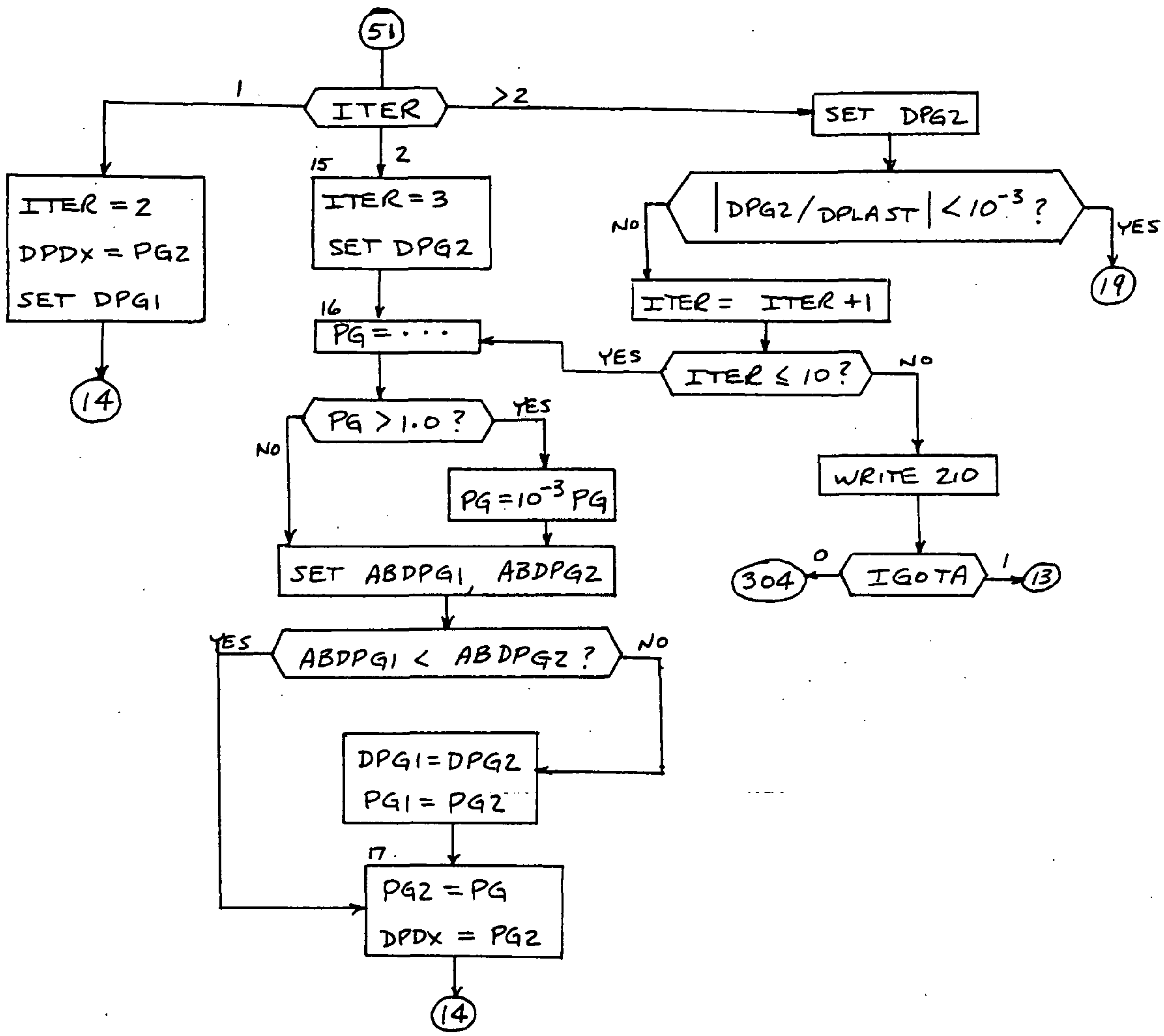
51
ITER
1
2
>2
ITER = 2
DPDX = PG2
SET DPG1
14
15
ITER = 3
SET DPG2
16
PG = . . .
PG > 1.0 ?
YES
NO
PG = 10⁻³ PG
SET ABDPG1, ABDPG2
ABDPG1 < ABDPG2 ?
YES
NO
DPG1 = DPG2
PG1 = PG2
17
PG2 = PG
DPDX = PG2
14
SET DPG2
\|DPG2/DPLAST\| < 10⁻³ ?
NO
YES
19
ITER = ITER + 1
ITER ≤ 10 ?
YES
NO
WRITE 210
IGOTA
0
1
304
13

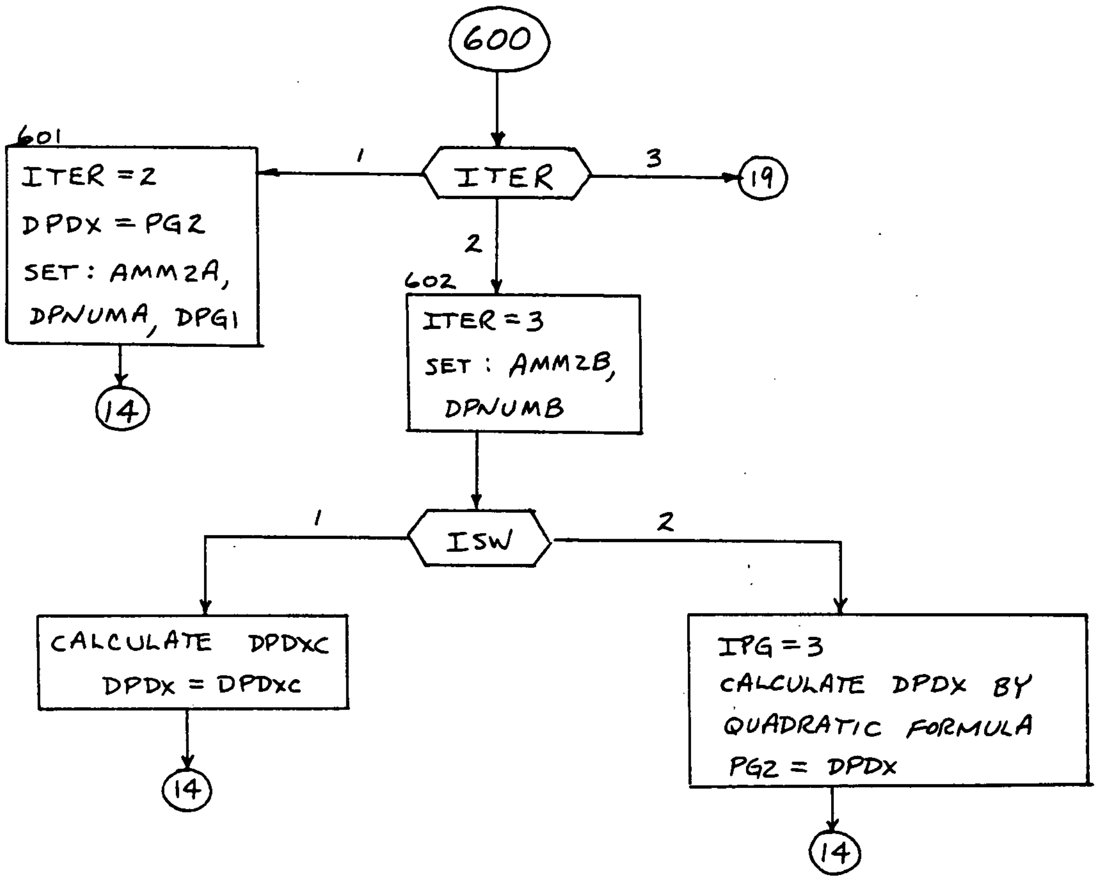
600
601
ITER = 2
DPDX = PG2
SET : AMM2A, DPNUMA, DPG1
14
ITER
1
2
3
19
602
ITER = 3
SET : AMM2B, DPNUMB
ISW
1
2
CALCULATE DPDXC
DPDX = DPDXC
14
IPG = 3
CALCULATE DPDX BY QUADRATIC FORMULA
PG2 = DPDX
14

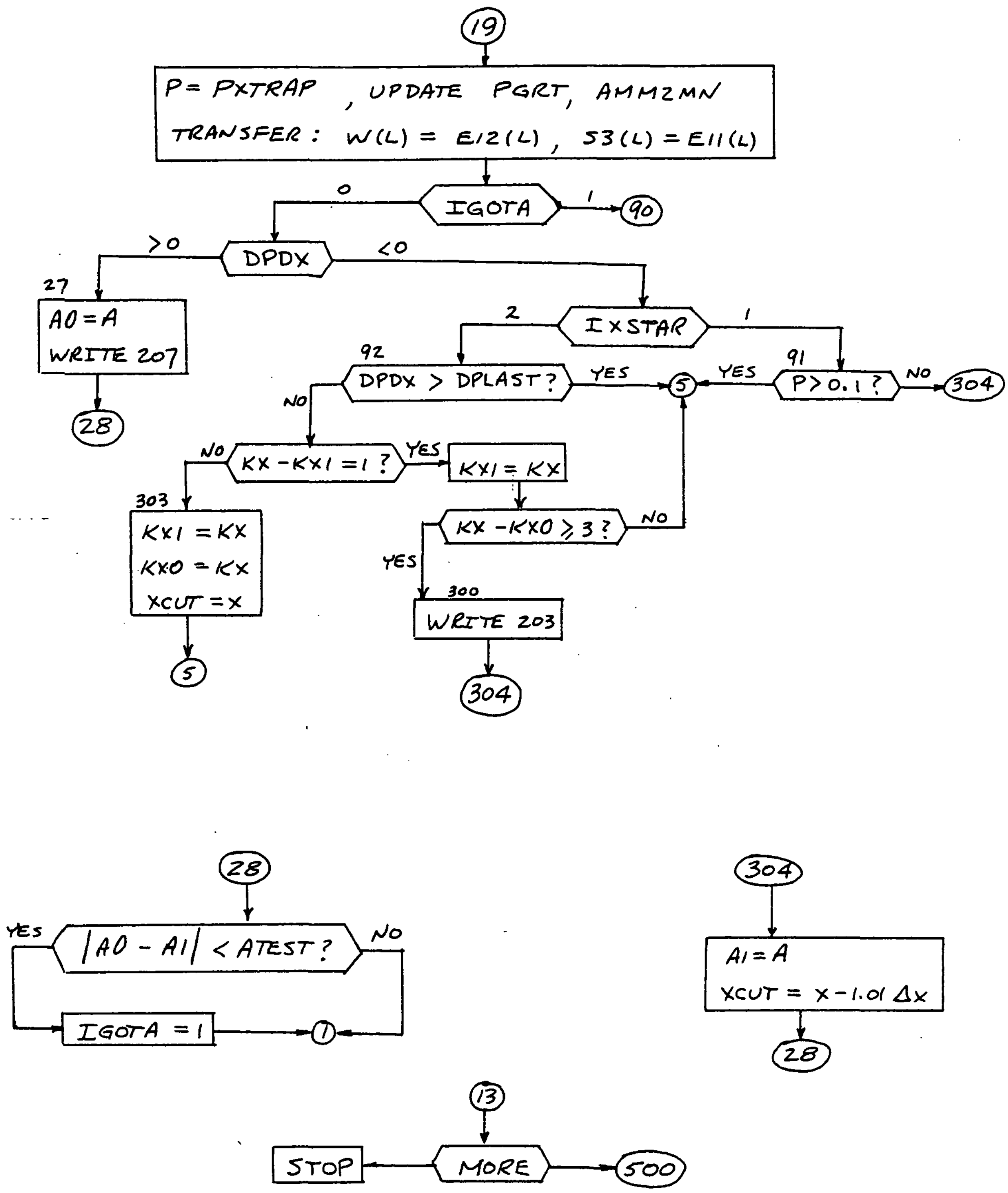
19
P= PXTRAP , UPDATE PGRT, AMMZMN
TRANSFER : W(L) = E12(L) , S3(L) = E11(L)
IGOTA
0
1
90
DPDX
>0
<0
27
A0=A
WRITE 207
28
IXSTAR
2
1
92
DPDX > DPLAST ?
YES
NO
5
YES
91
P>0.1 ?
NO
304
KX -KX1 =1 ?
NO
YES
KX1 = KX
303
KX1 = KX
KX0 = KX
XCUT = X
5
KX -KX0 ≥ 3 ?
NO
YES
300
WRITE 203
304
28
|A0 - A1| < ATEST ?
YES
NO
IGOTA = 1
7
304
A1 = A
XCUT = X - 1.01 ΔX
28
13
MORE
STOP
500

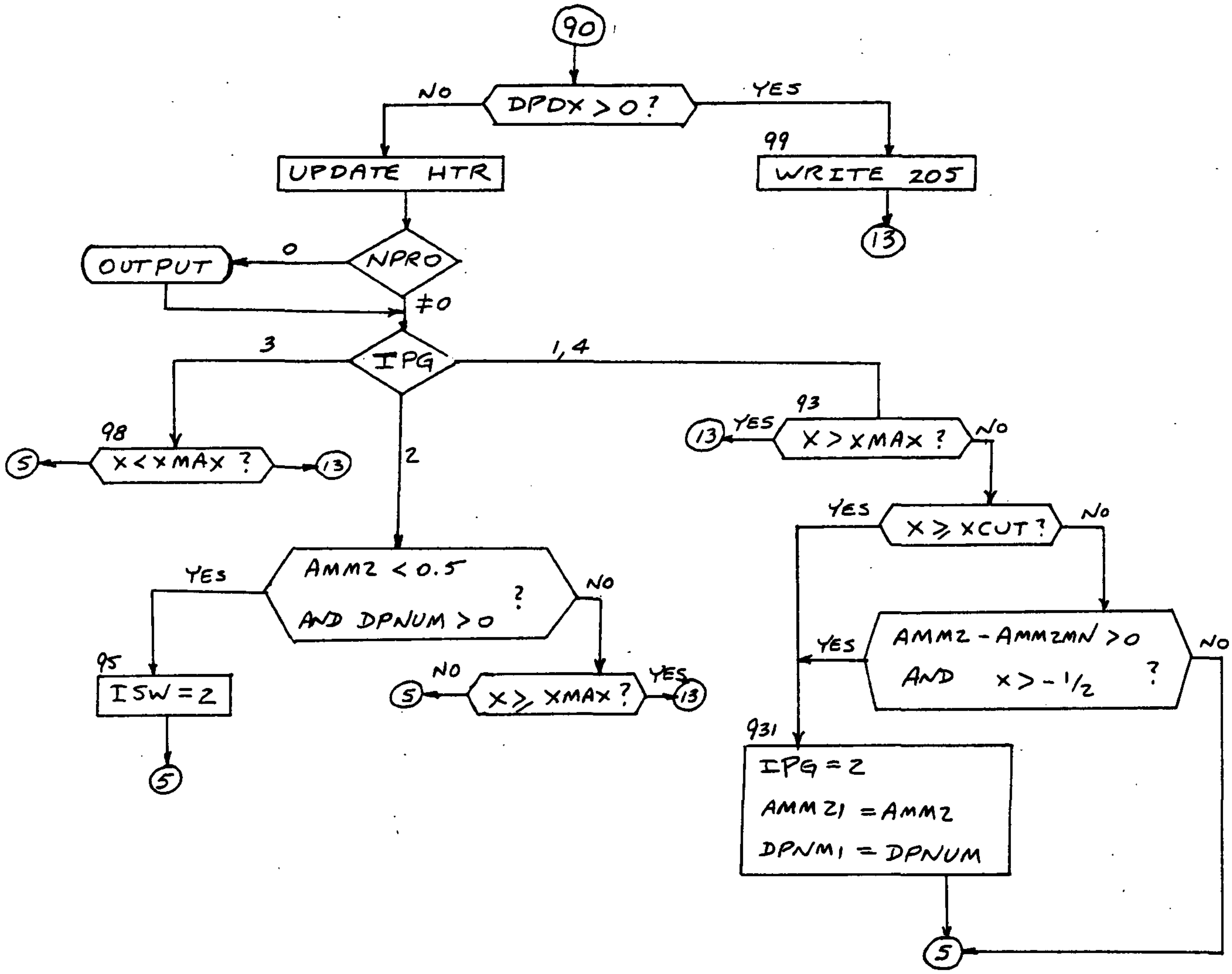
90
DPDX > 0 ?
NO
YES
UPDATE HTR
99
WRITE 205
13
OUTPUT
0
NPRO
≠0
3
IPG
1, 4
2
98
X < XMAX ?
5
13
93
X > XMAX ?
YES
NO
13
X ≥ XCUT ?
YES
NO
AMMZ < 0.5
AND DPNUM > 0 ?
YES
NO
AMMZ - AMMZMN > 0
AND X > -1/2 ?
YES
NO
95
ISW = 2
5
X ≥ XMAX ?
NO
YES
5
13
931
IPG = 2
AMMZ1 = AMMZ
DPNM1 = DPNUM
5

APPENDIX F

DEFINITION OF PROGRAM VARIABLES

FORTRAN Symbol	Algebraic Equivalent	Definition, Use, Comments
A	A	See Eq. (3-26)
ABDLP1, 2	$\lvert PN1,2 - PXTRAP \rvert$	Used to select the iteration that most nearly matches PNEW and PXTRAP
ABDPG1, 2	$\lvert (PGNP1)_{1,2} - DPDX \rvert$	Absolute value of the difference between the right-hand side of Eq. (3-34) and the value of dP/dx used to find it. Subscripts 1 and 2 refer to two iterations: the prior one that was saved, and the one just completed.
AEFF	A_{EFF}/A_*	Effective area ratio, Eq. (6-4)
ALPHT, ALPHU	α_T, α_u	Thermal and velocity accommodation coefficients
AMACH	$M = u/a = u \Big/ \sqrt{\frac{(\gamma-1)}{2}\Theta}$	Local Mach number
AMACH2	M^2	—
AMM2	$\int_0^1 \eta \, d\eta / M^2$	—
AMM2A, B, C	-	See Eq. (4-36)
AMM2AV	$\frac{1}{2}\left[(AMM2)_K + (AMM2)_{K+1}\right]$	-
AMM2MN	—	Minimum value of AMM2
AMM21	—	See Eq. (4-35)
AMSQ	$\int_0^1 M^2 \eta \, d\eta$	—
AM2LST	-	Value of AMM2 at previous step

FORTRAN Symbol	Algebraic Equivalent	Definition, Use, Comments
ARCHI	–	Area-change integral - see Eq. (4-25)
ARCH(L)	–	Area-change integrand - see Eq. (4-25)
ATEST	–	Tolerance for A
A0	–	Lower bound for A
A1	–	Upper bound for A
A11, A12, A21, A22	–	Matrix coefficients, Eq. (4-6)
B	$\rho\sqrt{2H_o}\, r_* / \mu_o$	Reynolds number
BRB, BR1, BR11, BR12, BR2, BR21, BR22	–	Coefficients in quadratic expression for dP/dx - see Eqs. (4-39) thru (4-42)
B11, B12, B21, B22	–	Matrix coefficients, Eq. (4-6)
C	$\sqrt{R_1^2 - x^2}$	–
CFBOT	$B\Delta\eta$	–
CONDI	–	Heat-conduction integral - see Eq. (4-27)
COND(L)	–	Heat-conduction integrand - see Eq. (4-27)
CPKU	K_u	Eq. (5-2)
C11, C12, C21, C22	–	Matrix coefficients, Eq. (4-6)
D	ρ/ρ_o	–
DELETA	$\Delta\eta$	$\Delta\eta$ = 0.01 throughout this program
DELX	Δx	–

FORTRAN Symbol	Algebraic Equivalent	Definition, Use, Comments
DELXS	–	"Saved" value of Δx, i. e., the value used for $x_0 \leq x \leq x_1$, $x \geq x_2$
DFBRDX	$d\bar{F} / dx$	See Eq. (3-29)
DLP1, 2	PN1, 2 − PXTRAP	–
DLSTR	δ_1 / r_*	See Eq. (6-3)
DPDX	dP / dx	–
DPG1, 2	–	Difference between right-hand side of Eq. (3-34) and the value of dP/dx used to find it
DPLAST	–	Value of DPDX at the previous station
DPNM1	–	See Eq. (4-35)
DPNUM	–	See Eq. (4-24)
DPNUMA, B	–	See Eq. (4-36)
DTDN	$\partial \Theta / \partial \eta$	See Eq. (4-29) for difference formula
DUDN	$\partial u / \partial \eta$	"
DUDNSQ	$\left(\partial u / \partial \eta \right)^2_{\eta = 1}$	$\left(\dfrac{u_K^{101} - u_K^{100} + u_K^{101} - u_K^{100}}{2 \Delta \eta} \right)^2$
DVDN	$\partial v / \partial \eta$	–
D1, D2	–	Matrix coefficients, Eq. (4-6)
D2TDN2	$\partial^2 \Theta / \partial \eta^2$	–
D2UDN2	$\partial^2 u / \partial \eta^2$	–
EM11, EM12, EM21, EM22	–	Matrix coefficients, Eq. (4-17)

FORTRAN Symbol	Algebraic Equivalent	Definition, Use, Comments
ETA(L)	η	–
ETTBU2	–	Used in finding $\int_0^1 \eta\Theta\, dx/\mathcal{U}^2$, hence AMM2
E11(L), E12(L), E21(L), E22(L)	E_{ij}	Matrix coefficients, Eq. (4 - 7). E11(L) is also used at various times to store $\mathcal{U}\eta/\Theta$, and $\left(P\sigma_w^2\int_0^\eta \frac{\mathcal{U}_\eta\, d\eta}{\Theta}\right)_{K+1}$ E12(L) stores $\mathcal{U}^2\eta/\Theta$, and later W_{K+1}^L E22(L) stores $\eta\Theta/\mathcal{U}^2$ and PGRD(L) E21(L) stores ARCH(L)
FACT	$2\gamma/(\gamma-1)B\bar{\sigma}_w$	–
FN1, FN2	–	Matrix coefficients, Eq. (4-17)
F1(L), F2(L)	f_i^L	Matrix coefficients, Eq. (4 - 7)
GAMMA	γ	–
GAMMAP	$\gamma\left(P + \frac{\Delta x}{2}\frac{dP}{dx}\right)$	–
GENRI	–	Generation integral - Eq. (4-28)
GENR(L)	–	Generation integrand - Eq. (4-28)
G1 thru G21	–	Intermediate quantities used in determining the matrix coefficients
G4BGM1	$4\gamma/(\gamma-1)$	–
HDELX	$\Delta x/2$	–
HFLUX	$\sigma_w^2\int_0^1 \eta D\mathcal{U}\,(\Theta+\mathcal{U}^2)\,d\eta$	Dimensionless enthalpy flux, see Eq. (3-31)

FORTRAN Symbol	Algebraic Equivalent	Definition, Use, Comments
HTR	$\int_{x_0}^{x} Q\,dx$	–
IBC	–	Boundary-condition indicator
IETAPR	–	Print-control indicator
IGOTA	–	Equals 1 or 0 depending on whether A is or is not known
IPG	–	Indicator for pressure-gradient algorithm
ISW	–	Used in switching from IPG = 2 to 3
ITER	–	Counter for number of iterations on dP/dx
IX	–	Step-size indicator
IXSTAR	–	Equals 1 or 2 depending on whether solution is upstream or downstream of first minimum in dP/dx
IXTHW	–	Used to identify three regions of wall-temperature variation
KI	$x = x_0 + KI \cdot \Delta x$	–
KX	–	Counts the number of steps, regardless of step size
KX0, KX1	–	Used to determine number of steps with dP/dx decreasing and IXSTAR = 2
LC	–	Line counter
MORE	–	Indicates further cases are to be run

FORTRAN Symbol	Algebraic Equivalent	Definition, Use, Comments
NPRO	–	Equal to zero if profiles are desired
NRUN	–	Run number
OMPH	$\omega + 1/2$	–
OMEGA	ω	–
O1	$.16 A^2 Pr$	–
O2	$8 Ku / \sigma_w^3$	–
O3	$\frac{1}{2} (1 + TW2)$	Parameters used in wall-temperature variation - see Eq. (6-2)
O4	$\frac{1}{2} (1 - TW2)$	
O5	$\pi / (XTW2 - XTW1)$	
P	P, p/p_0	–
PDA	$P \frac{d}{dx} (\sigma_w^2)$	See Eq. (3-29)
PG	–	Trial value for dP/dx, Eq. (4-20) or (4-31)
PGNP1	–	See Eq. (4-21)
PGRT	–	Pressure-gradient ratio, Eq. (4-34)
PG1	–	Initial trial for dP/dx
PG2	–	Second trial for dP/dx
PHW	$P_K + \frac{\Delta x}{2} \cdot \frac{dP}{dx}$	–
PI3	π_3	–
PNEW	–	See Eq. (4-18)
PN1, PN2	–	Values of PNEW used in extrapolating for PG - see Eq. (4-20)
PR	Pr	Prandtl number

FORTRAN Symbol	Algebraic Equivalent	Definition, Use, Comments
PSGW2	$P\left(\sigma_{w,K+1}\right)^2$	–
PSI	ψ	Stream function
PXTRAP	$P_K + \Delta x \cdot \frac{dP}{dx}$	–
Q	$\frac{1}{B}\left[\Theta^{\omega}\frac{\partial}{\partial\eta}\left(\frac{\Theta}{Pr} + \mathcal{U}^2\right)\right]_{\eta=1}$	Local dimensionless heat-transfer rate, see Eq. (3-31)
RTPB2	$\sqrt{\pi/2}$	–
RTZ8Z7	$\sqrt{2\gamma/(\gamma-1)}$	–
RT2GM1	$\sqrt{2/(\gamma-1)}$	–
R1	$R_1 = r_1/r_*$	–
R1ST1	$R_1 \sin\theta_1$	–
R1ST2	$R_1 \sin\theta_2$	–
R12	R_1^2	–
SAME	$\Theta + \omega\eta\frac{\partial\Theta}{\partial\eta}$	–
SA1	$\frac{2-\alpha_u}{\alpha_u}\sqrt{\frac{\pi}{2}}$	–
SC1	$\frac{2-\alpha_T}{\alpha_T}\sqrt{\frac{\pi}{2}}\;\frac{2\gamma}{(\gamma+1)Pr}$	–
SGDX	$\sigma_{w,K+1}/\Delta x$	–
SHERI	–	Shear integral, Eq. (4-26)
SHER(L)	–	Integrand for shear integral
SIGBAR	$\left.\sigma_w\right)_{x=x_K+\Delta x/2}$	Wall radius, halfway across the step
SIGDP	$\sigma_{w,K+1}\cdot\frac{dP}{dx}$	–
SIGMAW	$\sigma_w \quad , \quad \sigma_{w,K+1}$	Wall radius at the end of the step

FORTRAN Symbol	Algebraic Equivalent	Definition, Use, Comments
SW2	σ_w^2	–
SW3	σ_w^3	–
SW4	σ_w^4	
S3(L)	$\left(P\sigma_w^2 \int_0^\eta \frac{\mathcal{U}\eta\, d\eta}{\Theta} \right)_K$	–
S4(L)	In subroutine START: $S4(L) = \mathcal{U}\eta / \Theta$ In the MAIN program, through statement 10: $S4(L) = \int_0^\eta \frac{\mathcal{U}\eta\, d\eta}{\Theta}$	–
T(L, K)	Θ_K^L	–
TANBAR	$\bar{\sigma}_w'$	Wall slope halfway across the step
TANTHP	σ_w'	Wall slope at the end of the step
TAU	$\frac{4\gamma}{B(\gamma-1)} \left[\Theta^\omega \frac{\partial \mathcal{U}}{\partial \eta} \right]_{\eta=1}$	See Eq. (3-29)
THCOEF	$\bar{F}$	See Eq. (3-30)
THETAP	–	A dummy, used in subroutine GEOM for θ_w
THETAW	$\theta_w = \arctan d\sigma_w/dx$	–
THETA1, 2	θ_1 , θ_2	–
TOMF	$\frac{2\gamma}{(\gamma-1) B \bar{\sigma}_w} \left(\Theta_{K+1}^L \right)^{\omega-1}$	–
TW2	–	See Eq. (6-2)
U(L, K)	$\mathcal{U}_K^L$	–
U2ETAT	–	Used in finding $\int_0^1 \frac{\mathcal{U}^2 \eta\, d\eta}{\Theta}$

FORTRAN Symbol	Algebraic Equivalent	Definition, Use, Comments
V	V	–
W(L)	W	–
X	X	–
XCUT	–	Point where extrapolation through the saddle point is started
XHW	$X_K + \frac{\Delta x}{2}$	–
XIPG	–	Point where switch from IPG = 4 to IPG = 1 is made
XMAX	–	Point where calculation is terminated
XPLAST	–	Previous print station
XPRINT	–	Interval between print stations
XTW1, XTW2	–	See Eq. (6-2)
X0	–	Initial station
X1, X2	–	Boundaries of reduced step-size region
Y1 - Y9		Dummies used in calculation of matrix coefficients
Z1	$\tan\theta_1$	–
Z2	$\tan\theta_2$	–
Z5	$\cos\theta_1$	–
Z7	$\gamma - 1$	–
Z8	2γ	–
Z10	$1 + R_1(1-\cos\theta_1) - R_1\sin\theta_1\tan\theta_1$	–
Z11	$1 + R_1$	–

FORTRAN Symbol	Algebraic Equivalent	Definition, Use, Comments
Z12	$1 + R_1(1-\cos\theta_2) - R_1 \sin\theta_2 \tan\theta_2$	—
Z13	$\Delta\eta/3 = 0.01/3$	—
Z15	$\sqrt{\frac{2\gamma}{\gamma-1}}\ \frac{\cos\theta_1}{B}$	—
Z16	$4A$	—
Z23	$\Delta\eta/12 = 0.01/12$	—
Z31	$(\Delta\eta)^2 = 0.0001$	—
Z32	$\omega - 1$	—
Z33	$2\Delta\eta = 0.02$	—
Z34	$4\Delta\eta = 0.04$	—
Z35	$B(\Delta\eta)^2 = 0.0001\,B$	—
Z41	$4\Delta\eta\,\Delta x = 0.04\,\Delta x$	—
Z42	$2(\Delta\eta)^2 = 0.0002$	—
Z43	$2\Delta\eta/3(\gamma-1) = 0.02/3(\gamma-1)$	

Table 1: SUMMARY OF CASES

Case No.	$\mathcal{B}$	A	θ_1(deg.)	R_1	θ_2(deg.)	$\Theta_w(x)$	$x_{\text{Saddle Point}}$
1	1250	0.1122	-20	13.356	21.77	adiabatic wall	4.95
2	1250	0.121	"	0.5	22.4	" "	1.05
3	1250	0.1222	-30	"	"	" "	-
4	800	0.1188	-20	"	"	" "	1.15
5	400	0.1138	"	"	"	" "	> 20
6	800	0.1188	"	"	25.0	" "	0.65
7	800	0.1188	"	"	21.0	" "	2.35
8	800	0.1188	"	"	18.0	" "	> 20
9	800	0.1188	"	"	15.0	" "	"
10	100	See text	"	"	15.0	" "	"
11	1250	0.1208	"	"	22.4	$\Theta_w = 1.0$	1.45
12	1250	0.1370	"	"	22.4	$1.0 \leq \Theta_w \leq 0.2$ (see text)	0.75
13	1220	0.118	-25	2.8	25.0	adiabatic wall	1.15

```
11 JUL 1967

NRUN= MC-2    IOC= 1    MORE= 0    NPRO= 0    IFTAPR= 2

       R1              THETA1            THETA2              TW2              GAMMA
     OMEGA               PR                B                 XIPG             ATEST
       A0                A1              XCUT               XPRINT             DELX
       X0                X1                X2                XMAX             ALPHU
     ALPHT              XTW1              XTW2

  3.000000E 00     -2.000000E 01     3.000000E 01     5.000000E-01     1.299999E 00
  6.500000E-01      7.500000E-01     3.000000E 03     5.000000E 01     9.999999E-04
  7.999998E-02      1.400000E-01     0.0              5.000000E-01     9.999996E-02
 -5.000000E 00      5.000000E 01     2.000000E 01     1.500000E 01     1.000000E 00
  1.000000E 00      5.000000E-01     1.500000E 00

HEAT TRANSFER IS ALLOWED

THE OUTPUT FORMAT OF THE P ITERATION PRINTOUT FOLLOWS

       X            DPDX          PGNP1         PXTRAP         PNEW        U(1,KP1)     T(1,KP1)
                    ARCHI         SHERI         CONDI          GENRI       DPNUM        AMSO
                    HFLUX         SIGBAR        SIGMAW         TANBAR      TANTHP       AMM2
                  U(101,KP1)    T(101,KP1)      AEFF           DLSTR       Q

A DESCRIPTION OF THE VARIABLES PRINTED ABOVE IS CONTAINED IN THE PROGRAM REPORT
```


TABLE 2.1

A= 1.100000E-01

-4.90	-1.067073E-04	-2.145706E-04	9.997327E-01	1.024953E 00	6.379074E-02	9.969516E-01
	-4.730369E-01	4.373428E 01	-3.580705E-04	4.713555E-04	-4.420740E 01	4.534598E-03
	1.100556E-01	2.609118E 00	2.590919E 00	-3.639703E-01	-3.639703E-01	1.579297E 05
	5.656196E-05	9.999994E-01	3.354556E 00	7.593756E-01	2.151151E-07	
-4.90	-1.077743E-04	-2.167738E-04	9.997326E-01	1.024933E 00	6.379098E-02	9.969516E-01
	-4.730369E-01	4.415247E 01	-3.573820E-04	4.721419E-04	-4.462558E 01	4.534680E-03
	1.100554E-01	2.609118E 00	2.590919E 00	-3.639703E-01	-3.639703E-01	1.578034E 05
	5.658444E-05	9.999994E-01	3.354509E 00	7.593613E-01	2.151123E-07	
-4.90	-1.457259E-03	-4.169658E-03	9.995977E-01	1.001384E 00	6.403440E-02	9.969202E-01
	-4.730049E-01	3.787502E 02	-7.154243E-04	8.791254E-04	-3.792231E 02	4.636575E-03
	1.100547E-01	2.609118E 00	2.590919E 00	-3.639703E-01	-3.639703E-01	6.971675E 04
	8.502198E-05	9.999990E-01	3.420339E 00	7.415047E-01	3.380699E-07	
-4.90	-1.560207E-03	-4.553352E-03	9.995374E-01	9.996311E-01	6.405294E-02	9.969178E-01
	-4.730025E-01	3.932739E 02	-7.464474E-04	9.134030E-04	-3.937468E 02	4.644606E-03
	1.100547E-01	2.609118E 00	2.590919E 00	-3.639703E-01	-3.639703E-01	6.628706E 04
	8.719193E-05	9.999996E-01	3.425336E 00	7.401533E-01	3.377000E-07	
-4.80	-2.281235E-02	-3.824301E-03	9.973061E-01	7.623600E-01	6.813568E-02	9.963933E-01
	-4.724259E-01	3.356509E 02	-7.816579E-03	8.538708E-03	-3.361238E 02	6.995730E-03
	1.100621E-01	2.572721E 00	2.554523E 00	-3.639703E-01	-3.639703E-01	2.039769E 03
	5.008706E-04	9.999615E-01	4.220058E 00	5.002451E-01	3.085664E-06	
-4.80	-2.304046E-02	-3.311578E-03	9.972833E-01	7.604413E-01	6.817675E-02	9.963879E-01
	-4.724208E-01	3.343743E 02	-7.900331E-03	8.626141E-03	-3.348472E 02	7.024754E-03
	1.100624E-01	2.572721E 00	2.554523E 00	-3.639703E-01	-3.639703E-01	2.007473E 03
	5.049282E-04	9.999968E-01	4.228135E 00	4.982796E-01	3.124796E-06	
-4.80	5.454019E-03	4.462495E-07	1.000133E 00	1.108210E 00	6.305218E-02	9.970447E-01
	-4.730948E-01	-1.621953E 04	9.286827E-02	-1.550359E-02	1.621897E 04	4.335176E-03
	1.100578E-01	2.572721E 00	2.554523E 00	-3.639703E-01	-3.639703E-01	2.825413E 10
	-1.330282E-07	1.000000E 00	3.139173E 00	7.827520E-01	-9.800794E-08	
-4.80	-3.451919E-03	-2.646461E-03	9.992421E-01	9.697783E-01	6.465232E-02	9.968396E-01
	-4.728841E-01	2.947373E 02	-1.416186E-03	1.661929E-03	-2.952100E 02	4.973590E-03
	1.100531E-01	2.572721E 00	2.554523E 00	-3.639703E-01	-3.639703E-01	2.043073E 04
	1.573458E-04	9.999987E-01	3.497771E 00	6.942899E-01	9.213724E-07	
-4.80	-1.544089E-03	-1.395907E-03	9.994329E-01	9.964547E-01	6.430936E-02	9.968827E-01
	-4.729292E-01	1.780693E 02	-9.421494E-04	1.124984E-03	-1.785624E 02	4.821390E-03
	1.100537E-01	2.572721E 00	2.554523E 00	-3.639703E-01	-3.639703E-01	3.315621E 04
	1.235818E-04	9.999996E-01	3.422434E 00	7.045412E-01	7.185922E-07	
-4.80	-1.329569E-03	-1.221658E-03	9.994544E-01	9.995477E-01	6.427079E-02	9.968879E-01
	-4.729341E-01	1.591719E 02	-8.924133E-04	1.068322E-03	-1.596450E 02	4.804805E-03
	1.100540E-01	2.572721E 00	2.554523E 00	-3.639703E-01	-3.639703E-01	3.530207E 04
	1.197862E-04	9.999989E-01	3.413707E 00	7.068472E-01	6.771299E-07	
-4.70	-1.133024E-03	-1.120951E-03	9.993411E-01	1.004333E 00	6.445313E-02	9.968623E-01
	-4.728758E-01	9.541035E 01	-7.323604E-04	9.192300E-04	-9.588341E 01	4.964691E-03
	1.100534E-01	2.536324E 00	2.518126E 00	-3.639703E-01	-3.639703E-01	3.214898E 04
	1.255078E-04	9.999981E-01	3.387939E 00	6.774902E-01	8.359609E-07	
-4.70	-1.144354E-03	-1.131918E-03	9.993399E-01	1.004186E 00	6.445521E-02	9.968622E-01
	-4.728758E-01	9.621196E 01	-7.326142E-04	9.215442E-04	-9.668501E 01	4.965555E-03
	1.100534E-01	2.536324E 00	2.518126E 00	-3.639703E-01	-3.639703E-01	3.205390E 04
	1.256929E-04	9.999981E-01	3.388330E 00	6.773844E-01	8.359112E-07	

TABLE 2.2

A= 1.100000E-01

-0.30	-4.499116E-01	-4.417610E-01	6.314577E-01	6.314602E-01	3.287345E-01	8.963060E-01
	-3.986544E-02	1.668315E 00	-1.093252E-02	2.025108E-02	-1.777597E 00	3.560511E-01
	1.104233E-01	1.020488E 00	1.015038E 00	-1.174696E-01	-1.005044E-01	3.808195E 00
	1.330077E-02	9.976695E-01	9.499210E-01	4.039961E-02	3.835512E-04	
-0.20	-5.165902E-01	-5.108741E-01	5.797987E-01	5.812095E-01	3.555657E-01	8.786637E-01
	-6.583899E-02	1.363632E 00	-1.080798E-02	2.114974E-02	-1.439813E 00	4.261183E-01
	1.105000E-01	1.010435E 00	1.006675E 00	-8.362466E-02	-6.681579E-02	2.770259E 00
	1.597615E-02	9.969445E-01	9.353898E-01	3.951925E-02	4.498481E-04	
-0.20	-5.217557E-01	-5.151802E-01	5.792822E-01	5.805681E-01	3.558455E-01	8.784798E-01
	-6.581092E-02	1.371807E 00	-1.083883E-02	2.121703E-02	-1.447994E 00	4.269405E-01
	1.105018E-01	1.010435E 00	1.006675E 00	-8.362466E-02	-6.681579E-02	2.755065E 00
	1.602543E-02	9.969345E-01	9.354910E-01	3.946692E-02	4.510819E-04	
-0.20	-5.747738E-01	-5.586281E-01	5.739804E-01	5.740154E-01	3.587322E-01	8.765815E-01
	-6.552273E-02	1.451612E 00	-1.116809E-02	2.190934E-02	-1.527874E 00	4.354780E-01
	1.105202E-01	1.010435E 00	1.006675E 00	-8.362466E-02	-6.681579E-02	2.605408E 00
	1.653688E-02	9.968244E-01	9.365284E-01	3.393083E-02	4.635905E-04	
-0.10	-7.342884E-01	-7.251607E-01	5.005516E-01	5.053536E-01	3.972628E-01	8.489340E-01
	-3.496653E-02	1.126568E 00	-1.130828E-02	2.371383E-02	-1.173939E 00	5.548556E-01
	1.106830E-01	1.003753E 00	1.001668E 00	-5.006338E-02	-3.335263E-02	1.620222E 00
	2.201264E-02	9.952537E-01	9.303002E-01	3.714728E-02	5.852419E-04	
-0.10	-7.416307E-01	-7.309724E-01	4.998174E-01	5.045901E-01	3.976747E-01	8.486386E-01
	-3.494263E-02	1.131936E 00	-1.134466E-02	2.379845E-02	-1.179332E 00	5.562977E-01
	1.106868E-01	1.003753E 00	1.001668E 00	-5.006338E-02	-3.335263E-02	1.609279E 00
	2.210141E-02	9.952320E-01	9.304189E-01	3.708577E-02	5.870638E-04	
-0.10	-1.938165E 00	-1.186777E 00	3.801640E-01	3.895208E-01	4.732734E-01	7.943994E-01
	-3.104898E-02	1.265069E 00	-1.743715E-02	3.689777E-02	-1.315578E 00	8.659823E-01
	1.120805E-01	1.003753E 00	1.001668E 00	-5.006338E-02	-3.335263E-02	6.033643E-01
	4.168497E-02	9.904414E-01	9.480225E-01	2.800357E-02	8.613467E-04	
-0.10	5.042845E-01	2.999421E-01	6.244088E-01	6.461810E-01	3.350000E-01	8.936060E-01
	-3.899699E-02	-1.386732E 00	-5.558502E-03	1.011471E-02	1.343178E 00	3.640382E-01
	1.106074E-01	1.003753E 00	1.001668E 00	-5.006338E-02	-3.335263E-02	7.317356E 00
	1.036539E-02	9.980860E-01	9.081752E-01	4.868573E-02	2.698253E-04	
-0.10	-1.091450E 00	-9.687036E-01	4.648355E-01	4.690634E-01	4.179752E-01	8.340735E-01
	-3.380428E-02	1.306012E 00	-1.314261E-02	2.782402E-02	-1.354497E 00	6.305536E-01
	1.109201E-01	1.003753E 00	1.001668E 00	-5.006338E-02	-3.335263E-02	1.180654E 00
	2.669522E-02	9.941115E-01	9.359329E-01	3.423172E-02	6.728200E-04	

AMM2= 1.644942E-01

TABLE 2.3

A= 9.499997E-02

0.20	-2.417535E-02	-2.374732E-02	7.335247E-01	7.311646E-01	2.711894E-01	9.288110E-01
	4.781679E-02	5.327090E-01	-6.069820E-03	1.003346E-02	-4.888558E-01	2.187704E-01
	9.518427E-02	1.003753E 00	1.006675E 00	5.006192E-02	6.681454E-02	2.340041E 01
	4.997636E-03	9.993470E-01	8.900059E-01	5.327355E-02	1.246750E-04	
0.20	-2.441703E-02	-2.397308E-02	7.335005E-01	7.311139E-01	2.712027E-01	9.288037E-01
	4.781600E-02	5.371361E-01	-6.073177E-03	1.003811E-02	-4.932850E-01	2.187964E-01
	9.518427E-02	1.003753E 00	1.006675E 00	5.006192E-02	6.681454E-02	2.338223E 01
	4.999578E-03	9.993469E-01	8.900167E-01	6.326783E-02	1.247118E-04	
0.20	-2.631265E-03	-3.742492E-03	7.356791E-01	7.357613E-01	2.700238E-01	9.294399E-01
	4.788689E-02	1.243590E-01	-5.848181E-03	9.621691E-03	-8.024555E-02	2.164689E-01
	9.518480E-02	1.003753E 00	1.006675E 00	5.006192E-02	6.681454E-02	2.510602E 01
	4.830021E-03	9.993656E-01	8.888649E-01	6.387848E-02	1.209721E-04	
0.30	-1.489851E-04	8.898806E-04	7.356642E-01	7.313521E-01	2.700281E-01	9.294345E-01
	7.997489E-02	5.086252E-02	-5.598325E-03	8.947205E-03	2.576349E-02	2.135316E-01
	9.518415E-02	1.010435E 00	1.015038E 00	8.362317E-02	1.005028E-01	3.319926E 01
	4.161824E-03	9.994613E-01	8.942041E-01	6.941390E-02	1.042287E-04	
0.30	-1.504748E-04	6.884757E-04	7.356640E-01	7.313521E-01	2.700281E-01	9.294332E-01
	7.997489E-02	5.090373E-02	-5.598765E-03	8.947238E-03	2.572269E-02	2.135317E-01
	9.518415E-02	1.010435E 00	1.015038E 00	8.362317E-02	1.005028E-01	3.319899E 01
	4.161838E-03	9.994613E-01	8.942029E-01	6.941450E-02	1.042286E-04	
0.30	-4.330936E-02	-3.986688E-02	7.313482E-01	7.219505E-01	2.723649E-01	9.281718E-01
	7.974029E-02	1.127293E 00	-6.095853E-03	9.847593E-03	-1.051303E 00	2.181574E-01
	9.516307E-02	1.010435E 00	1.015038E 00	8.362317E-02	1.005028E-01	2.809000E 01
	4.515402E-03	9.994274E-01	8.968571E-01	6.801212E-02	1.112926E-04	
0.30	3.644176E-02	3.430655E-02	7.393233E-01	7.394541E-01	2.680575E-01	9.304979E-01
	8.017379E-02	-1.012074E 00	-5.186751E-03	8.201290E-03	1.089231E 00	2.096877E-01
	9.518588E-02	1.010435E 00	1.015038E 00	8.362317E-02	1.005028E-01	3.873813E 01
	3.865905E-03	9.994897E-01	8.919277E-01	7.061833E-02	9.821171E-05	

TOO LITTLE MASS FLOW

TABLE 2.4

11 JUL 1967

RUN 10-2 X= -5.00 A= 0.10854 SIGMAW= 2.727 SW2= 6.90 TANTHP=-0.364 P= 9.9975E-01 DPDX=-1.0534E-04

ARCHI= 0.0 CONDI= 0.0 SHERI= 0.0 GENRI= 0.0 AMSO= 0.0 THCOEF= 0.0

PDA= 0.0 TAU= 0.0 DERDX= 0.0 HFLUX= 1.0859E-01 HTR= 0.0 Q= 0.0

ETA	U	T	W	V	D	PSI	M	DA/DX	PGT	SHEAR	COND'N	GEN
0.0	0.06298	0.99703	0.0	0.0	1.003E 00	0.0	0.163	0.0	0.0	0.0	0.0	0.0
0.02	0.06296	0.99703	0.0	-0.0005	1.003E 00	0.0	0.163	0.0	0.0	0.0	0.0	0.0
0.04	0.06288	0.99704	0.0	-0.0009	1.003E 00	0.0	0.163	0.0	0.0	0.0	0.0	0.0
0.06	0.06276	0.99705	0.0	-0.0014	1.003E 00	0.0	0.162	0.0	0.0	0.0	0.0	0.0
0.08	0.06258	0.99707	0.0	-0.0018	1.003E 00	0.0	0.162	0.0	0.0	0.0	0.0	0.0
0.10	0.06235	0.99709	0.0	-0.0023	1.003E 00	0.0	0.161	0.0	0.0	0.0	0.0	0.0
0.12	0.06208	0.99711	0.0	-0.0027	1.003E 00	0.0	0.161	0.0	0.0	0.0	0.0	0.0
0.14	0.06175	0.99715	0.0	-0.0031	1.003E 00	0.0	0.160	0.0	0.0	0.0	0.0	0.0
0.16	0.06137	0.99718	0.0	-0.0036	1.003E 00	0.0	0.159	0.0	0.0	0.0	0.0	0.0
0.18	0.06094	0.99722	0.0	-0.0040	1.003E 00	0.0	0.158	0.0	0.0	0.0	0.0	0.0
0.20	0.06047	0.99726	0.0	-0.0044	1.002E 00	0.0	0.156	0.0	0.0	0.0	0.0	0.0
0.22	0.05994	0.99731	0.0	-0.0048	1.002E 00	0.0	0.155	0.0	0.0	0.0	0.0	0.0
0.24	0.05936	0.99736	0.0	-0.0052	1.002E 00	0.0	0.153	0.0	0.0	0.0	0.0	0.0
0.26	0.05873	0.99742	0.0	-0.0056	1.002E 00	0.0	0.152	0.0	0.0	0.0	0.0	0.0
0.28	0.05805	0.99748	0.0	-0.0059	1.002E 00	0.0	0.150	0.0	0.0	0.0	0.0	0.0
0.30	0.05732	0.99754	0.0	-0.0063	1.002E 00	0.0	0.148	0.0	0.0	0.0	0.0	0.0
0.32	0.05654	0.99761	0.0	-0.0066	1.002E 00	0.0	0.146	0.0	0.0	0.0	0.0	0.0
0.34	0.05571	0.99768	0.0	-0.0069	1.002E 00	0.0	0.144	0.0	0.0	0.0	0.0	0.0
0.36	0.05483	0.99775	0.0	-0.0072	1.002E 00	0.0	0.142	0.0	0.0	0.0	0.0	0.0
0.38	0.05390	0.99783	0.0	-0.0075	1.002E 00	0.0	0.139	0.0	0.0	0.0	0.0	0.0
0.40	0.05291	0.99790	0.0	-0.0077	1.002E 00	0.0	0.137	0.0	0.0	0.0	0.0	0.0
0.42	0.05188	0.99799	0.0	-0.0079	1.002E 00	0.0	0.134	0.0	0.0	0.0	0.0	0.0
0.44	0.05080	0.99807	0.0	-0.0081	1.002E 00	0.0	0.131	0.0	0.0	0.0	0.0	0.0
0.46	0.04967	0.99815	0.0	-0.0083	1.002E 00	0.0	0.128	0.0	0.0	0.0	0.0	0.0
0.48	0.04848	0.99824	0.0	-0.0085	1.002E 00	0.0	0.125	0.0	0.0	0.0	0.0	0.0
0.50	0.04725	0.99833	0.0	-0.0086	1.001E 00	0.0	0.122	0.0	0.0	0.0	0.0	0.0
0.52	0.04597	0.99842	0.0	-0.0087	1.001E 00	0.0	0.119	0.0	0.0	0.0	0.0	0.0
0.54	0.04463	0.99851	0.0	-0.0088	1.001E 00	0.0	0.115	0.0	0.0	0.0	0.0	0.0
0.56	0.04325	0.99860	0.0	-0.0088	1.001E 00	0.0	0.112	0.0	0.0	0.0	0.0	0.0
0.58	0.04181	0.99869	0.0	-0.0088	1.001E 00	0.0	0.108	0.0	0.0	0.0	0.0	0.0
0.60	0.04033	0.99878	0.0	-0.0088	1.001E 00	0.0	0.104	0.0	0.0	0.0	0.0	0.0
0.62	0.03379	0.99887	0.0	-0.0088	1.001E 00	0.0	0.100	0.0	0.0	0.0	0.0	0.0
0.64	0.03721	0.99896	0.0	-0.0087	1.001E 00	0.0	0.096	0.0	0.0	0.0	0.0	0.0
0.66	0.03557	0.99905	0.0	-0.0085	1.001E 00	0.0	0.092	0.0	0.0	0.0	0.0	0.0
0.68	0.03389	0.99914	0.0	-0.0084	1.001E 00	0.0	0.088	0.0	0.0	0.0	0.0	0.0
0.70	0.03215	0.99923	0.0	-0.0082	1.001E 00	0.0	0.083	0.0	0.0	0.0	0.0	0.0
0.72	0.03036	0.99931	0.0	-0.0080	1.000E 00	0.0	0.078	0.0	0.0	0.0	0.0	0.0
0.74	0.02852	0.99939	0.0	-0.0077	1.000E 00	0.0	0.074	0.0	0.0	0.0	0.0	0.0
0.76	0.02664	0.99947	0.0	-0.0074	1.000E 00	0.0	0.069	0.0	0.0	0.0	0.0	0.0
0.78	0.02470	0.99954	0.0	-0.0070	1.000E 00	0.0	0.064	0.0	0.0	0.0	0.0	0.0
0.80	0.02271	0.99962	0.0	-0.0066	1.000E 00	0.0	0.059	0.0	0.0	0.0	0.0	0.0
0.82	0.02067	0.99968	0.0	-0.0062	1.000E 00	0.0	0.053	0.0	0.0	0.0	0.0	0.0
0.84	0.01858	0.99974	0.0	-0.0057	1.000E 00	0.0	0.048	0.0	0.0	0.0	0.0	0.0
0.86	0.01644	0.99980	0.0	-0.0051	9.999E-01	0.0	0.042	0.0	0.0	0.0	0.0	0.0
0.88	0.01425	0.99985	0.0	-0.0046	9.999E-01	0.0	0.037	0.0	0.0	0.0	0.0	0.0
0.90	0.01201	0.99989	0.0	-0.0039	9.999E-01	0.0	0.031	0.0	0.0	0.0	0.0	0.0
0.92	0.00972	0.99993	0.0	-0.0033	9.998E-01	0.0	0.025	0.0	0.0	0.0	0.0	0.0
0.94	0.00738	0.99996	0.0	-0.0025	9.998E-01	0.0	0.019	0.0	0.0	0.0	0.0	0.0
0.96	0.00499	0.99998	0.0	-0.0017	9.998E-01	0.0	0.013	0.0	0.0	0.0	0.0	0.0
0.98	0.00255	1.00000	0.0	-0.0009	9.998E-01	0.0	0.007	0.0	0.0	0.0	0.0	0.0
1.00	0.00006	1.00000	0.0	-0.0000	9.997E-01	0.0	0.000	0.0	0.0	0.0	0.0	0.0

TABLE 2.5

A= 1.085936E-01

-0.10	-4.905088E-01	-4.876641E-01	5.603429E-01	5.514313E-01	3.651371E-01	8.717991E-01
	-3.806460E-02	1.209056E 00	-1.028845E-02	2.054848E-02	-1.257379E 00	4.514642E-01
	1.090834E-01	1.003753E 00	1.001668E 00	-5.006338E-02	-3.335263E-02	2.629166E 00
	1.647352E-02	9.967793E-01	9.236392E-01	4.061121E-02	4.527266E-04	
-0.10	-4.954135E-01	-4.918567E-01	5.598524E-01	5.608525E-01	3.654010E-01	8.716188E-01
	-3.804364E-02	1.216401E 00	-1.031652E-02	2.061077E-02	-1.264742E 00	4.522722E-01
	1.090910E-01	1.003753E 00	1.001668E 00	-5.006338E-02	-3.335263E-02	2.615202E 00
	1.652275E-02	9.967682E-01	9.237247E-01	4.056203E-02	4.538996E-04	
-0.10	-5.510448E-01	-5.386205E-01	5.542893E-01	5.543186E-01	3.684093E-01	8.695741E-01
	-3.786761E-02	1.295452E 00	-1.064087E-02	2.131944E-02	-1.343998E 00	4.615404E-01
	1.091091E-01	1.003753E 00	1.001668E 00	-5.006338E-02	-3.335263E-02	2.463564E 00
	1.708739E-02	9.966449E-01	9.248065E-01	3.999937E-02	4.671116E-04	
-0.00	-6.950330E-01	-6.914757E-01	4.847260E-01	4.890072E-01	4.048734E-01	8.427035E-01
	-1.125739E-02	1.027289E 00	-1.071557E-02	2.291403E-02	-1.050744E 00	5.783643E-01
	1.092527E-01	1.000418E 00	1.000000E 00	-1.666962E-02	-6.357832E-07	1.574304E 00
	2.239805E-02	9.951075E-01	9.244313E-01	3.852654E-02	5.800931E-04	
-0.00	-7.025838E-01	-6.971723E-01	4.840305E-01	4.883104E-01	4.052678E-01	8.424163E-01
	-1.125045E-02	1.032286E 00	-1.074362E-02	2.299315E-02	-1.055779E 00	5.797729E-01
	1.092561E-01	1.000418E 00	1.000000E 00	-1.666962E-02	-6.357832E-07	1.563920E 00
	2.248628E-02	9.950857E-01	9.245458E-01	3.846699E-02	5.818417E-04	
-0.00	-5.149534E-01	-5.350446E-01	5.027939E-01	5.073296E-01	3.949403E-01	8.500232E-01
	-1.145376E-02	8.719342E-01	-9.872380E-03	2.086471E-02	-8.943797E-01	5.431954E-01
	1.091830E-01	1.000418E 00	1.000000E 00	-1.666962E-02	-6.357832E-07	1.878239E 00
	2.020182E-02	9.956434E-01	9.213899E-01	4.010946E-02	5.345547E-04	
0.10	-4.812257E-01	-5.266793E-01	4.546713E-01	4.654148E-01	4.199005E-01	8.303038E-01
	1.037347E-02	6.375126E-01	-8.771304E-03	1.994598E-02	-6.363137E-01	6.278846E-01
	1.092462E-01	1.000418E 00	1.001668E 00	1.666817E-02	3.335105E-02	1.544669E 00
	2.273116E-02	9.947262E-01	9.227516E-01	4.106838E-02	5.782195E-04	
0.10	-4.860376E-01	-5.314896E-01	4.541301E-01	4.649688E-01	4.201627E-01	8.300970E-01
	1.036825E-02	6.413119E-01	-8.788753E-03	1.999576E-02	-6.421506E-01	6.288947E-01
	1.092477E-01	1.000418E 00	1.001668E 00	1.666817E-02	3.335105E-02	1.537172E 00
	2.279617E-02	9.947091E-01	9.228304E-01	4.102737E-02	5.794850E-04	
0.10	-5.223954E-01	-5.676359E-01	4.505544E-01	4.616084E-01	4.221530E-01	8.285255E-01
	1.032836E-02	6.690437E-01	-8.920759E-03	2.037220E-02	-6.701662E-01	6.365957E-01
	1.092539E-01	1.000418E 00	1.001668E 00	1.666817E-02	3.335105E-02	1.482031E 00
	2.329227E-02	9.945812E-01	9.234145E-01	4.072344E-02	5.890524E-04	
0.20	-5.299445E-01	-6.151813E-01	3.975599E-01	4.167081E-01	4.504505E-01	8.046309E-01
	2.759783E-02	5.213934E-01	-8.225553E-03	1.997140E-02	-5.055412E-01	7.455553E-01
	1.093408E-01	1.003753E 00	1.006675E 00	5.006192E-02	6.681454E-02	1.155376E 00
	2.733162E-02	9.931544E-01	9.310054E-01	4.178858E-02	6.446603E-04	
0.20	-5.352436E-01	-6.210107E-01	3.970300E-01	4.162613E-01	4.507511E-01	8.043762E-01
	2.758059E-02	5.242257E-01	-8.241501E-03	2.002228E-02	-5.084258E-01	7.468736E-01
	1.093426E-01	1.003753E 00	1.006675E 00	5.006192E-02	6.681454E-02	1.149261E 00
	2.742006E-02	9.931295E-01	9.310883E-01	4.174566E-02	6.460890E-04	
0.20	-4.872565E-01	-5.680094E-01	4.013287E-01	4.203097E-01	4.480402E-01	8.066653E-01
	2.773673E-02	4.975404E-01	-8.101486E-03	1.956158E-02	-4.812636E-01	7.350575E-01
	1.093268E-01	1.003753E 00	1.006675E 00	5.006192E-02	6.681454E-02	1.206196E 00
	2.662842E-02	9.933494E-01	9.303392E-01	4.213387E-02	6.329378E-04	

TABLE 2.6

A= 1.085936E-01

1.00	-1.723466E-01	-2.938502E-01	1.579721E-01	1.929405E-01	6.015723E-01	6.485605E-01
	7.229934E-02	8.123755E-02	-1.129265E-02	1.152366E-02	-9.168725E-03	1.576427E 00
	1.090848E-01	1.154389E 00	1.171573E 00	3.338466E-01	3.535523E-01	5.124360E-01
	4.200120E-02	7.665508E-01	1.213594E 00	6.994057E-02	-9.156887E-04	
1.00	-1.740699E-01	-3.188887E-01	1.577998E-01	1.928351E-01	6.017140E-01	6.483935E-01
	7.226241E-02	8.165158E-02	-1.128955E-02	1.153650E-02	-9.646125E-03	1.577672E 00
	1.090847E-01	1.154389E 00	1.171573E 00	3.338466E-01	3.535523E-01	5.107851E-01
	4.209192E-02	7.665457E-01	1.213659E 00	6.991100E-02	-9.147101E-04	
1.00	-1.716424E-01	-2.840492E-01	1.580425E-01	1.929834E-01	6.015145E-01	6.486285E-01
	7.231510E-02	8.106387E-02	-1.129359E-02	1.151844E-02	-8.973613E-03	1.575917E 00
	1.090848E-01	1.154389E 00	1.171573E 00	3.338466E-01	3.535523E-01	5.131113E-01
	4.196423E-02	7.665526E-01	1.213568E 00	6.995296E-02	-9.160859E-04	
1.10	-1.455216E-01	2.069379E 00	1.434903E-01	1.741729E-01	6.135212E-01	6.341806E-01
	7.323027E-02	6.842047E-02	-1.213128E-02	1.095371E-02	5.987372E-03	1.669521E 00
	1.088348E-01	1.189751E 00	1.208942E 00	3.736314E-01	3.941148E-01	4.917532E-01
	4.033041E-02	6.965225E-01	1.288953E 00	7.362270E-02	-1.253780E-03	
1.10	-1.469766E-01	2.744234E 00	1.433448E-01	1.740869E-01	6.136470E-01	6.340298E-01
	7.319498E-02	6.878382E-02	-1.212859E-02	1.096467E-02	5.575087E-03	1.670699E 00
	1.088343E-01	1.189751E 00	1.208942E 00	3.736314E-01	3.941148E-01	4.903039E-01
	4.046044E-02	6.965247E-01	1.289019E 00	7.359314E-02	-1.252855E-03	
1.10	-1.458772E-01	2.194113E 00	1.434547E-01	1.741518E-01	6.135520E-01	6.341440E-01
	7.322162E-02	6.850940E-02	-1.213062E-02	1.095638E-02	5.886462E-03	1.669809E 00
	1.088347E-01	1.189751E 00	1.208942E 00	3.736314E-01	3.941148E-01	4.913990E-01
	4.039992E-02	6.965229E-01	1.288970E 00	7.361507E-02	-1.253554E-03	
1.20	-1.239795E-01	-8.763469E-01	1.310568E-01	1.568768E-01	6.243210E-01	6.209257E-01
	7.405591E-02	5.912377E-02	-1.242490E-02	1.049967E-02	1.685736E-02	1.759931E 00
	1.085521E-01	1.229169E 00	1.250454E 00	4.150366E-01	4.364344E-01	4.773020E-01
	3.831551E-02	6.317554E-01	1.376915E 00	7.703400E-02	-1.494024E-03	
1.20	-1.252192E-01	-8.232753E-01	1.309328E-01	1.568063E-01	6.244339E-01	6.207876E-01
	7.402247E-02	5.944411E-02	-1.242224E-02	1.050921E-02	1.649140E-02	1.761047E 00
	1.085514E-01	1.229169E 00	1.250454E 00	4.150366E-01	4.364344E-01	4.760075E-01
	3.838537E-02	6.317627E-01	1.376979E 00	7.700729E-02	-1.493162E-03	
1.20	-1.587421E-01	-1.756266E-01	1.275805E-01	1.548898E-01	6.275186E-01	6.170022E-01
	7.311809E-02	6.757790E-02	-1.234725E-02	1.076563E-02	7.121809E-03	1.791925E 00
	1.085368E-01	1.229169E 00	1.250454E 00	4.150366E-01	4.364344E-01	4.426202E-01
	4.032836E-02	6.319699E-01	1.378706E 00	7.627106E-02	-1.469902E-03	
1.20	-1.595400E-01	-1.684916E-01	1.275007E-01	1.548440E-01	6.275927E-01	6.169107E-01
	7.309657E-02	6.775910E-02	-1.234521E-02	1.077170E-02	6.910987E-03	1.792679E 00
	1.085366E-01	1.229169E 00	1.250454E 00	4.150366E-01	4.364344E-01	4.418620E-01
	4.037593E-02	6.319751E-01	1.378746E 00	7.625389E-02	-1.469353E-03	
1.20	-1.604403E-01	-1.606579E-01	1.274107E-01	1.547921E-01	6.276764E-01	6.168078E-01
	7.307231E-02	6.796288E-02	-1.234310E-02	1.077854E-02	6.673984E-03	1.793527E 00
	1.085362E-01	1.229169E 00	1.250454E 00	4.150366E-01	4.364344E-01	4.410080E-01
	4.042967E-02	6.319802E-01	1.378795E 00	7.623366E-02	-1.468734E-03	
1.20	-1.604627E-01	-1.604717E-01	1.274084E-01	1.547909E-01	6.276789E-01	6.168056E-01
	7.307172E-02	6.796795E-02	-1.234326E-02	1.077871E-02	6.668311E-03	1.793547E 00
	1.085363E-01	1.229169E 00	1.250454E 00	4.150366E-01	4.364344E-01	4.409872E-01
	4.043099E-02	6.319807E-01	1.378795E 00	7.623386E-02	-1.468721E-03	

TABLE 2.7

11 JUL 1969

RUN MC-2 X= 2.00 A= 3.106594 SIGMAW= 1.621 SW2= 2.86 TANTHP= 0.577 P= 5.1591E-02 DPDX=-5.1776E-02

ARCHI= 4.0665E-02 CONDI=-4.1146E-03 SHEARI= 1.9470E-02 GENRI= 6.5260E-03 AMSQ= 2.8489E 00 THCOEF= 1.4543E 00

PDA= 6.8993E-02 TAU=-3.3341E-02 DFFPDX= 6.5652E-02 HFLUX= 1.0693E-01 HTR=-5.3499E-04 Q=-7.6753E-04

ETA	U	T	W	V	D	PSI	M	DA/DX	PST	SHEAR	COND'N	GEN
0.0	0.71582	0.49939	0.0	0.0	1.033E-01	0.0	2.615	0.0	0.0	0.0	0.0	0.0
0.02	0.71582	0.49939	-3.081E-04	0.0080	1.033E-01	0.000	2.615	1.561E-03	1.489E-03	-4.685E-09	1.041E-07	3.541E-14
0.04	0.71582	0.49939	-6.164E-04	0.0159	1.033E-01	0.002	2.615	3.123E-03	2.978E-03	1.085E-08	3.770E-09	6.741E-16
0.06	0.71582	0.49939	-9.247E-04	0.0239	1.033E-01	0.004	2.615	4.684E-03	4.467E-03	2.145E-08	1.583E-07	9.561E-13
0.08	0.71581	0.49940	-1.233E-03	0.0318	1.033E-01	0.007	2.615	6.246E-03	5.956E-03	5.795E-08	2.752E-07	2.947E-12
0.10	0.71581	0.49941	-1.542E-03	0.0398	1.033E-01	0.011	2.615	7.807E-03	7.445E-03	-7.496E-08	3.841E-07	4.915E-12
0.12	0.71580	0.49941	-1.850E-03	0.0477	1.033E-01	0.016	2.615	9.368E-03	8.934E-03	-8.039E-08	4.849E-07	7.900E-12
0.14	0.71579	0.49942	-2.158E-03	0.0557	1.033E-01	0.022	2.615	1.093E-02	1.042E-02	-1.208E-08	6.108E-07	9.893E-12
0.16	0.71578	0.49944	-2.467E-03	0.0637	1.033E-01	0.029	2.615	1.249E-02	1.191E-02	-8.130E-09	4.152E-07	1.096E-11
0.18	0.71578	0.49945	-2.776E-03	0.0716	1.033E-01	0.037	2.615	1.405E-02	1.340E-02	-7.768E-08	4.497E-07	1.673E-11
0.20	0.71577	0.49947	-3.085E-03	0.0796	1.033E-01	0.046	2.615	1.561E-02	1.489E-02	-1.010E-08	7.038E-07	2.144E-11
0.22	0.71576	0.49949	-3.394E-03	0.0875	1.033E-01	0.055	2.615	1.717E-02	1.638E-02	-2.319E-07	9.828E-07	3.347E-11
0.24	0.71575	0.49951	-3.703E-03	0.0955	1.033E-01	0.066	2.615	1.874E-02	1.787E-02	2.668E-08	3.805E-07	3.965E-11
0.26	0.71573	0.49953	-4.013E-03	0.1034	1.033E-01	0.077	2.615	2.030E-02	1.935E-02	2.546E-08	1.045E-06	5.974E-11
0.28	0.71572	0.49955	-4.322E-03	0.1114	1.033E-01	0.089	2.615	2.186E-02	2.084E-02	1.173E-07	6.889E-07	8.319E-11
0.30	0.71570	0.49957	-4.631E-03	0.1193	1.033E-01	0.103	2.615	2.342E-02	2.233E-02	1.607E-07	8.351E-07	1.104E-10
0.32	0.71568	0.49959	-4.941E-03	0.1273	1.033E-01	0.117	2.614	2.498E-02	2.382E-02	-2.152E-07	7.319E-07	1.487E-10
0.34	0.71566	0.49961	-5.252E-03	0.1352	1.033E-01	0.132	2.614	2.654E-02	2.531E-02	3.442E-07	4.043E-07	1.827E-10
0.36	0.71564	0.49964	-5.562E-03	0.1432	1.033E-01	0.148	2.614	2.810E-02	2.680E-02	8.455E-08	9.588E-07	2.273E-10
0.38	0.71562	0.49966	-5.873E-03	0.1511	1.033E-01	0.165	2.614	2.966E-02	2.828E-02	2.436E-07	1.030E-06	2.786E-10
0.40	0.71559	0.49969	-6.185E-03	0.1591	1.032E-01	0.183	2.614	3.122E-02	2.977E-02	3.405E-07	8.930E-07	3.400E-10
0.42	0.71556	0.49971	-6.496E-03	0.1670	1.032E-01	0.201	2.614	3.278E-02	3.126E-02	1.894E-07	7.648E-07	3.862E-10
0.44	0.71554	0.49974	-6.807E-03	0.1750	1.032E-01	0.221	2.613	3.434E-02	3.275E-02	5.081E-07	1.244E-06	4.639E-10
0.46	0.71551	0.49976	-7.118E-03	0.1829	1.032E-01	0.241	2.613	3.590E-02	3.424E-02	-8.455E-08	1.472E-06	5.215E-10
0.48	0.71548	0.49979	-7.430E-03	0.1908	1.032E-01	0.263	2.613	3.746E-02	3.572E-02	2.594E-08	1.492E-06	5.730E-10
0.50	0.71544	0.49982	-7.742E-03	0.1988	1.032E-01	0.285	2.613	3.902E-02	3.721E-02	-7.983E-08	1.651E-06	6.104E-10
0.52	0.71541	0.49985	-8.054E-03	0.2067	1.032E-01	0.308	2.613	4.058E-02	3.870E-02	3.316E-07	1.835E-06	7.027E-10
0.54	0.71538	0.49988	-8.367E-03	0.2147	1.032E-01	0.333	2.612	4.214E-02	4.019E-02	4.284E-07	2.715E-06	8.078E-10
0.56	0.71534	0.49992	-8.679E-03	0.2226	1.032E-01	0.358	2.612	4.370E-02	4.167E-02	3.062E-07	3.475E-06	9.024E-10
0.58	0.71530	0.49997	-8.991E-03	0.2305	1.032E-01	0.384	2.612	4.526E-02	4.316E-02	-2.836E-07	6.190E-06	1.013E-09
0.60	0.71527	0.50003	-9.303E-03	0.2385	1.032E-01	0.411	2.612	4.682E-02	4.465E-02	7.703E-07	1.093E-05	1.085E-09
0.62	0.71523	0.50011	-9.613E-03	0.2464	1.032E-01	0.438	2.611	4.839E-02	4.613E-02	1.469E-06	1.743E-05	1.402E-09
0.64	0.71518	0.50023	-9.922E-03	0.2543	1.031E-01	0.467	2.611	4.996E-02	4.762E-02	2.732E-06	3.385E-05	1.900E-09
0.66	0.71512	0.50042	-1.023E-02	0.2623	1.031E-01	0.497	2.610	5.154E-02	4.910E-02	7.068E-06	5.758E-05	3.449E-09
0.68	0.71504	0.50071	-1.052E-02	0.2702	1.030E-01	0.527	2.609	5.314E-02	5.058E-02	1.522E-05	1.024E-04	8.663E-09
0.70	0.71490	0.50119	-1.080E-02	0.2781	1.029E-01	0.559	2.607	5.476E-02	5.206E-02	3.271E-05	1.774E-04	2.725E-08
0.72	0.71464	0.50199	-1.106E-02	0.2860	1.028E-01	0.591	2.604	5.644E-02	5.352E-02	7.023E-05	3.010E-04	9.994E-08
0.74	0.71414	0.50331	-1.126E-02	0.2938	1.025E-01	0.624	2.599	5.818E-02	5.497E-02	1.443E-04	4.896E-04	3.933E-07
0.76	0.71316	0.50544	-1.143E-02	0.3015	1.021E-01	0.658	2.590	6.002E-02	5.639E-02	2.845E-04	7.562E-04	1.533E-06
0.78	0.71128	0.50875	-1.149E-02	0.3088	1.014E-01	0.692	2.575	6.197E-02	5.776E-02	5.413E-04	1.080E-03	5.716E-06
0.80	0.70779	0.51363	-1.143E-02	0.3155	1.004E-01	0.727	2.550	6.396E-02	5.903E-02	9.769E-04	1.388E-03	1.984E-05
0.82	0.70156	0.52038	-1.124E-02	0.3209	9.914E-02	0.762	2.511	6.592E-02	6.017E-02	1.699E-03	1.525E-03	6.351E-05
0.84	0.69093	0.52895	-1.094E-02	0.3241	9.754E-02	0.797	2.453	6.765E-02	6.107E-02	2.848E-03	1.281E-03	1.869E-04
0.86	0.67358	0.53879	-1.055E-02	0.3239	9.575E-02	0.832	2.369	6.907E-02	6.162E-02	4.677E-03	4.913E-04	5.097E-04
0.88	0.64637	0.54879	-1.010E-02	0.3183	9.401E-02	0.866	2.253	7.035E-02	6.160E-02	7.612E-03	-8.321E-04	1.306E-03
0.90	0.60524	0.55752	-9.438E-03	0.3050	9.254E-02	0.898	2.093	7.223E-02	6.055E-02	1.235E-02	-2.431E-03	3.181E-03
0.92	0.54543	0.56369	-8.425E-03	0.2813	9.152E-02	0.928	1.876	7.580E-02	5.744E-02	1.994E-02	-4.192E-03	7.402E-03
0.94	0.46245	0.56619	-6.591E-03	0.2444	9.112E-02	0.954	1.587	8.207E-02	4.954E-02	3.247E-02	-7.159E-03	1.653E-02
0.96	0.35338	0.56326	-3.986E-03	0.1919	9.159E-02	0.976	1.216	9.092E-02	2.744E-02	5.797E-02	-1.568E-02	3.660E-02
0.98	0.21688	0.55084	-1.296E-03	0.1214	9.366E-02	0.992	0.754	1.004E-01	-6.368E-02	1.499E-01	-4.817E-02	9.188E-02
1.00	0.05090	0.51998	0.0	0.0294	9.922E-02	1.000	0.182	0.0	-2.629E 00	2.729E 00	-5.137E-01	5.372E-01

TABLE 2.8

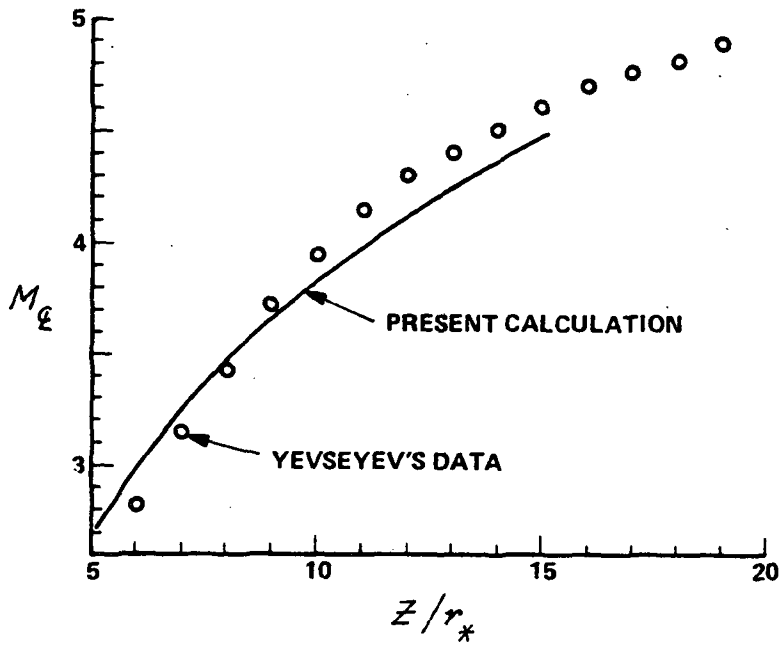

Figure 1 DISTRIBUTION OF CENTERLINE MACH NUMBER, CASE 1

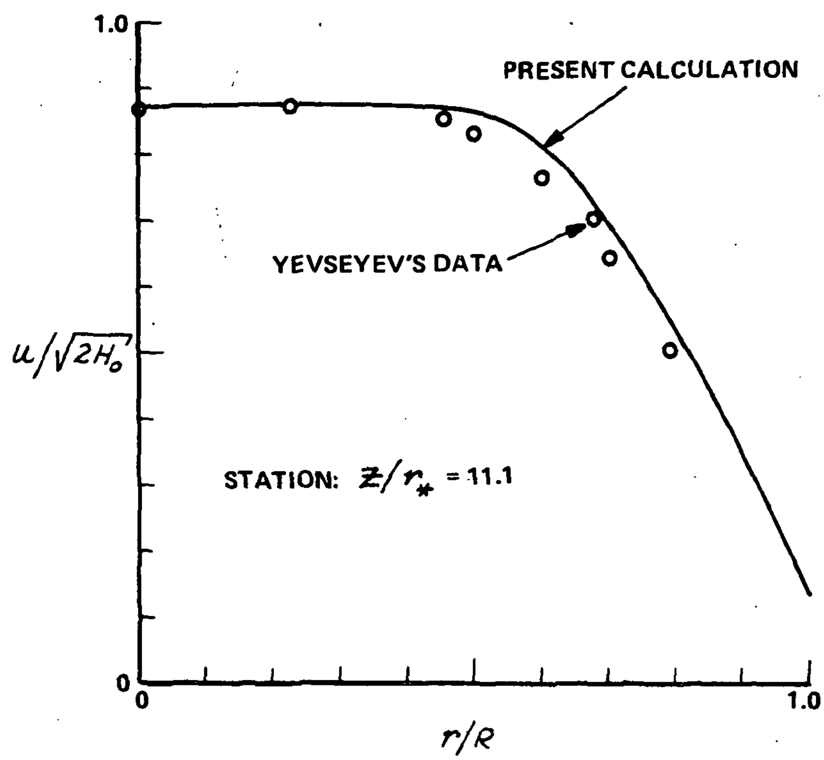

Figure 2 VELOCITY - PROFILE PREDICTION CASE 1

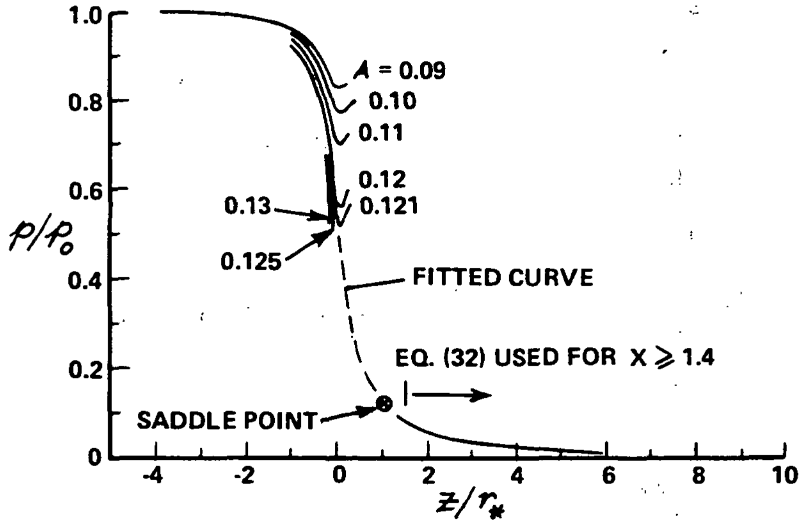

Figure 3 PRESSURE DISTRIBUTIONS FOR VARIOUS MASS FLOWS,(CASE 2)

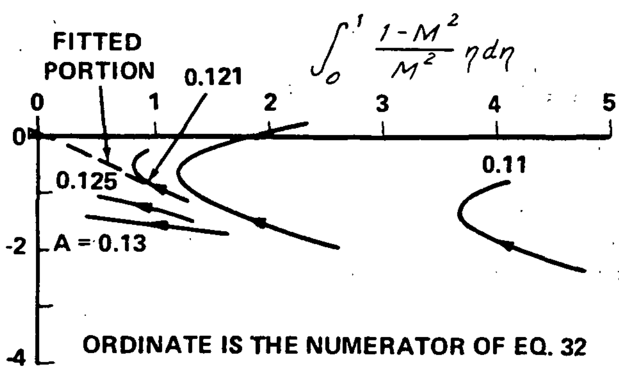

Figure 4 SOLUTION CURVES FOR VARIOUS MASS FLOWS (CASE 2)

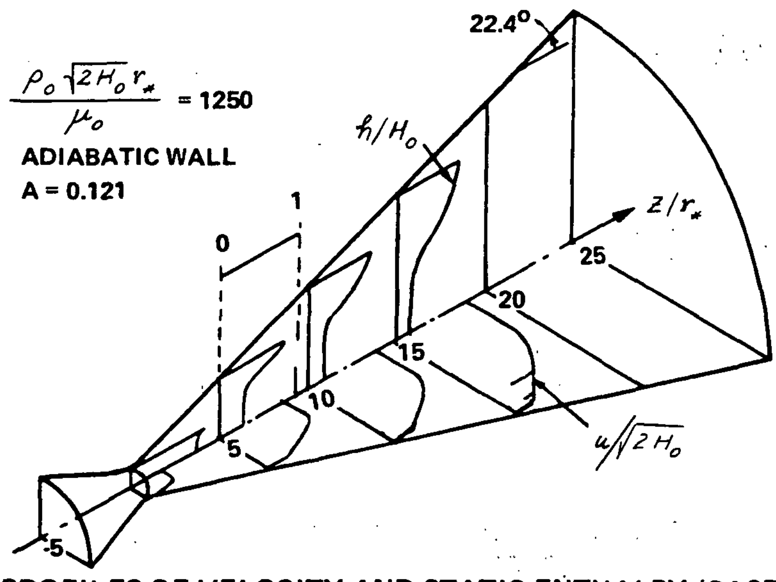

Figure 5 PROFILES OF VELOCITY AND STATIC ENTHALPY (CASE 2)

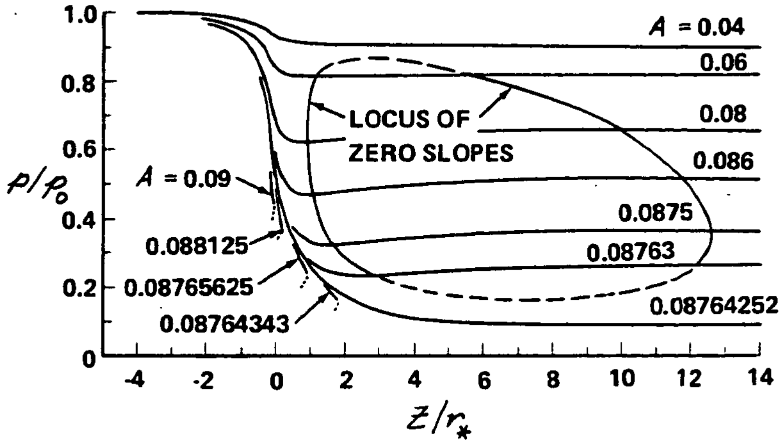

Figure 6 PRESSURE DISTRIBUTIONS FOR VARIOUS MASS FLOWS, CASE 10

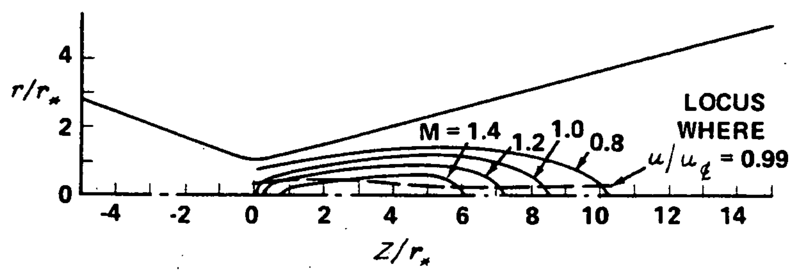

Figure 7 CONTOURS OF CONSTANT MACH NUMBER CASE 10, A = 0.08764252

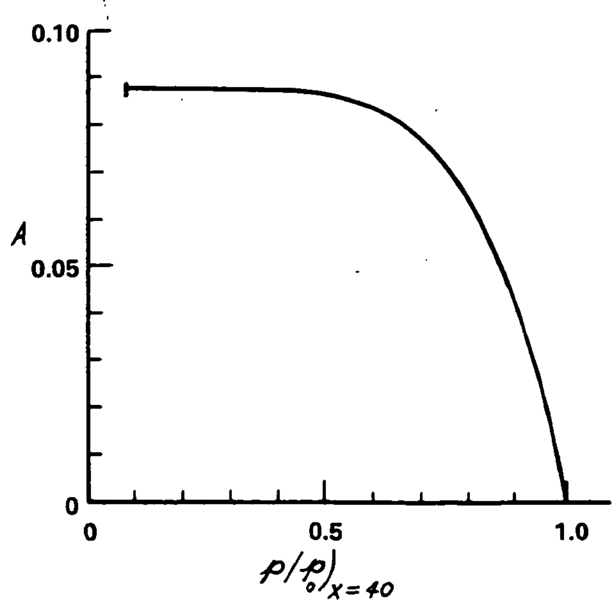

Figure 8 MASS-FLOW VARIATION WITH EXIT-PLANE PRESSURE (EXIT STATION AT X = 40), CASE 10

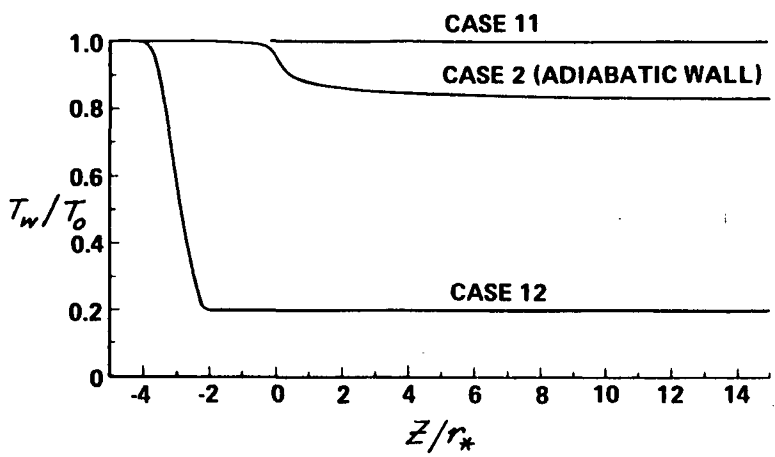

Figure 9a WALL-TEMPERATURE DISTRIBUTIONS

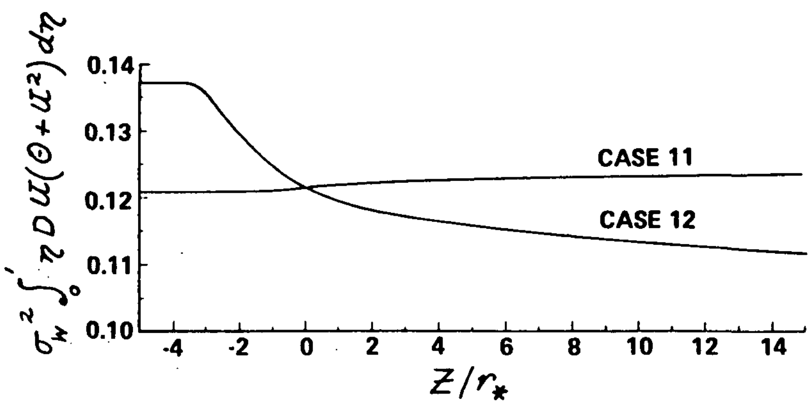

Figure 9b ENTHALPY-FLUX DISTRIBUTIONS

$$Q \equiv 1/B \left[\Theta^{\omega}\, \partial/\partial\eta \left(\Theta/Pr + \mathcal{U}^2\right)\right]_{\eta=1}$$

$Q > 0$ CORRESPONDS TO HEAT TRANSFER FROM THE WALL TO THE GAS

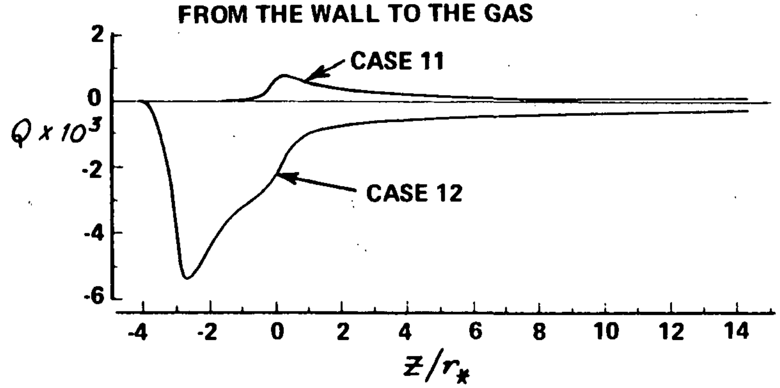

Figure 9c HEAT-TRANSFER DISTRIBUTIONS

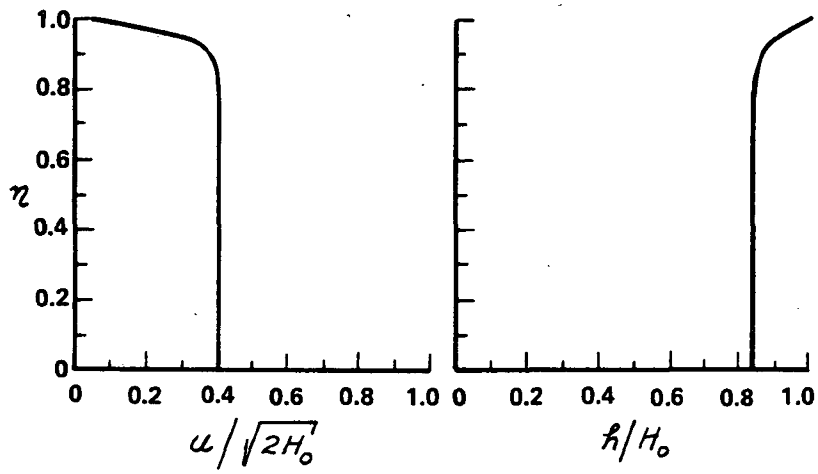

Figure 10a VELOCITY AND ENTHALPY PROFILES
CASE 11, X = 0

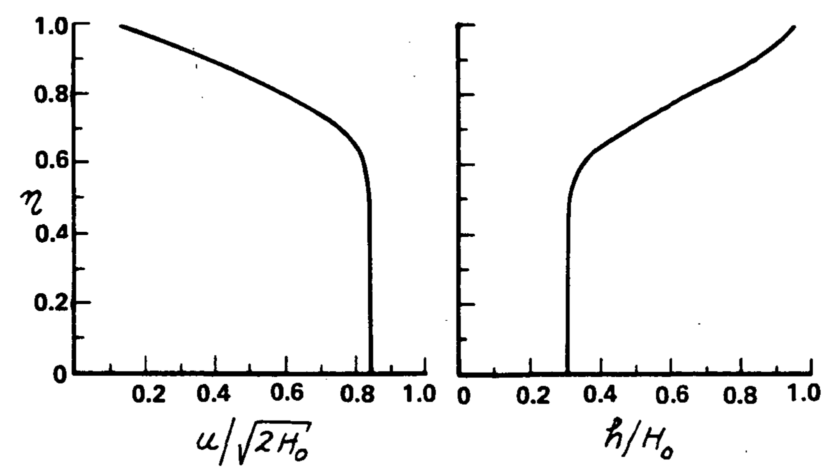

Figure 10b VELOCITY AND ENTHALPY PROFILES
CASE 11, X = 5

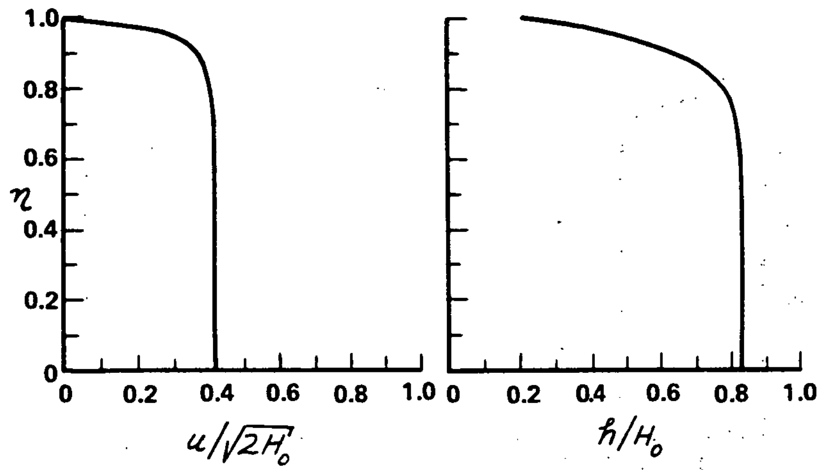

Figure 10c VELOCITY AND ENTHALPY PROFILES CASE 12, X = 0

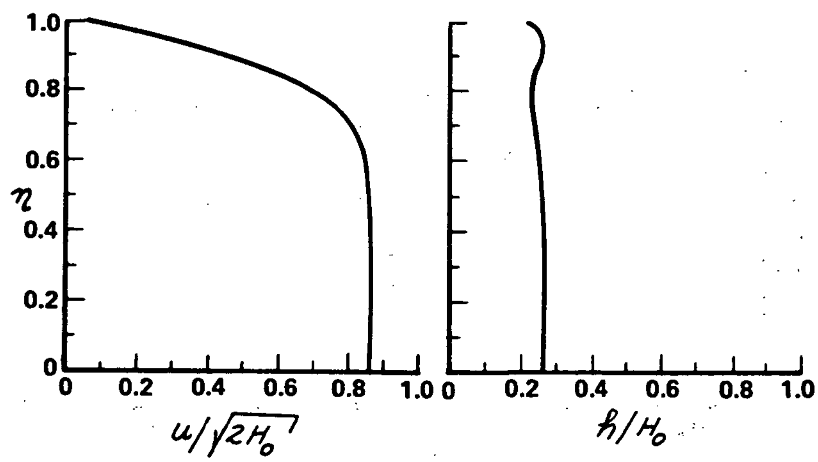

Figure 10d VELOCITY AND ENTHALPY PROFILES CASE 12, X = 5

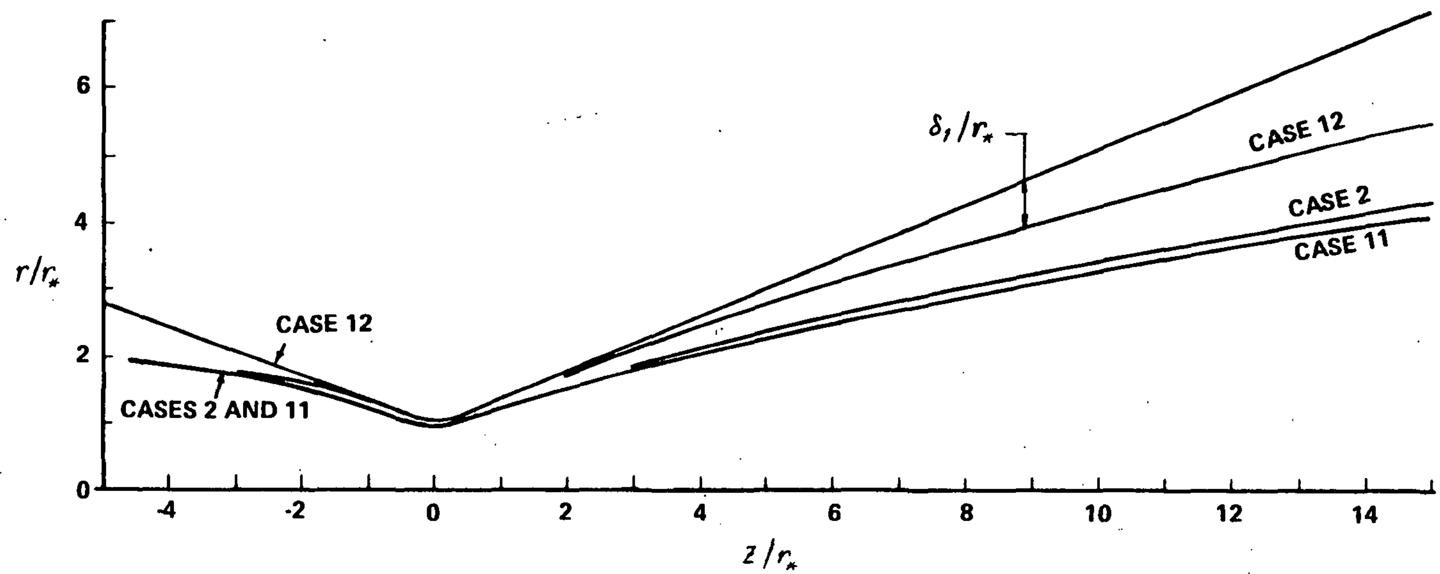

Figure 11 VARIATION OF DISPLACEMENT THICKNESS

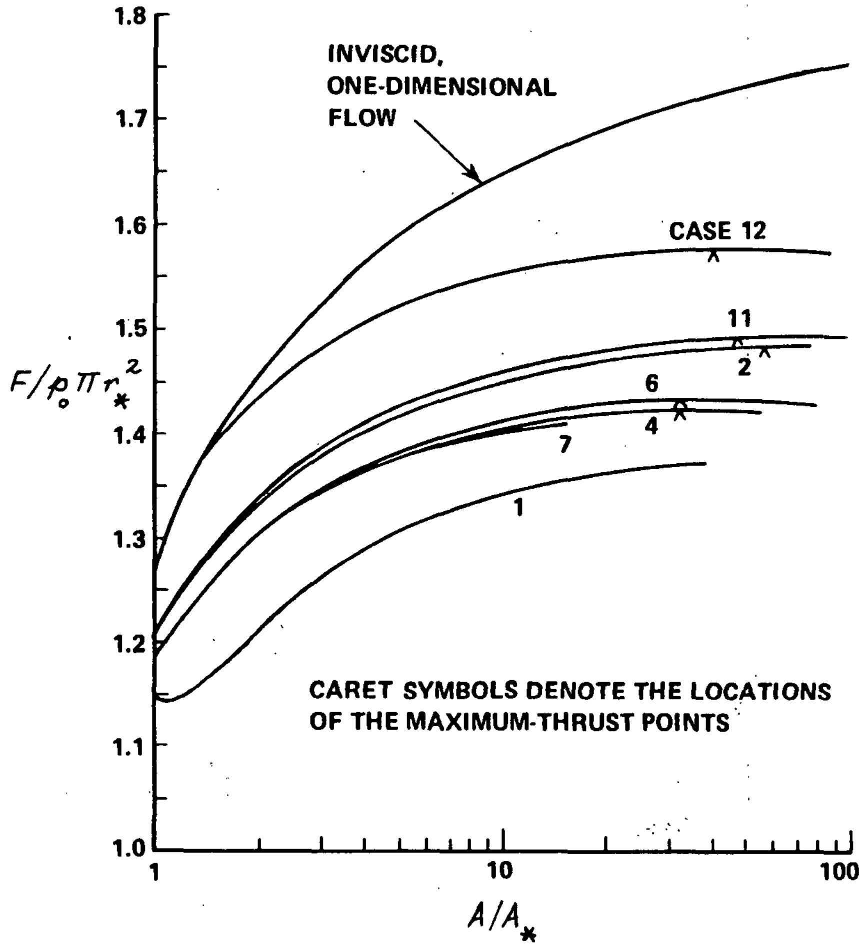

Figure 12 THRUST-COEFFICIENT DEPENDENCE ON AREA RATIO

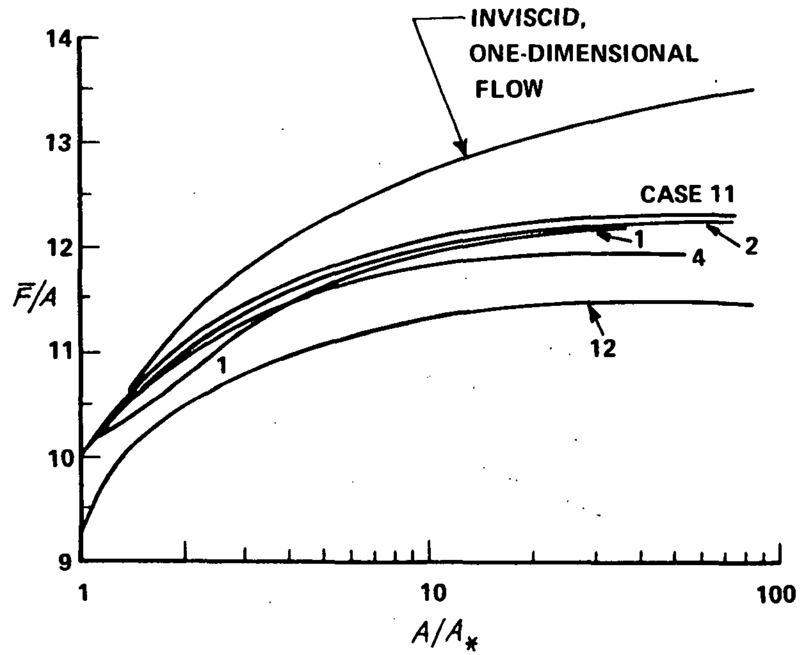

Figure 13 VARIATION OF SPECIFIC-IMPULSE PARAMETER

APPENDIX G

DISTRIBUTION LIST

COPIES	RECIPIENT	DESIGNEE
	NASA Headquarters, Washington, D. C.20546	
1	Contracting Officer, DHC	( )
1	Patent Office,	( )
	NASA Lewis Research Center	
	21000 Brookpark Road, Cleveland, Ohio 44135	
1	Office of Technical Information	( )
1	Contracting Officer	( )
1	Patent Office	( )
	NASA Marshall Space Flight Center	
	Huntsville, Alabama 35812	
2	Office of Technical Information,MS-IP	( )
1	Technical Library	( )
1	Purchasing Office, PR-EC	( )
1	Patent Office, M-PAT	( )
1	Keith Chandler, R-P&VE-PA	( )
1	Technology Utilization Office MS-T	( )
	NASA Pasadena Office	
	4800 Oak Grove Drive	
	Pasadena, California 91103	
1	Patents and Contracts Management	( )
	Western Support Office	
	150 Pico Boulevard	
	Santa Monica, California 90406	
1	Office of Technical Information	( )

COPIES	RECIPIENT	DESIGNEE
1	Technical Monitor	( )
4	Chief, Liquid Propulsion Technology Code: RPL Office of Advanced Research & Technology NASA Headquarters Washington, D. C. 20546	(X)
25	NASA Scientific and Technical Information Facility P.O. Box 33 College Park, Maryland 20740	(X)
1	Mr. Vincent L. Johnson Director, Launch Vehicles and Propulsion Office of Space Science and Applications NASA Headquarters Washington, D. C. 20546	(X)
1	Mr. George S. Trimble Director, Advanced Manned Missions Code: MT Office of Manned Space Flight NASA Headquarters Washington, D. C. 20546	(X)
1	Mr. A. Gessow Chief, Physics of Fluids Branch Office of Advanced Research and Technology NASA Headquarters Washington, D. C. 20546	(X)
1	Mr. Leonard Roberts Mission Analysis Division NASA Ames Research Center Moffett Field, California 24035	(X)

NASA FIELD CENTERS

COPIES	RECIPIENT	DESIGNEE
2	Ames Research Center Moffett Field, California 94035	H. J. Allen Mission Anal. Division
2	Goddard Space Flight Center Greenbelt, Maryland 20771	Merland L. Moseson Code: 620
2	Jet Propulsion Laboratory California Institute of Tech. 4800 Oak Grove Drive Pasadena, California 91103	Henry Burlage, Jr. J. H. Rupe
2	Langley Research Center Langley Station Hampton, Virginia 23365	Dr. Floyd Thompson Director
2	Lewis Research Center 21000 Brookpark Road Cleveland, Ohio 44135	Dr. A. Silverstein Director R. J. Priem E. W. Conrad
2	Marshall Space Flight Center Huntsville, Alabama 35812	Hans G. Paul R. J. Richmond
2	Manned Spacecraft Center Houston, Texas 77058	Dr. Robert R. Gilruth Director J. G. Thibodaux
1	Western Support Office 150 Pico Boulevard Santa Monica, California 90406	Robert W. Kamm Director
2	John F. Kennedy Space Center, NASA Kennedy Space Center, Florida 32899	Dr. Kurt H. Debus Director

GOVERNMENT INSTALLATIONS

COPIES	RECIPIENT	DESIGNEE
1	Aeronautical System Division Air Force Systems Command Wright-Patterson Air Force Base Dayton, Ohio 45433	D. L. Schmidt Code: ASRCNC-2
1	Air Force Missile Development Center Holloman Air Force Base New Mexico	Maj. R.E. Bracken Code: MDGRT
1	Air Force Missile Test Center Patrick Air Force Base, Florida	L. J. Ullian
1	Air Force Systems Division Air Force Unit Post Office Los Angeles 45, California	Col. Clark Technical Data Center
1	Arnold Engineering Development Center Arnold Air Force Station Tullahoma, Tennessee	Dr. H. K. Doetsch
1	Bureau of Naval Weapons Department of the Navy Washington, D. C.	J. Kay RTMS-41
1	Chemistry Research Laboratory Building 450 Wright-Patterson Air Force Base Dayton, Ohio 45433	K. Scheller ARL (ARC)
1	Department of the Navy Office of Naval Research Washington, D. C. 20360	R. O. Jackel Code: 429
1	Headquarters U. S. Air Force Washington, D. C.	Col. C. K. Stambaugh AFRST

GOVERNMENT INSTALLATIONS

COPIES	RECIPIENT	DESIGNEE
1	Headquarters Research and Technology Division Air Force Systems Command Bolling Air Force Base, Washington, D. C. 20332	L. Green,Jr. (RTGS)
1	Picatinny Arsenal Dover, New Jersey 07801	I. Forsten, Chief Liquid Propulsion
1	Air Force Rocket Propulsion Lab. Research and Technology Division Air Force Systems Command Edwards, California 93523	RPRR
1	U. S. Atomic Energy Commission Technical Information Services Box 62 Oak Ridge, Tennessee	A. P. Huber Oak Ridge; Gaseous Diffusion Plant
1	U. S. Army Missile Command Redstone Arsenal Huntsville, Alabama 35808	W. W. Wharton AMSMI-RRK
2	U. S. Naval Ordnance Test Station China Lake, California 93555	E. W. Price D. Couch
1	Air Force Office of Scientific Research Propulsion Division 1400 Wilson Blvd. Arlington, Va. 22209	B. T. Wolfson

CPIA

2	Chemical Propulsion Information Agency Applied Physics Laboratory 8621 Georgia Avenue Silver Spring, Maryland 20910	Neil Safeer T. W. Christian W. G. Berl

INDUSTRY CONTRACTORS

COPIES	RECIPIENT	DESIGNEE
1	Aerojet-General Corporation P. O. Box 296 Azusa, California 91703	L. F. Kohrs
1	Aerojet-General Corporation P.O. Box 15847 Sacramento, California 95809	R. J. Hefner R. Stiff
1	Aeronautronic Philco Corporation Ford Road Newport Beach, California 92663	D. A. Carrison
1	Aerospace Corporation 2400 East El Segundo Boulevard P.O. Box 95085 Los Angeles, California	O. W. Dykema W. C. Strahle
1	Astrosystems International ,Inc. 1275 Bloomfield Avenue Fairfield, New Jersey 07007	A. Mendenhall
1	Atlantic Research Corporation Edsall Road and Shirley Highway Alexandria, Virginia 23314	R. Friedman
1	Beech Aircraft Corporation Boulder Division Box 631 Boulder, Colorado	J.H. Rodgers
1	Bell Aerosystems Company P.O. Box 1 Buffalo, New York 14205	Dr. Kurt Berman
1	Bendix Corporation Bendix Systems Division 3300 Plymouth Road Ann Arbor, Michigan	John M. Brueger

INDUSTRY CONTRACTORS

COPIES	RECIPIENT	DESIGNEE
1	Boeing Company P.O. Box 3707 Seattle, Washington 98124	J. D. Alexander
1	Chrysler Corporation Missile Division P.O. Box 2628 Detroit, Michigan 48231	John Gates
1	Curtiss-Wright Corporation Wright Aeronautical Division Wood-Ridge, New Jersey 07075	G. Kelley
1	Dartmouth University Hanover, New Hampshire 03755	P. D. McCormack
1	Defense Research Corporation P.O. Box 3587 Santa Barbara, California 93105	B. Gray
1	Douglas Aircraft Company, Inc. Missile and Space Systems Division 3000 Ocean Park Boulevard Santa Monica, California 90406	R. W. Hallett Chief Engineer Advanced Space Tech.
1	Dynamic Science Corporation 1900 Walker Avenue Monrovia, California 91016	Dr. Kliegel R. J. Hoffman
1	Fairchild Hiller Corporation Aircraft Missiles Division Hagerstown, Maryland	J. S. Kerr
1	General Dynamics/Astronautics Library & Information Services Code: 128-00 P.O. Box 1128 San Diego, California 92112	Frank Dore
1	General Electric Company Re-Entry Systems Department 3198 Chestnut Street Philadelphia, Pennsylvania 19101	F. E. Schultz

INDUSTRY CONTRACTORS

COPIES	RECIPIENT	DESIGNEE
1	General Electric Company Advanced Engine & Technology Dept. Cincinnati, Ohio 45215	D. Suichu
1	Geophysics Corporation of America Technical Division Burlington Road Bedford, Massachusetts 01730	A. C. Toby
1	Georgia Institute of Technology Aerospace School Atlanta, Georgia 30332	B. T. Zinn
1	Grumman Aircraft Engineering Corp. Bethpage, Long Island New York	Joseph Gavin
1	Ling-Temco-Vought Corporation Astronautics P.O. Box 5907 Dallas, Texas 75222	Warren C. Trent
1	Arthur D. Little, Inc. 20 Acorn Park Cambridge, Massachusetts 02140	E. Karl Bastress
1	Lockheed California Company 2555 North Hollywood Way Burbank, California 91503	G. D. Brewer
1	Lockheed Missiles and Space Company Attn: Technical Information Center P.O. Box 504 Sunnyvale, California 94088	Y. C. Lee
1	Lockheed Propulsion Company P.O. Box 111 Redlands, California 92374	H. L. Thackwell
1	The Marquardt Corporation 16555 Saticoy Street Van Nuys, California 91409	W. P. Boardman, Jr.

INDUSTRY CONTRACTORS

COPIES	RECIPIENT	DESIGNEE
1	Martin Marietta Corporation Baltimore Division Baltimore, Maryland 21203	John Calathes Code: 3214
1	Martin Marietta Corporation Denver Division P.O. Box 179 Denver, Colorado 80201	J. D. Goodlette Code: A-241
1	Massachusetts Institute of Tech. Department of Mechanical Engineering Cambridge, Massachusetts 02139	T. Y. Toong
1	McDonald-Douglas Aircraft Company Astropower Division 2121 Paularino Newport Beach, California 92663	Dr. George Moc Director, Research
1	McDonnell Aircraft Corporation P.O. Box 516 Municipal Airport St. Louis, Missouri 63166	R. A. Herzmark
1	Multi-Tech. Inc. 601 Glenoaks Boulevard San Fernando, California	F. B. Cramer
1	North American Aviation, Inc. Space & Information Systems Div. 12214 Lakewood Boulevard Downey, California 90241	D. Simkin
1	North American Aviation, Inc. ROCKETDYNE 6633 Canoga Avenue Canoga Park, California 91304	E. C. Clinger R. B. Lawhead
1	Northrop Space Laboratories 3401 West Broadway Hawthorne, California	Dr. William Howard
1	The Pennsylvania State University Mechanical Engineering Department 207 Mechanical Engineering Boulevard University Park, Pennsylvania 16802	G. M. Faeth

INDUSTRY CONTRACTORS

COPIES	RECIPIENT	DESIGNEE
1	Polytechnic Institute of Brooklyn Graduate Center Route 110 Farmingdale, New York	V. D. Agosta
1	Pratt and Whitney Aircraft (United Aircraft Corporation) Florida Research and Development P.O. Box 2691 West Palm Beach, Florida 33402	G. D. Lewis
1	Princeton University Forrestal Research Center Guggenheim Laboratories Princeton, New Jersey 08540	I. Glassman D. T. Harrje
1	Purdue University School of Mechanical Engineering Lafayette, Indiana 47907	J. R. Osborn
1	Ohio State University Department of Aeronautical & Astronautical Engineering Columbus, Ohio 43210	R. Edse
1	Radio Corporation of America Astro-Electronics Division Princeton, New Jersey 08540	S. Fairweather
1	Republic Aviation Corporation Farmingdale, Long Island New York	Dr. William O'Donnell
1	Sacramento State College Engineering Division 60000 J. Street Sacramento, California 95819	F. H. Reardon
1	Space General Corporation 9200 East Flair Avenue El Monte, California 91734	C. E. Roth

INDUSTRY CONTRACTORS

COPIES	RECIPIENT	DESIGNEE
1	Stanford Research Institute 333 Ravenswood Avenue Menlo Park, California 94025	G. Marxman
1	TRW Incorporated TRW Systems Group One Space Park Redondo Beach, California 90278	G. W. Elverum
1	TRW Incorporated TAPCO Division 23555 Euclid Avenue Cleveland, Ohio 44117	P. T. Angeli
1	Thiokol Chemical Corporation Huntsville Division Huntsville, Alabama	John Goodloe
1	Thiokol Chemical Corporation Reaction Motors Division Denville, New Jersey 07832	Arthur Sherman
2	United Aircraft Corporation Research Laboratories 400 Main Street East Hartford, Connecticut 06108	Erle Martin D. H. Utvick
1	United Technology Center 587 Methilda Avenue P.O. Box 358 Sunnyvale, California 94088	R. H. Osborn
1	University of California Department of Chemical Engineering 6161 Etcheverry Hall Berkeley, California 94720	A. K. Oppenheim
1	University of California Department of Mechanical Engineering Thermal Systems Berkeley, California 94720	E. Starkman

INDUSTRY CONTRACTORS

COPIES	RECIPIENT	DESIGNEE
1	University of Michigan Aerospace Engineering North Campus Ann Arbor, Michigan 48104	J. A. Nicholls
1	University of Southern California Department of Mechanical Engineering University Park Los Angeles, California 90007	M. Gerstein
1	University of Wisconsin Department of Mechanical Engineering 1513 University Avenue Madison, Wisconsin 53705	P. S. Myers
1	Walter Kidde and Company, Inc. Aerospace Operations 567 Main Street Belleville, New Jersey 07109	R. J. Hanville Director Research Engineering
1	Warner-Swasey Company Control Instrument Division 32-16 Downing Street Flushing, New York 11354	R. H. Tourin
1	Rocket Research Corporation 520 South Portland Street Seattle, Washington 98108	Foy McCullough, Jr.
1	Illinois Institute of Technology 3300 S. Federal Street Chicago, Illinois 60616	T. P. Torda
1	Cetec Corporation 188 Whisman Road Mountain View, California	Dr. R. S. Channapragada
1	Technology Incorporated 6461 Edsall Road Alexandria, Virginia 22312	Donald A. Waters
1	Aerospace Division Library Mail Station R3679 Honeywell, Inc. 2600 Ridgway Parkway Minneapolis, Minnesota 55413	Mr. R. E. Michel